Published in final edited form as:
Mol Cell Biomech. 2009 March ; 6(1): 1–55.

Creation of Functional Micro/Nano Systems through Top-down and Bottom-up Approaches

Tak-Sing Wong[*], **Branden Brough**[†], and **Chih-Ming Ho**[*,‡]

[*]Mechanical and Aerospace Engineering Department, University of California, Los Angeles, CA 90095, USA

[†]Muscle Biology Proteomics and Nanotechnology Section, Laboratory of Muscle Biology, National Institutes of Health, Bethesda, MD 20892, USA

Abstract

Mimicking nature's approach in creating devices with similar functional complexity is one of the ultimate goals of scientists and engineers. The remarkable elegance of these naturally evolved structures originates from bottom-up self-assembly processes. The seamless integration of top-down fabrication and bottom-up synthesis is the challenge for achieving intricate artificial systems. In this paper, technologies necessary for guided bottom-up assembly such as molecular manipulation, molecular binding, and the self assembling of molecules will be reviewed. In addition, the current progress of synthesizing mechanical devices through top-down and bottom-up approaches will be discussed.

Keywords

bottom-up fabrication; complexity; emergent properties; self-assembly; top-down fabrication

1 Introduction

Nature has long been a source of wonderment for its ability to produce extremely complex yet elegant and functional structures and life forms across a multitude of length scales (1–3). The remarkable sophistication of these naturally evolved complex structures originates from the guided bottom-up assembly. This can be illustrated by radiolarian *Actinomma* micro skeletons (see Figure 1), which exist in unicellular organisms (4). These highly symmetrical and concentric structures are synthesized, through a reiteration of tangential and radial crystallization of inorganic ions, inside vesicles distributed over intracellular scaffolds at successive levels within the cell (4,5). In the language of manufacturing, the vesicles attached to the intracellular scaffolds are served as structural templates to provide geometrical constraints for the synthesis of inorganic structures through the process of crystallization.

Apart from their interesting structural complexity, naturally synthesized geometries often exhibit remarkable structural hierarchy for specific functionality. An example can be found in the skeleton of *Euplectella sp.*, which is a deep sea, sediment-dwelling sponge from the Western Pacific (6). To serve the purpose of filtering, metabolite trapping, and providing the ability to withstand continuous ocean currents, the skeleton has evolved into a special structural architecture (see Figure 2). These structures are synthesized from nanoscale silica particles

‡Corresponding Author: chihming@seas.ucla.edu.

(see Figure 2I), which are arranged in well-defined microscopic concentric rings (see Figure 2G and H) and glued together by an organic matrix (see Figure 2E) to form laminated spicules. The spicules are assembled into bundles (see Figure 2D), which eventually result in a macroscopic cylindrical square-lattice and cagelike structure with diagonal ridges for structural enhancement (see Figure 2A–C). This mechanical design can effectively strengthen the rigidity of the overall structure to serve its purposes even though the constituent material (i.e., bio-silica) is relatively brittle.

Very often, natural structures with simple functionalities interacting together will result in a system featuring extremely complex functionalities. The cell is a typical example of such a system with multiple levels of complexity. Unlike the previously mentioned naturally evolved structures, cells can perform higher-order functions, such as replication (e.g., mitotic cell division (7)) and locomotion (e.g., actin and myosin system, see Figure 3 (8,9)). The fundamental unit that dictates the eventual morphology and functions of the cell is DNA (10). DNA carries the genetic code necessary for the proper synthesis of proteins, which dictates the functions of the cellular system. Molecules inside the cell interact together, causing the transduction of different signal pathways for initiating cell functions (11,12). Furthermore, cells can interact together to form tissues which emerge to higher-order functionalities or so called emergent properties(13–15). These hierarchies of complex systems constitute the framework of the biological systems that exist in nature.

To create devices with similar functional complexity as those found in nature, the primary step is to understand the force fields required to bring simple molecules together and assemble them in a controlled manner. In nature, diffusion is the dominant transport mechanism to bring molecules from a far-field region to a near-field region (see Figure 4). Once a molecule enters the near-field region, termed the recognition or binding site, near-field forces enable the molecules to assemble together. This mechanism is stochastic in nature. To better utilize nature's methodology (i.e., guided bottom-up approach) to create artificial engineered devices, we need to develop techniques that transport molecules more effectively from the far-field region to the desired near-field regions where they will initiate bottom-up synthesis, guided in a deterministic way by the use of top-down fabrication techniques.

In this paper, we will first present an introductory theoretical background of the fundamental force fields operating at the molecular scale in a self-assembling system. We will then discuss the common types of molecules, or so called molecular components for the bottom-up assembly process in a liquid medium. The current state-of-the-art technologies used to define recognition sites through top-down approaches will also be reviewed. Next, we will discuss the recent efforts in manipulating molecules, from the far-field region to the near-field region, for the effective transport of molecular components. Examples of recent advances in constructing functional devices through both the top-down and bottom-up synthesis approaches will be discussed. In concluding this article, we will evaluate the current progress of synthesizing functional devices through both the top-down and bottom-up approaches and some future directions within the field.

2 Force Fields and Thermodynamics of Self-assembly at the Molecular Scale

In a self-assembled system, the architecture of the structure is dictated by the geometries of the constituent molecules and the molecular interactions within and between the molecules in the surrounding liquid medium. Consequently, the ability to manipulate the spatial distribution of the molecules (or equivalently speaking, the local concentration of the molecules) is essential in directing growth in predefined locations. Therefore, understanding the force fields required to bring molecules together is fundamental. In this section, we are going to give a brief overview of the pertinent molecular interactions in a self-assembled system. In a later section, we will

touch on the physical mechanisms that can induce bulk transportation of molecules from a far-field region to near-field region for initiation of self- assembly at specific recognition sites (see Figure 4).

2.1 Force Fields at the Molecular Scale

Molecules possess thermal energy which set them into random motion at any temperature higher than absolute zero. This thermal energy is generally characterized by kT, where k is the Boltz-mann constant ($k = 1.381 \times 10^{-23}$J/K) and T is the temperature of the system. In order for the molecules to initiate any kind of self-assembly action, the interaction energy between the molecules has to overcome this intrinsic thermal energy barrier. According to Trouton's rule, it has been shown that as long as the interaction energy between two molecules in close proximity exceeds $\frac{3}{2}kT$ at standard temperature and pressure, the molecules will be condensed into a solid or liquid phase (16). Therefore, the thermal energy term, kT, is a good indicator to gauge the strength and effective range of any type of intermolecular interactions in a self-assembled system. Unless otherwise specified, T is assumed to be 298K throughout this article that involves kT in the calculations.

For simplicity, we will consider two atoms in a vacuum environment. If the interaction between the atoms is covalent (which is quantum mechanical in nature), the bond strength is on the order of $100kT$ (or equivalent to 250kJ/mol) and the range of the interaction is ~0.1 – 0.2nm (16,17). This type of interaction is very strong, but the effective interaction range is on the order of an atomic radius. On the other hand, for Coulomb interactions between ions, the potential function (or pair potential function), $w(r)$, can be described as,

$$w(r)=\frac{Q_1 Q_2}{4\pi\varepsilon\varepsilon_0 r} \tag{1}$$

where Q_1 and Q_2 are the charges of the ions, ε and ε_0 are the relative permittivity of the medium and absolute permittivity of vacuum, respectively, and r is the intermolecular distance. When compared to covalent interactions, Coulomb interactions are on the same order of strength, but with a longer effective range. For example, for isolated K^+ and Cl^-ions in vacuum (the sum of their ionic radii is ~0.332nm (17)), the interaction energy between this ion pair is ~$170kT$ (or ~420kJ/mol). According to Equation (1), the Coulomb interaction is still higher than the intrinsic thermal energy, kT, at a distance ~56nm, which gives us a sense of the relatively long range interactions between ions and atoms.

Apart from the inter-atomic strong interactions described earlier, there is another type of interaction, called van der Waals' interactions, which act on any type of atoms or molecules. Although the physical origin of van der Waals' interactions arises from dipole-dipole interactions, these interactions can be further sub-divided into three different categories. This sub-division is mainly due to the slightly different physical mechanisms (18), namely, the dispersion interaction, the induction interaction, and the orientation interaction. The potential function of van der Waals' interactions can be described as,

$$w(r)=-\frac{C_{\text{dispersion}}+C_{\text{orientation}}+C_{\text{induction}}}{r^6} \tag{2}$$

where $C^{\text{dispersion}}$, $C^{\text{orientation}}$, and $C^{\text{induction}}$ are the coefficients related to the dispersion, orientation, and induction interactions, respectively. All of these interactions have the same scaling factor which gives rise to the one-sixth scaling effect of van der Waals' interactions.

Unlike the previously mentioned strong covalent and Coulomb interactions, van der Waals' interactions are much weaker in terms of strength (on the order of 1kJ/mol or equivalent to ~0.4*kT*) (16) and influence. Clearly, the scaling factor of 1/*r*6 results in the strength of the interactions decaying much faster than that of Coulomb interactions which scales at 1/*r*. In general, the van der Waals' interactions can be effective from ~10nm down to atomic spacing (0.2nm) (16). However, the attractive nature of van der Waal's interactions can only partially describe the force fields between atoms and molecules. To have a complete picture, one has to account for the electrostatic repulsive nature of atoms or molecules when they are in very close proximity. These repulsive interactions arise from the electron cloud repulsion contributed from individual atoms or molecules. Therefore, the total pair potential function between atoms and molecules can be more precisely represented by the Mie potential (16),

$$w(r) = -\frac{A}{r^n} + \frac{B}{r^m} \tag{3}$$

where *A* and *B* are constants depending on the type of interactions and *n* and *m* are two positive integers. The first term is related to an attractive potential and the second term is related to a repulsive potential. Among the different constants (*n* and *m*) used, the most commonly used total pair potentials is the Lennard-Jones (19) potential, which adopts $n = 6$ and $m = 12$ because the function retains the one-sixth power nature of van der Waals' interactions. The Lennard-Jones potential has been adopted by scientists and engineers worldwide for numerical simulations of molecular interactions at the nanoscale level.

Another type of intermolecular interaction which is significant in dictating the three-dimensional structures of macromolecules is that of hydrogen bonding. This type of interaction arises when a hydrogen atom interacts between two electronegative atoms (i.e., atoms that tend to attract electrons to itself, such as oxygen, fluorine, nitrogen). The effective range of this particular type of interaction is between that of covalent interactions and van der Waals' interactions. For example, the covalent bond length of O-H is 0.10nm and the hydrogen bond length of O···H is 0.176nm. Comparatively, the sum of van der Waals radii of O and H is approximately 0.26nm (16). While the strength of hydrogen bonding interactions is between 10 – 40kJ/mol (or equivalent to 4*kT* – 16*kT*) (16,20), the significance of this type of interaction can be signified by the double helix DNA structures that originate from the hydrogen bonding interactions between the intramolecular bases on the sugar phosphate backbone structures (10).

So far we have briefly reviewed the typical types of interactions between atoms and molecules ranging from the strongest interactions, such as covalent and Coulomb interactions, to the weakest interactions, such as van der Waals' interactions. There exist other types of interactions (e.g., hydration, steric, and hydrophobic interactions, etc.) whose strength and effective ranges rank in between those mentioned earlier. Interested readers are suggested to refer to the detailed treatments from Israelachvili (16).

2.2 Thermodynamics of Self-assembly Processes

The energy distribution possessed by individual molecules (or a population of molecules) in ther mal equilibrium follows the Boltzmann distribution (21),

$$p_i = \frac{1}{Z} e^{-\frac{U_i}{kT}} \tag{4}$$

where p_i is the probability of finding a molecule (or a sub-population of molecules) at energy state U_i, and Z is the partition function to ensure that the probability sums up to unity. With the foundation set by the Boltzmann distribution function, Equation (4) can be further extended to describe a system of self-assembled molecules. The dynamics of the molecules that self-assemble together are dictated by the local concentration of the constituent molecules and the local interactions between individual molecules and the solvent molecules. Depending on the local interactions between the molecules, different populations of self-assembled structures of varying sizes may result, which can be described by statistical thermodynamics. For instance, the thermodynamic state for a system of self-assembled molecules in thermal equilibrium can be completely defined by the following two equations (16),

$$X_N = N\left(X_1 e^{\frac{\mu_1^0 - \mu_N^0}{kT}}\right)^N \tag{5}$$

where X_N is the concentration of the aggregates (or self-assembled structures) with N constituent molecules in the medium, and μ_N^0 is the mean interaction free energy per molecule in the aggregates, and

$$C = \sum_{N=1}^{\infty} X_N \tag{6}$$

where C is the total concentration of the solute molecules inside a solution.Equation (5) describes the dependency of the population of self-assembled structures (with different numbers of constituent molecules, N) in a system to the interaction energy of individual constituent molecules (i.e., μ_N^0). On the other hand, Equation (6) describes the conservation of the number of constituent molecules in a system following the mass conservation argument.

Depending on the dimensionality of the self-assembled structures, the mean interaction free energy per molecule (i.e., μ_N^0) will be varied with the size of the aggregates (which is equivalent to the number of constituent molecules self-assembled together) which can be described by the following equation,

$$\mu_N^0 = \mu_\infty^0 + \frac{\alpha kT}{N^p} \tag{7}$$

where μ_∞^0 is the bulk interaction free energy per molecule for an aggregate of infinite size, α is a positive constant dependent on the strength of the intermolecular interactions, and p is a number dependent on the shape and dimensionality of the self-assembled structures. For example, p will be equal to unity for molecules self-assembled into a linear-chain structure. An example such as actin, which is one of the most abundant cytoskeleton proteins known, and it is able to polymerize into linear chain of actin filaments. Detailed accounts for this particular type of protein will be presented in Section 3.3. By using Equations (4–7), one can predict the critical molecular concentration for which the molecules start to self-assemble into aggregates and the population density of the resulting self-assembled structures.

In general, the effective range of all intermolecular interactions seldom exceeds 100nm (16). Consequently, in order to initiate any form of self-assembly process (i.e., bottom-up approach), we have to control the local concentrations of the molecules and bring them in very close proximity (<100nm) to the surface binding area. To achieve this purpose, global force fields,

such as fluidic motion, are required by a guided assembly system to transport molecules within close proximity of their binding surfaces, in order for the short range interactions to take over. Before discussing the force-fields that result in the bulk transportation of molecules from the far-field region to the close proximity of a surface, a thorough understanding of the molecular components available as structural materials for bottom-up synthesis is necessary, especially with regards to their optimal incorporation into top-down fabricated structures. In the next section, we will examine the properties of a few natural molecular components and describe how these molecular components can be used in engineering applications.

3 Natural Molecular Components

Nature has produced a variety of complex patterns and structures from a wide range of constituent materials. These materials range from structurally simple inorganic salts to geometrically more involved molecules, such as deoxyri-bonucleic acid (DNA), as well as highly complex structural molecules such as cytoskeleton and motor proteins. On the other hand, chemists have made synthetic molecular components on the order of nanometers that are able to perform mechanical work. This rich toolset of natural and synthetic molecular components has enabled limitless potential for device and material construction. The following section will first introduce the basic functionality of each individual natural molecular component and then briefly describe how they can potentially be utilized in engineering applications. For detailed accounts on synthetic molecular components, readers are suggested to refer to review articles by Balzani et al. (22,23).

3.1 Inorganic Salts

Among the naturally occurring constituent molecules, inorganic salts feature among the simplest form of material construction, yet a variety of crystal forms can result based on the molecular geometry and arrangement (24,25). Inorganic ions join together to form crystal structures through ionic interactions featuring inter-atomic spacing on the order of 0.1 – 0.2nm (17). The crystal morphology is therefore highly dependent on the inter-atomic arrangement of individual ionic species. Examples, such as NaCl and KCl, are simple diatomic molecules which can form cubic crystals as seen in everyday life.

Despite the geometrical simplicity of inorganic ions, a number of control parameters (e.g., chemical and biological additives or temperature, etc.) can be introduced to influence the growth dynamics of the inorganic crystals, resulting in different crystal morphologies (4,26). The knowledge of how to control the crystal morphology comes from the emerging research field of biomineralization, which studies how biological species are able to precisely control the formation of different crystal morphologies *in vivo* (4) (see Figure 1). A typical example is calcium carbonate, which can exist in the form of calcite and aragonite in the shell layer of a mollusk, depending on the biological additives and ionic species present in the growth environment (27,28) (see Figure 5). One remarkable feature is that these two crystal forms cannot be found at the same location in these biomineralized tissues, which implies that the determination of the form of grown crystal is highly regulated. By understanding how biological species can exert such exacting control on their crystal formation, we can gain further insight into the integration of inorganic crystals of specific forms, with top-down fabricated structures, to create new types of functionality.

Apart from the control of crystal morphology, the crystallographic planes of the growing crystals can be precisely controlled under well designed micro-environments (29). Different crystallographic planes can withstand a varying degree of stress owing to the difference in atomic packing density. To illustrate, let us consider a very well studied inorganic material, silicon (30). The calculated Young's modulus of the single crystalline silicon for crystallographic planes of {100}, {110} and {111} are 149.6GPa (mean value), 158.9GPa

(mean value) and 168.9GPa, respectively (31). By growing the crystals to a specific crystallographic plane, we can make use of the mechanical anisotropy advantage in device construction.

Besides the control of crystallographic planes to enhance the material's mechanical strength, the inclusion of biological additives as an organic matrix within the crystal structures can have a tremendous effect on the material's mechanical properties. In the previously mentioned mollusk shell, the characteristic skeletal structure, or nacre, has exceptional structural strength (tensile strength from 35MPa to 110MPa) especially when considering that the constituent material (i.e., $CaCO_3$) is relatively brittle. Quantitatively, it is approximately 3000 times more resistant to fracture than the single crystal of the same constituent molecules (32–34), which is not seen in any other form of natural calcium carbonate (32). This exceptional mechanical behavior of nacre originates from the interactions of the unfolding proteins and the mineral bridges between the aragonite platelets inside the skeleton structure (35–37). Therefore, by controlling the growth of the inorganic crystal to a certain crystallographic plane with the inclusion of an organic matrix, we can fully utilize mechanical anisotropy and elasticity in the design of a new class of mechanical devices, analogous to natural materials such as bones or nacre (38,39).

The interesting examples of calcium carbonate crystals have provided us insight into the use of inorganic crystals. When used wisely with biological molecules, emergent materials can feature unexpected structural performance. Nevertheless, there are a variety of crystal structures which can be directly grown from aqueous solution and each of them has different physical properties for different purposes. A database of different inorganic crystal structures was constructed in the early 1980s (40) and to date, it features ~90000 inorganic crystal structures on the world-wide-web. Interested readers are suggested to refer to the database for acquiring various inorganic crystal structures (41). In addition, recent progress towards simulating crystal growth from solution has provided an indispensable tool in the prediction of crystal shape and morphology as well as their physical properties (42). This will help our future understanding of how to grow inorganic crystals with specific specifications for functional device construction.

3.2 DNA

The seminal discovery of the structural architecture of DNA by Watson and Crick in 1953 (10) marked the beginning of modern molecular biology. DNA is a linear polymer chain composed of monomers called nucleotides. The length of DNA macromolecules can be on the order of hundreds of millions of nucleotides. Each nucleotide consists of an organic base that is linked to a five-carbon sugar with a phosphate group. There are 4 different types of organic bases (resulting in 4 different types of nucleotides), namely adenine (A), thymine (T), guanine (G) and cytosine (C). In its natural state (i.e., at room temperature and neutral pH), two single strands of DNA (ssDNA) will form a double helix structure (i.e., double-stranded DNA or dsDNA). This structure can be held precisely by the organic base pairs, where A is paired with T and G is paired with C through hydrogen bonding (43). Specifically, the A-T base pair is held by two hydrogen bonds whereas the G-C base pair is held by three hydrogen bonds. Recent single molecule force measurements have revealed that the unbinding force for individual base pairs is on the order of 10pN (44,45).

Most DNA exists in the form of a right-handed double helix structure with the spacing between the stacked bases being 0.34nm apart along the helix axis. The helix structure repeats itself every 3.4nm (10), which is about 10 – 10.5 base pairs (bp) per turn (10,46,47). The diameter of the double helix structure is about 2nm. This common configuration of DNA is called B-form DNA. There exist other forms of DNA such as A-form and Z-form DNA. A-form DNA is a compacted form of B-form DNA with 11bp per turn and a diameter of 2.6nm whereas Z-

form DNA is a left-handed double helix with 12bp per turn and measuring 1.8nm in diameter (43,48). Recent single molecule experiments have shown that mechanical manipulations of DNA can result in a S-form (0.58nm per rise, ~70% longer than B-form DNA) when the molecules are stretched under large tension forces (>65pN) (49) or P-form (2.7bp per turn) when the molecules are twisted (50). Along the longitudinal axis of the helix structure, there are no hydrogen bonds between the base pairs, therefore the structure is flexible to bend. The flexibility and the specific hydrogen bonding between the individual bases are important features for utilizing DNA as a programmable assembling structural material.

3.2.1 DNA Mechanics—Quantifying the mechanical properties of DNA has important implications to both DNA mechanics and DNA-related enzymatic studies (51). Understanding the mechanical properties of DNA is the primary step to utilize them for higher-order structure construction. With the rapid development of single molecule spectroscopy technologies (e.g., optical nanometry and scanning probe microscopy), the characterization of DNA mechanics on the single molecule level can now be achieved (51,52). There are a few important parameters that can quantify the mechanical properties of a DNA molecule; namely persistence length, flexural rigidity, and torsional rigidity. Persistence length is a measure of the filament's structural resistance to thermal forces (21). Owing to the negatively charged phosphate backbone in dsDNA, all mechanical properties, especially persistence length, are contingent on the surrounding ionic environment (53). Indeed, optical nanometry studies have verified that the persistence length of dsDNA molecules ranges from 40 – 50nm (54) (compared to ssDNA whose persistence length is 0.75nm (49)), which is comparable to the measurements of DNA mechanics in bulk quantities (55).

In addition, torsional rigidity is a measure that quantifies a rod-like structure's tendency to resist rotational motion along the centerline whereas flexural rigidity is a measure of the tendency to resist bending (56). If we assume DNA molecules are isotropic rod-like structures (which is generally true when the DNA is stretched under very low tension, i.e., <0.3pN (57)), there is a simple relationship correlating persistence length, L_p, and flexural rigidity, EI, (where E is the Young's modulus and I is the area moment of inertia about the longitudinal direction of the filament cross section) which is (21),

$$L_{\mathrm{p}}=\frac{EI}{kT} \tag{8}$$

By using this simple relationship, the flexural rigidity can be estimated from the measured persistence length (or vice versa). Based on the measured persistence length from single DNA mechanical studies, the flexural rigidity of a dsDNA molecule at 298K is estimated to be ~0.16 – 0.21nN·nm^2. In addition, single molecule measurements of dsDNA has shown that the torsional rigidity of dsDNA is ~0.44nN·nm^2 (50).

Apart from the three mechanical properties mentioned earlier, a very recent study has shown that when a dsDNA molecule is stretched under low tension (<30pN), it will start to overwind. Similarly, if the dsDNA molecule is twisted, its length will increase accordingly (i.e., increment of ~0.5nm per turn) (58). This twist-stretch coupling mechanism of DNA molecules may be accounted for their mechanical anisotropy. In addition, the mechanical properties of dsDNA have shown to be sequence dependent (44,59). Therefore, by manipulating the sequence of a dsDNA molecule, its mechanical properties can be tailored for different applications. More in-depth treatments on DNA mechanics on the single molecule level can be found in review articles by Bustamante et al. (51,60).

3.2.2 DNA for Geometric Construction—Through creative designs of DNA sequences, DNA molecules can be utilized for geometrical and topological construction. Normally, DNA macromolecules exist in linear duplex structures in eukaryotic cells (e.g., supercoiled structure (43,61), similar to a twisted rubber band). However, DNA macromolecules can form branched structures in the intermediate steps of DNA metabolism such as replication (62,63) and recombination (64). The famous example is the Holliday junction (64,65) which contains 4 strands of DNA arranged in 4 double helix armed structures. Branched DNA structures are important elements in creating 2-dimensional and 3-dimensional structures. To illustrate how branched DNA can be used for this purpose, let us consider a simple hypothetical DNA linear sequence, 5'-ATTC-3' and a longer DNA complimentary sequence, 3'-TAAGCA-5'. After these two linear sequences combine (or hybridize) to form a double helix structure, $5\prime - ATTC - 3\prime$
$3\prime - TAAGCA - 5\prime$, the extra bases, C and A are now available for additional binding with other DNA double helix structures with a matched base end-sequence of G and T. The iteration of this process will eventually yield a long, linear double helix structure of DNA. As this mechanism is applied to every arm of a branched DNA structure, more complicated 2-D and 3-D structures can be formed by joining the structures together.

In order to realize the 2-D and 3-D structures made from DNA molecules, the first step is to obtain stable, branched DNA structures *in vitro* since those structures are inherently unstable *in vivo*. In the early 1980s, pioneering work of Seeman and coworkers have shown the possibility of forming branched DNA structures in solution by imposing sequence symmetry constraints with equilibrium calculations (66), thereby laying down the foundation of this exciting research field of DNA nanotechnology (67,68). Thus far, a variety of 2-D and 3-D objects have been synthesized by joining those short branched DNA molecules together (usually the length of each individual branch is <100 bases). Examples of successfully synthesized structures using this technique include, cube (69), truncated octahedron (70), quadrilateral (71), Borromean rings (i.e., three mutually interlocked rings) (72), equilateral triangle (73,74), and 2-D periodic crystalline structures (75). Besides using short strands of branched DNA molecules for structural construction, recent demonstrations have shown that 2-D and 3-D structures can be assembled by folding a long, single strand of DNA molecules (>1000kb, kb = kilobase) with a few short strands of DNA molecules (<0.1kb) as molecular "staples". This approach, compared to the previous DNA nanoconstruction methods using short, branched DNA molecules, presents a much higher yield since the DNA purification and sequence optimization steps are not necessary (e.g., the yield for the construction of rectangles with patterns and sharp triangles can be at least 70% using this approach). Thus far, a 3-D object (i.e., an octahedron (76)) and arbitrary 2-D objects (77) (see Figure 6), have been successfully produced using this method.

3.2.3 DNA for Nanomechanical Devices—Apart from using them as nanoconstruction materials, DNA molecules have recently been utilized for the creation of nanomechanical devices with simple functionalities, such as performing partially reversible rotational motion (78), unidirectional (79) and bidirectional (80) linear motion, and opening and closing actions (81,82). To illustrate how DNA can be used for mechanical functions, consider the partial rotary DNA nanomachine as an example (78). This early demonstration of using DNA for a nanomechanical device is based on the transition from B-form DNA to Z-form DNA, induced by the presence of metallic ions. The device is constructed from two rigid "double-crossover" (or DX) DNA molecules (83) connected by a DNA molecule with 4.5 double-helical turns (see Figure 7). By switching the device under B-promoting or Z-promoting ionic conditions, the DNA molecule (that connected to the rigid DX molecules) can configure from B-form to Z-form or vice versa, resulting in ~128° rotational motion and ~2 – 6nm atomic displacement. Nevertheless, B-Z transition (or vice versa) of DNA induced by metallic ions is just one of the demonstrated mechanisms in utilizing DNA as a nanomechanical machine.

Other mechanisms (e.g., protonation (84), hybridization and branch migration (81)) have also been proven to propel DNA exhibiting nanoscale motion. Interested readers are suggested to refer to Seeman, and Simmel and Dittmer (48,85) for the recent developments on the current topic.

In this section, we have briefly summarized the use of DNA molecules for static and dynamic structural construction. When compared with inorganic salt, DNA has the programming capability for creating a wide range of structures and devices. In the next section, we are going to introduce another class of complex natural molecules, namely cytoskeleton and motor proteins, to see what kind of functionalities they can provide for more intricate device construction.

3.3 Cytoskeleton and Motor Proteins

Cytoskeleton and motor proteins play a pivotal role in sustaining the body's metabolism and locomotion through a series of inter-cooperative microscopic and nanoscopic movements at intracellular levels (e.g., muscle contraction (86) and chromosome splitting during mitosis (87)). As an example of the inter-cooperative motion of cytoskeleton and motor proteins, consider the intriguing process of mitosis. Mitosis is a process where replicated chromosomes (consisting mostly of DNA molecules) inside the nucleus of a eukaryotic cell are separated equally during the process of cell division (see Figure 8). During this process, the cell dynamically assembles and disassembles a specialized set of microtubule structures (microtubules belong to the class of cytoskeleton and motor proteins), which is known as the mitotic apparatus. Through the energy released from nucleotide hydrolysis, the mitotic apparatus can attach and capture chromosomes. Then, they align the chromosomes and separate them into equally halves, so that the genetic material is partitioned evenly in the daughter cells (43) (see Figure 8). The molecular origin that contributes to the relative motion of microtubules in the mitotic process is believed to be caused by the dynamic instability (which will be explained in detailed later) of microtubules. It is also related to a number of ATP-fuelled (ATP stands for adenosine triphosphate) force-generating enzymes, namely kinesins and dyneins, that 'walk' along the molecular track of microtubules (88).

Over the past 30 years, the progress of discovering new classes of cytoskeleton and motor proteins has been accelerated due to the advancement of related biotechnologies (e.g., two or more new classes of actin-binding proteins are discovered every year (89)). Thus far, more than 150 cytoskeleton and motor proteins along with their corresponding functions have been successfully identified (89). We have selected a few commonly used cytoskeleton and motor proteins that have been employed in the engineering community and for discussion here. For cytoskeleton proteins, we will mainly focus on the structural functionalities of actin, some of the actin-binding and actin-related proteins, and tubulin (the monomer of microtubules); whereas for motor proteins, we will focus on linear motors such as myosin (actin-based motor) and kinesin (microtubule-based motor). For detailed treatments of the cytoskeleton and motor proteins, readers are suggested to refer to the review articles and books given by Bray (8), Cleveland and Sullivan (90), Howard (21), Kreis and Vale (89), Vale (91,92), Pollard (93), and Warrick and Spudich (94). Since cytoskeleton and motor proteins have shown a rich amount of structural and dynamic functionality (see the example of mitosis), we have collected some useful data on the mechanical properties of individual proteins described in the following text to give a feel for how these individual molecular components can be used for engineering applications (see Table 1 – Table 3).

3.3.1 Actin and Actin Filaments

3.3.1.1. Molecular Structures of Actin and Actin Filaments: Actin (actin monomers or globular actin, G-actin) is a protein responsible for the structural architecture and intracellular

transportation of eukaryotic cells as well as cellular motility (8,95). It is a highly conserved protein throughout evolution, which means the genetic sequence differences of the actin protein among other animals and protozoa are very small (<5%) (89,93,96). Actin is a bi-lobed molecule that consists of a large and small domain with overall dimensions of ~3.3nm × 5.6nm × 5.0nm (93). Each individual G-actin has specific binding sites allowing it to self-assemble into a long filament chain, so-called F-actin, through reversible non-covalent binding (96,97). Some of the binding sites of the G-actin are for metal ions such as Mg^{2+}, nucleotides such as adenine, and motor proteins such as myosin (98). It is suspected that the interactions between G-actin may be of the nature of hydrogen bonds (8). Recent single molecule optical nanometry and glass needle micromanipulation studies have shown that the actin-actin bond breaking force is ~100 – 600pN (99,100). Based on these force measurements, we can estimate that the bond strength between individual actin-actin molecules is ~20kT, assuming the distance between actin-actin interactions is ~0.2nm (101) and a breaking force of 400pN. This bond strength is much weaker than covalent bonds but is within the range of hydrogen bonding interactions.

3.3.1.2. From Actin to F-actin – Self-assembly Dynamics: The F-actin can be viewed as a two-stranded, right-handed double helix which repeats itself every 35.8 – 37nm with 13 subunits (8,93,96). The filament width is 7nm with subunit spacing of 5.5nm (96). The polymerization from G-actin to F-actin essentially involves four different steps (93); 1) salt binding and conformational changes in G-actin, 2) formation of nuclei (the nuclei is most likely formed by three actin molecules clustered together in the form of a trimer structure (93)), 3) bidirectional association and dissociation of G-actin to form F-actin, and 4) annealing of short F-actin to form longer F-actin. The rate determining step in the polymerization process is the formation of nuclei. Owing to the nature of non-covalent binding, the growth of F-actin is highly influenced by the ionic environment; normally the addition of Ca^{2+} and Mg^{2+} can accelerate the nuclei formation process. For example, it has been shown that activated Mg^{2+}-actin forms nuclei more than 10 times faster than unactivated G-actin (93,102). With the presence of ATP, the F-actin will polymerize gradually until an equilibrium is reached (93, 103–105). The growth of F-actin is a dynamic association/dissociation process dictated by diffusion (105). If the association rate of G-actin is faster than the dissociation rate, there will be a net growth of F-actin. Interestingly, the growth rates at both ends of the F-actin are very different where the net growth of one end can be 10 times faster than that of the other end (8, 103). The fast growing end of F-actin is referred to as the barbed end, whereas the slow growing end is termed the pointed end. The critical concentration, $C_{critical}$, of G-actin in a solution to induce a net growth of F-actin can be formulated as (8),

$$C_{\text{critical}} = \frac{k_{\text{off}}}{k_{\text{on}}} \tag{9}$$

where k_{on} and k_{off} are the monomer association rate and the dissociation rate, respectively. In particular, there is a biological term, known as treadmilling, which describes the process where the barded end polymerizes (or increases in length) while the pointed end depolymerizes at the same moment. This process is important in cell motility (8). It has been shown that the rate of the barbed end growth correlates to the rate of the movement of the lamellipodium extension, which provides the first evidence of the relationship between actin assembly and cell motility (95,106,107).

3.3.1.3. Mechanical Properties of F-actin: Since F-actin is used within the structural architecture and for molecular transportation on an intracellular level, it is important to understand the mechanical properties of F-actin on the single filament level. Similar to DNA mechanics, we will describe actin mechanical properties through persistence length, flexural

rigidity, and torsional rigidity. Torsional rigidity is an interesting parameter to study for F-actin because it has been shown that F-actin will undergo axial rotation when myosin travels along the filament (108). The measured torsional rigidity of a single F-actin, measured by optical trapping nanometry and Brownian motion-induced shape fluctuation analysis, is ~50 – 80nN·nm^2 (100,109,110) and the measured flexural rigidity is ~15 – 73nN·nm^2 (109–112). The persistence length of a single F-actin can be deduced fromEquation (8),Based on the data from (109,112), the estimated persistence length of a single F-actin is ~4 – 18μm.

3.3.2 Actin-binding and Actin-related Proteins—The growth dynamics of F-actin is highly regulated in time and space (104). Global locomotion of cells and higher ordered structures consisting of F-actin networks result from the well-controlled incorporation of specific proteins, namely actin-binding proteins (ABPs) and actin-related proteins (ARPs), at the proper time and space. The fundamental step here is to understand what kind of ABPs and ARPs are utilized for higher ordered structure construction and the regulation of F-actin growth.

3.3.2.1. Molecular Structures of ABPs and ARPs: A variety of 2-D and 3-D actin networks can be formed from a few ABPs with unique molecular geometries that can crosslink F-actin. For instance, fimbrin has two actin-binding sites arranged side-by-side which can be used as a molecular spacer to separate two individual F-actin filaments ~12 – 14nm apart (8,113–115). Another molecular spacer that can bundle F-actin is known as α-actinin, which is a long rod-shaped molecule that is 3 – 4nm wide and 30 – 40nm in length. It has two actin binding sites arranged on each end (8,116–118). Fimbrin and α-actinin are relatively short molecular spacers when compared to spectrin. Spectrin can take the form of a tetramer with two actin binding sites on opposite ends, measuring ~10nm in width and ~150 – 200nm in length (8, 119,120). Apart from these linear molecular spacers, biological spacers with other geometries do exist. For example, filamin (121), which is ~80nm in length, has two actin-binding sites which are arranged in a flexible, V-shape geometry (8,119). Also, instead of bundling F-actin together with molecular spacers, F-actin can form branched structures with the aid of other proteins. For example, the Arp2/3 complex can form side-branched F-actin at ~70° with respect to the main F-actin branch, producing Y-branched dendrite structures (122) (see Figure 9). The structural dimensions of selected molecular components are summarized in Table 1. The data is obtained from published atomic models of the corresponding proteins and high resolution electron micrographs.

3.3.2.2. Functions of ABPs and ARPs: In addition to the construction of higher-order structures, ABPs are also responsible for regulating the dynamics of actin assembly/disassembly for the purpose of cell motility (95,123). For example, it has been shown that the process of treadmilling can be accelerated by 125 times with the synergistic effects of cofilin and profilin (95,124). Cofilin (or known as actin depolymerizing factor, ADF) can accelerate the depolymerization of the pointed-end of F-actin by forming the ADF-ADP-G-actin complex (89,104). On the other hand, profilin can specifically bind to ATP-G-actin, which in turn binds exclusively to the barbed ends of F-actin (89,104,125). It has been shown that ATP-G-actin can polymerize into F-actin more effectively than ADP-G-actin (103,104,126). Therefore, in order to polymerize F-actin more efficiently, the ADP-G-actin needs to be converted to ATP-G-actin. Profilin can accelerate this process by promoting the exchange of ADP for ATP bound to actin, and thus enhances the polymerization at the barbed-end of F-actin (8,89,95,104). Other important ABPs for cell motility are capping proteins and gelsolin. Capping proteins can bind to the barbed end of F-actin with a strong affinity (89,104), which in turn inhibits the growth of F-actin from the barbed end. As a result, F-actin without capping proteins will grow much faster than those with them. This can result in selective F-actin growth in different locations within a cell. Besides influencing the growth of F-actin, the length of F-actin can be altered by cutting a filament with specific ABPs. Gelsolin is one of the ABPs that can perform this function

(127). The F-actin cutting process is accomplished by the binding of gelsolin to the side of a long F-actin, which when cut into two halves leaves two short F-actin filaments with one featuring gelsolin capped onto its end (104,128).

3.3.3 Tubulin and Microtubules

3.3.3.1. Molecular Structures of Tubulin and Microtubules: In addition to G-actin, another protein that is able to polymerize into long filament chains under suitable growing conditions is tubulin. Tubulin exists in three different isoforms; namely α-tubulin, β-tubulin, and γ-tubulin (129). Instead of forming a long, solid linear chain-like F-actin, tubulin (in the form of the αβ-tubulin heterodimer) can polymerize into microtubules, which are hollow tube structures with 8 – 19 protofilaments (130) (the 13-protofilament configuration is the most common configuration *in vivo* (8)). The dimensions of the αβ-tubulin heterodimer are ~4.6nm ×8.0nm × 6.5nm (131,132). For the 13-protofilament microtubule, its inner and outer diameters are ~10nm and ~22nm, respectively, with wall thickness of ~5 – 6nm (130).

3.3.3.2. Mechanics of Microtubules: When compared to F-actin, microtubules are much stiffer. The measured persistence length of a microtubule ranges from 100μm to 8000μm (including pure and chemical-stabilized microtubules at temperature ranges from 22°C to 37° C) (110,133–139). The persistence length distribution for microtubules is relatively broad (~ two orders of magnitude discrepancy). These persistence length measurements may be contingent on the use of different single molecule force measurement techniques, the chemical stabilizing agents (133), the growth history of the microtubules (137), or the number of microtubule protofilaments in the specific experiments (e.g., microtubules exist in the form of 13 – 16 protofilaments with 14-protofilaments being the most common case (110,139)). However, there is still no consensus explanation for the discrepancy. Recent reports have shown that the persistence length of a microtubule is dependent on their corresponding length (138,140). Particularly, Pampaloni et al. have shown a systematic increase of persistence lengths of microtubules, from 110μm to 5035μm, as the length of the microtubules varied from 2.6μm to 47.5μm (138). From the persistence length data, we have estimated that the flexural rigidity of microtubules (Equation 8) range from $452 nN \cdot nm^2$ to $2.1 \times 10^4 nN \cdot nm^2$ (see Table 2). As long as the microtubule is sufficiently long (»21μm), the persistence length is shown to converge to ~6300μm theoretically. The underlying reason for this length dependency is suggested to be caused by the strong material anisotropy of microtubules (138).

3.3.3.3. Dynamic Instability of Microtubules: Apart from the difference in mechanical properties between F-actin and microtubules, there are a number of similarities between these two microfilament structures. First, microtubules have structural polarity with the α-tubulin end as the minus end and the β-tubulin end as the plus or fast-growing end (132). The scenario where a microtubule changes from the polymerization phase to the depolymerization phase is known as the catastrophe. The reverse process (i.e., from depolymerization phase to polymerization phase) is known as the rescue. These two processes are regulated by guanasine triphosphate (GTP) hydrolysis (as opposed to ATP hydrolysis in the case of actin polymerization). The phenomenon where the microtubule switches from catastrophe to rescue (or vice versa) is generally termed as dynamic instability (141), which is central to the process of mitosis. Similar to F-actin, there are a number of drugs (e.g., taxol (142)) and microtubule-associated proteins (MAPs, e.g., MAP2 (89)) that can affect the dynamics of microtubule polymerization and its structural functionalities. The detailed processes of how microtubules and MAPs can form higher ordered structures and regulate growth dynamics will not be addressed, but interested readers can refer to the following sources (89,141).

As mentioned earlier, in the process of mitosis the dynamic instability of microtubule assembly/ disassembly plays a central role in the separation of chromosomes. Therefore, it is important

to know the amount of force that microtubules can generate during this process. Thermodynamically speaking, the maximum pushing force available from the free energy of microtubule growth is related to tubulin association/dissociation kinetics, which can be predicted from the following equation (143–146),

$$F = \frac{kT}{d} \ln\left(\frac{k'_{on}}{k'_{off}}\right) \tag{10}$$

where d is the added microtubule length per dimer, k'_{on} is the dimer association rate, and k'_{off} is the dimer dissociation rate. Based on Equation (10), the force generated from the microtubule assembly/disassembly will be ~ 15 – 47pN for a k'_{on}/k'_{off} ratio from 10 to 1000 and d = 0.61nm (i.e., 8nm/13 protofilaments) (145). However, a recent study by Kolomeisky and Fisher has suggested that the parameter d in Equation (10) should be considered as the distance bounded by the dimer length (i.e., d = 8.0nm) instead of the one defined earlier (147). This yields good agreement with the experimental results performed by Dogterom and Yurke, who have shown the maximum force exerted by growing microtubules to be ~4pN (135). Kolomeisky and Fisher have found k'_{on} to be 1887min^{-1} and k'_{off} to be 0.33min^{-1} based on the experimental data provided by Dogterom and Yurke. This leads to estimated stall forces of ~4.3pN (d = 8.2nm was used instead of 8.0nm, Table 1) (147).

3.3.4 Molecular Motors –Myosin and Kinesin—Apart from the important role of microtubules and F-actin in powering cell movement and intracellular manipulation, these microfilament systems are utilized as “molecular railways” for motor proteins for the purpose of cell motility and intercellular transportation. Here, we are going to look into the structures and functionalities of two linear molecular motors, namely myosin (motor protein for F-actin) and kinesin (motor protein for microtubule), and their respective mechanical performances from recent single molecule measurements.

3.3.4.1. Structures and Functions of Myosin and Kinesin: Linear molecular motors, such as myosin and kinesin, can be thought of as a series of lever systems that mechanically amplify a sub-nanometer binding event into tens of nanometers of motion. Understanding the basic structures of these linear molecular motors is therefore important to gain insight on the mechanical amplification mechanism. Myosin and kinesin motor molecules are structurally similar (148). Both of them can be simply described as a composition of a head region for motion generation and an elongated tail region for load carrying or mechanical anchoring (21,94,149–153). Specifically, a conventional myosin II motor molecule is composed of three portions: S1, S2, and LMM (94,152). S1 is the head region that powers the motion of motor molecules through nucleotide hydrolysis (152). S2 and LMM are the tail regions that connect to S1 at one end with the other end connected to other molecular components for the purpose of anchoring (21,153). S1 consists of three different domains, namely the light chain binding domain, the converter domain, and the catalytic domain (21,153). The light chain binding domain can be thought of as a lever arm that connects to the converter domain and the catalytic domain. The catalytic domain consists of binding sites for nucleotides and actin (154). The binding of nucleotides and subsequent nucleotide hydrolysis can induce a conformational change of the catalytic domain, whose motion can be amplified by the light chain binding domain through the transmission of the converter domain (153,155). This mechanism is known as the swinging crossbridge model, originally proposed by H.E. Huxley (86). Thus far, eighteen different myosin molecules have been identified whose classification depends on the composition of their head and tail regions (156,157). Some of the myosins exist as a monomer form (i.e., one head region), whereas others exist in a dimer form (i.e., two head regions). For example, myosins II, V, and VI have two head regions while myosins I, III, and IV only have

one head region (21). The size of the subfragment S1 for myosin II is ~ 16.5nm × 6.5nm × 4.0nm (154). The step size of myosin is dependent on the length of the lever arm in the S1 domain (158). For example, myosin V, with an S1 length of ~31nm (159), takes a center-of-mass step of 37nm (one complete helical turn of F-actin) (160,161), whereas myosin II, with an S1 length of 16.5nm, takes a step of ~5 – 15nm (153,158,162–165). Comparatively, the motor domain of kinesin is structurally similar to that of myosin (166). The motor domain size for kinesin is ~7.0nm ×4.5nm × 4.5nm (166) and the center-of-mass step size for kinesin is ~8.3nm (167).

Interestingly, the movements of myosin and kinesin (particularly myosin V (160) and conventional kinesin (167,168)) are highly analogous to the walking motion of a human (i.e., hand-overhand) with the exception that the molecular motors can only take finite discrete steps (see Figure 10). Specifically, myosin V "walks" on the helical repeat of the F-actin (160,161) whereas kinesin "walks" strictly on a single microtubule protofilament (169). In particular, the center-of-mass step sizes for kinesin and myosin V are 8.3nm and 37nm, respectively (160, 167). Both of them are plus-end directed motors on their respective microfilament system. On the other hand, myosin VI is a minus-end directed motor that takes a 11nm step towards the plus-end and a 27nm step towards the minus-end (170).

3.3.4.2. ATP as a Fuel: ATP hydrolysis is the chemical energy source that powers the mechanical motion of myosin and kinesin on their corresponding "molecular tracks". In the chemical reaction of ATP hydrolysis, ATP is converted to ADP and phosphate ions which can be reversible depending on the chemical environment of the surrounding media (21). The energy released through this process is ~54×10^{-21}J (or 54pN·nm which is equivalent to ~13kT) when at 298K, pH = 7, a concentration of free magnesium ions of 10mM, and an ionic strength of 0.25M (171). However, the actual free energy released may be higher than this value depending on the concentration of the respective species in the hydrolysis reaction. Nor mally speaking, 20kT (or 80pN·nm) is commonly assumed for ATP hydrolysis in the literature (21,172). The mechanical and chemical energy exchange by myosin and kinesin is highly coupled during the "walking" motion. The ATP binding and the hydrolysis process dictates the attachment and detachment of the molecular motors to their respective "molecular tracks". In the case of myosin in the presence of actin, phosphate ions are released from the myosin when it binds to the actin (i.e., with myosin-ADP attaching to the actin). When the ATP binds to the myosin, it will be detached from the actin by the conformational change induced by the binding (153,161,173). On the other hand, kinesin takes a different route in achieving this mechanochemical energy cycle. When the kinesin binds to the microtubule, ADP will be released and ATP hydrolysis is required for the detachment of kinesin from the microtubule (21,151).

3.3.4.3. Mechanical Performances of Myosin and Kinesin: Similar to macroscopic motor systems, we are interested in the mechanical performance of linear molecular motors in terms of speed, force generation, and energy efficiency. Since the linear molecular motors "walk" on "molecular tracks" (see Figure 10) through ATP hydrolysis, the quantification of their mechanical performance can be specified by the walking speed, the stall force, and the energy efficiency of ATP-to-mechanical energy coupling.

Depending on the nature of the molecular motors (e.g., number of head regions), they may or may not stay on the track permanently (e.g., two-headed kinesin will more likely remain on its track than one-headed kinesin (174)). Processivity is the term that describes whether a motor can continuously "walk" on the "molecular track" without detachment for many ATP hydrolysis cycles. A processive motor can travel for a long distance (compared to the cellular length scale, i.e., ~ μm) before detachment from the "molecular track". For example, myosin V and VI are processive motors which can travel a distance ranging from a few hundred

nanometers to a micron on F-actin before detachment (160,170). Conventional kinesin is another processive motor that can travel on the order of a micrometer before detachment from the microtubule, which is equivalent to ~100 steps or more (175,176). As a general reference, the *in vitro* speeds for myosin motors (i.e., Myosin IB, II, V, VI, XI) are ~ −6 – 60000nm/s while the *in vitro* speeds for kinesin motors (i.e., conventional kinesin, Nkin, Unc104/KIF, Fla10/KinII, BimC/Eg5 and Ncd) are ~ −90 – 1800nm/s (21). The forces generated by individual motor molecules have been quantified through single molecule optical nanometry measurements. For example, recent studies have shown that the stall force associated with a kinesin molecule can be up to 5 – 7pN at saturated ATP concentrations (177–179) and for myosin II, V, and VI, the stall force is on the order of ~3 – 4pN (165,170,180). A striking universal trend for molecular motors and macroscopic motors has recently been discovered which shows that the maximum force output of those molecular motors scale as two-thirds power of their mass (181). This scaling law may allow us to predict the maximum force output for a variety of yet unmeasured linear molecular motors.

In regards to the energy consumption of molecular motors, it has been shown that kinesin hydrolyses one ATP per 8nm under low load conditions (182,183). For a ball-park value estimation, assuming the kinesin motor can generate a force of 5 – 7pN throughout this 8nm step while consuming 1 ATP during the process, the mechanical energy consumed is ~40 – 56pN·nm. Comparing this energy consumption to the energy released by ATP hydrolysis (i.e., ~80pN·nm), one will appreciate the excellent energy conversion efficiency of those molecular motors (i.e., energy efficiency ~50 – 70%) (172).

A nicely complied table of the mechanical performance of motor proteins has previously been published by Howard (21). To augment the table, we have included additional mechanical parameters, such as step size, speed, and force generation of selected motor proteins obtained from recent single molecule measurements for general references in addition to those for a synthetic linear motor molecule to be used for comparison (see Table 3).

Thus far, we have discussed the properties of a few natural molecular components and their respective utilization for engineering applications. To incorporate them further into top-down fabricated structures, strategies to immobilize them specifically on a solid surface have to be developed. In the next section, we will provide a brief review on the current state-of-the-art technologies for interfacing these molecular components on a solid surface with high specificity.

4 Patterning Technologies for Guiding Molecular Growth

Specific placement of molecular components on a substrate is a pre-requisite towards achieving the construction of higher-order structures. Doing so with molecular precision requires length-scale matching with the individual binding sites. Immobilizing molecular components at lithographically defined locations is an integrated top-down and bottom-up process. In the past decades, the quest of the semiconductor industry to maximize the packing of circuit components on a single chip has pushed the capabilities of micro and nanolithography technologies forward. These technological advancements have been the cornerstone for the maturity of Micro-Electro-Mechanical Systems and the emergence of bio-nanotechnology.

The goal for all lithography technologies is to transfer predefined patterns onto a new substrate (i.e., replication). Although a variety of lithography technologies have been developed over the past decade (184–192), three make up the majority of the approaches used to achieve the end goal of pattern transfer. The first one, which is the most widely employed, is based on irradiation through a lithography mask. This process can be summarized as follows: 1) Coating of a radiation sensitive layer (RSL) on a substrate; 2) Image transfer of the lithography mask patterns to the RSL by irradiation; and 3) Pattern development of the image on the RSL by

selective etching (see Figure 11a). The second method is known as directwrite patterning, where no mask is required for the pattern transfer. In this approach, an energy beam is projected on the RSL surface to directly write the patterns. The written patterns are then developed by selective etching (see Figure 11b). A derivative of this method substitutes the energy beam for a mechanical probe. This is used to engrave a thin coating (normally it is a single layer of self-assembled molecules) to create patterns (see Figure 11c). This technique does not require subsequent selective etching. The third method is known as stamping. Here, a stamp, normally made of polymeric materials, is fabricated using the lithography approaches mentioned earlier. The stamp is then inked with the target molecules and transferred onto a substrate (see Figure 11d). In the following, we will briefly overview how molecular components can be patterned at a specific location on a substrate through a combination of the lithography technologies.

4.1 Patterning of Inorganic Crystal Structures

Natural organisms have the ability to control the formation of inorganic crystal structures with precise spatial dimensions at cellular and sub-cellular levels. An example is the magnetite nanocrystals existing in magnetotactic bacteria. These magnetite nanocrystals, which are about 50nm in dimension and precisely arranged with nanometer resolution, are utilized as a biological “compass” for the bacteria to navigate (4). Reproducing these natural functional crystal structures *in vitro* poses a great challenge to those in the material science and engineering disciplines.

4.1.1 Control of Growth Locations—In order to achieve the eventual goal of synthesizing these functional natural crystals, three primary steps need to be addressed: precise spatial patterning of crystals, size control of the crystals, and the control of crystal structural orientation. To pattern inorganic structures on a solid substrate, one existing approach utilizes surface hydrophobicity to locally trap liquids with dissolved inorganic ions on a substrate. Since the inorganic ions will self-assemble as the solvent evaporates, the patterning of the structure synthesis location becomes reliant on the final location of the solvent. There are a variety of methods to pattern a surface with spatial varying hydrophobicity (193–196). For example, hydrophobic molecules, such as CH_3-terminated alkanethiols, can be patterned on a gold surface through microcontact printing while the rest of the area is passivated by hydrophilic molecules, such as COOH-terminated alkanethiols, thereby creating hydrophilic and hydrophobic patterns (193). Another approach is to deposit a layer of hydrophobic molecules (e.g., hexamethyldisilazane) on a hydrophilic surface (e.g., Si/SiO_2). By the patterning (either by optical/electron beam lithography) and subsequent etching of the molecules, a surface of hydrophilic and hydrophobic regions can be created (196) (see Figure 12).

4.1.2 Control of Crystal Sizes—Apart from controlling the spatial location of the structure synthesis, the size of the structures can be controlled through manipulating the ionic concentration or volume of liquid being trapped on the hydrophilic area (193) or confining nanostructures (197). Recent demonstrations have shown that a confined liquid on the order of zeptoliters (10^{-21}L) can be trapped for the synthesis of inorganic structures on the order of 10nm (196,197) (see Figure 12). Thus far, the above mentioned techniques (198) have been demonstrated for the synthesis of simple inorganic crystals (194,196,197), quantum dots (193), magnetic nanoparticles (195) and colloidal nanoparticle assembly (199,200).

4.1.3 Control of Crystallographic Planes—In addition to patterning of inorganic crystals with controlled size and location, the structural orientation of these crystals can be controlled as well. Earlier crystallization studies have shown that the crystallographic plane is dictated by the structural information provided by a monolayer of molecules formed at the air/liquid interface (201–203) or deposited on a solid surface (204). This rationale argues that the

monolayer of molecules provides a structural support for the continuation of crystalline growth in a particular crystallographic plane due to the matching of their respective atomic arrangements (202). By controlling the density and the type of molecules used for the monolayer, the desired crystallographic plane of the crystal can be induced. More elaborate explanations on the underlying mechanisms of crystal orientation control have been provided in a review article by Mann (202).

Incorporating this strategy for controlling the structural orientation of crystals in conjunction with microfabrication technologies, researchers have demonstrated the complete control of the location, size, and crystallographic plane of a growing crystal on a solid substrate on the microscale domain. In particular, Aizenberg et al. (29) have demonstrated the control of crystallographic plane orientations of grown crystals, as well as the crystal nucleation locations and number densities, through a self-assembled monolayer of molecules patterned by micro-contact printing. In their work, a self-assembled monolayer of $HS(CH_2)_{15}X$ (where X = CO_2H, SO_3H, OH) was stamped on a gold/silver-coated silicon surface with an elastomer stamp while the remaining area was passivated by a self-assembled monolayer of $HS(CH_2)_{15}CH_3$. The chip was immersed in a crystallization solution (for the growth of $CaCO_3$) where the regions terminated by the X group (which will subsequently be ionized in the solution) attracted Ca^{2+} ions and induced crystal growth. Through the use of different terminal groups, a variety of crystal orientations of calcium carbonate have been successfully induced and patterned with controlled size and location (see Figure 13).

4.2 Patterning of DNA Molecules

From the earlier discussion, DNA can be utilized as a programmable material to construct static (e.g., 2D and 3D structures) and dynamic structures (e.g., DNA nanomachine). For each of these examples, the structures are synthesized in a bulk solution without defined physical confinements on a solid surface. Unfortunately, this characteristic prohibits their incorporation with other molecular components for higher ordered functions, which is a necessary requirement for the production of useful structures. In the past years, technologies for patterning DNA molecules on a solid surface have been established through the development of highly sensitive DNA detection systems (205). In the following, we will sample through some of the recent developments of DNA patterning techniques by a variety of lithography technologies.

4.2.1 Physical Adsorption—The phosphate backbone of DNA results in the molecule possessing a negative charge in physiological conditions. By controlling the surface charge density of a substrate through external radiation, DNA molecules can be physically absorbed on a surface through electrostatic interactions. For instance, Chi et al. utilized electron beam energy to create positively charged regions on a glass surface to electrostatically trap DNA molecules. The technique is capable of generating DNA line patterns down to 50nm (206). In addition, the use of micromolding in capillaries (MIMIC) (207) can physically confine the deposition of DNA molecules on a solid surface. Specifically, Bystrenova et al. (208) demonstrated the use of the MIMIC technique to pattern DNA molecules in continuous strips or ordered dot arrays through the control of the concentration of DNA in a liquid medium. Another approach used to define DNA molecules specifically on a surface through physical adsorption is surface dewetting and condensation on a heterogeneous patterned surface (209). The concept of this technique is similar to that of confining inorganic crystals on a patterned hydrophilic/hydrophobic surface.

4.2.2 Molecular Combing—Patterning DNA molecules through physical adsorption yields randomly aligned DNA structures on a surface. External force fields are required to align and orient DNA molecules in a controlled manner. A technique called molecular combing was

developed in the mid-90s, which is capable of stretching and orienting DNA molecules on a solid surface by utilizing the surface tension forces produced by a receding meniscus to manipulate DNA (210,211). While the DNA is bound on a surface at one end, the meniscus stretches the molecule to its full contour length. By controlling the shape of the liquid/air interface through the use of a microfluidic channel, micropatterns of fully stretched and oriented DNA molecules can be created through molecular combing (212). However, in this method, DNA molecules were patterned inside a microfluidic channel, which may hinder the patterning of additional molecular components if needed. Instead, it is desirable to create patterned DNA molecules on a solid surface without any physical confinement. For instance, Björk et al. recently developed a soft lithography technique combined with molecular combing to create patterned, stretched, and oriented DNA molecules on a solid surface (213). In one of their methods, patterns of hydrophobic and hydrophilic regions were created on a substrate through PDMS stamping allowing DNA molecules to be stretched and aligned exclusively in the hydrophobic region (see Figure 14).

4.2.3 Surface Chemistry and Ligand-pair Binding—Apart from physically adsorbing DNA molecules onto a surface, they can be chemically grafted onto a surface through specific surface chemistry or ligand-pair binding. Chemically bound DNA molecules on a surface are more stable than those immobilized through physical adsorption by electrostatic interactions. Silane (214–216) and thiol (214,217) chemistries are commonly used as chemically functionalization agents to specifically bound DNA to a surface. Particularly, patterning of DNA molecules utilizing chemically functionalization schemes have been demonstrated through a variety of lithography approaches such as electron beam lithography (215,216), optical lithography (218), and dip-pen lithography (214). On the other hand, ligand-pairs such as streptavidin and biotin have been utilized for DNA binding to a surface (219). Specific details on the nature of streptavidin and biotin binding will be given in the later section.

4.2.4 DNA as Molecular Glue—In addition to binding the native form of DNA specifically on a surface, DNA molecules have been utilized as “molecular glue” to assemble nanoparticles at a specific location. For example, in the work of Städler et al. (219), single strands of biotinylated DNA were specifically fixed to a surface through streptavidinbiotin interactions. When irradiated by light, the fluorescence molecules attached to the streptavidin molecules generate singlet oxygen that locally damages the DNA molecules. By patterning a DNA-bound surface with light, regions of DNA that were irradiated by light were damaged. Nanoparticles that are tagged with complementary DNA molecules can then be specifically attached to the regions where the DNA molecules were not damaged. In addition, Kannan et al. have utilized the silane chemistry functionalization scheme and demonstrated the assembly of multi-layered nanoparticles through using DNA molecules as the molecular linker (220). These demonstrations have shown that DNA molecules can be used to self-assemble nanostructures to higher-order dimensions.

Other than assembling nanoparticles with DNA molecules, biological entities such as cells can be surface functionalized with DNA to achieve specific adhesion on a surface. Particularly, Chandra et al. have developed a surface chemistry scheme to modify the surfaces of live cells with ssDNA, which can subsequently be attached to a surface patterned with their complementary DNA sequences (221). Owing to the unique programmable capability of DNA molecules, the establishment of the chemistry has laid down an important foundation for the precision patterning of multiple types of cells on a surface.

4.3 Patterning of Cytoskeleton and Motor Proteins

With the promise of ultra-sensitive biomedical diagnostics (222,223), the use of lithography technologies to define the locations of proteins on micro and nanoscale domains have recently

garnered significant attention in the area of bioMEMS and bionanotechnology. Conveniently, the same technologies allow for the specific placement of functional protein molecules (e.g., actin and myosin) for structure construction on the micro/nanoscale domain. Specifically, patterning of cytoskeleton and motor proteins at specific locations ensures directed transportation of molecular cargo. In this section, we will sample through some of the recent developments in defining cytoskeleton and motor proteins on a solid surface in both two-dimensional space, as well as the controlled orientations of cytoskeleton proteins for three-dimensional construction. In addition, technologies that can define multiple proteins with high spatial resolution on a substrate will be discussed. For comprehensive reviews on the use of lithography technologies to pattern proteins on the micro and nanoscale domain, readers can refer to review articles by Blawas and Reichert (224), Kane et al. (225), and Christman et al. (223).

4.3.1 Physical Adsorption—Similar to the surface binding of DNA, attaching proteins to a surface can be approached by either physical adsorption or chemically binding, which is achieved via specific surface chemistry or ligand-pair binding. In the case of physical adsorption, proteins, due to their multivalent nature in physiological conditions, can attach to surfaces that possess surface charges through electrostatic, hydrophobic, or van der Waals' interactions (224). These physical interactions are the main cause for non-specific binding. Therefore, in order for high specificity protein patterning to occur in the case where each element possess opposite charges, an intermediate layer (e.g., poly(ethylene glycol) (226)) must exist to shield the charges from each other, thereby preventing non-specific physical interactions. The patterning of this intermediate layer centers on leaving portions of the surface exposed, which allow for protein attachment. For example, Wong et al. recently developed a technique based on capillary force lithography (227) to pattern a self-assembled monolayer of poly(ethylene glycol) on a Si/SiO_2 surface for specific protein patterning (228). The resultant patterning has been utilized for supporting actin polymerization from the patterned locations (229,230).

For the case where the proteins and the surface possess the same charge, patterning of the proteins can be achieved by first patterning an intermediate layer which possesses the opposite charge. The proteins can then be attached to the intermediate layer electrostatically. For example, Yokokawa et al. has devised a method combining soft lithography with microfluidics to achieve specific patterning of microtubules on a glass surface (231). In this approach, arrays of microfluidic channels (10 – 100μm wide and 50μm depth) were fabricated using a PDMS molding technique. After the PDMS mold was created, it was then attached to a glass surface. Subsequently, a Poly-L-Lysine (PLL) solution was flowed into the channels. Microtubules, because of their negative surface charge in physiological conditions (232), do not have a strong affinity to the negatively charged glass surface. Therefore, PLL was used as an adhesion layer between the microtubules and glass substrate. As a result, microtubules bound to those areas patterned with PLL specifically. In this technique, the location of the microtubules was confined, but the polarity of the "molecular railways", which dictates the movement of the molecular motors, was still randomly distributed on the PLL patterns.

Even with the above techniques, non-specific binding of proteins may still occur (i.e., on non-patterned areas). One way to circumvent the problem is to cover up the non-patterned area with a sacrificial layer and then remove this layer after the proteins are deposited. For example, Atsuta et al. have demonstrated the patterning of motor proteins using a PDMS molding technique (233). In their work, a perforated PDMS sheet was made and attached against a glass substrate. A solution of proteins was then poured into the PDMS sieve. The number of molecules being patterned is dependent on the size of the sieve, which can be controlled from ~2μm to ~10μm. After rinsing the excessive amount of protein solution, the PDMS sieve was peeled off within an aqueous environment. Based on this technique, they have demonstrated

the patterning of arrays of F_1-ATPase (a rotary molecular motor), which were still functional after the patterning.

The previously discussed techniques are based on soft lithography in conjunction with microfluidic approaches. One drawback of such methods is the fact that multi-layer alignments can become an issue as more complex structures are built. For example, if one wants to pattern motor proteins specifically in between patterned electrodes with a tight tolerance, high resolution alignment is required. In general, resolution for multi-PDMS alignment can only approach ~10μm (234). Therefore, it is desirable for conventional lithography technology (e.g., optical lithography) to be used to define the "molecular tracks". Specifically, Yoshida et al. recently developed a parylene lift-off technique to pattern cytoskeleton and motor proteins (235). In their technique, a glass substrate was first coated with bovine serum albumin (BSA) followed by the deposition of parylene C polymer. The purpose of the BSA was to reduce the adhesion between the polymer and the glass substrate for the purpose of the subsequent release. Then the parylene C was lithography defined and etched to bring forth the patterns. Solutions of cytoskeleton proteins, such as microtubules, and motor proteins, such as kinesin, were then injected on top of the patterns and incubated for a period of time. Finally, the parylene polymer was peeled off and the patterned proteins remained in the patterned area. This technique may also be used to specifically create patterns within microfluidic channels due to the conformality of the parylene coating.

4.3.2 Surface Chemistry and Ligand-pair Binding

4.3.2.1. Patterning of Single Type of Protein on Surfaces: After going through examples of patterning cytoskeleton and motor proteins through physical adsorption, we will shift our focus into the patterning of proteins through chemical binding schemes, that are comprised of specific surface chemistry and ligand-pair binding. In general, attaching proteins to a surface through chemical means ensures a more stable immobilization of the proteins on a surface. For example, proteins can specifically bind to a surface through covalent bonds using bi-functional cross-linkers (e.g., silane chemistry) that bind to the surface on one-end and to the proteins on the other (224). In addition, proteins can be linked to a chemically functionalized surface through high affinity ligand pairs. A well-known example of such ligand pairs is streptavidin/avidin and biotin. Although the interaction between biotin/avidin-streptavidin is non-covalent, their bond strengths are relatively strong. Early single molecule measurements revealed that the unbinding forces for biotin-streptavidin and biotin-avidin are ~260pN and ~160pN, respectively with rupture lengths of ~1nm (101,236). More recent loading rate studies (237, 238) have produced unbinding force values for streptavidin/avidin-biotin interactions to range from 5pN to 170pN for loading rates from ~1pN/s to 10^5pN/s (237). As a ball-park value estimation using the bond characteristics from these studies, an interaction energy of ~6.5kT was calculated. The nature of the bonding is attributed to the formation of hydrogen bonding networks and van der Waals' interactions (239,240).

To utilize these interactions for anchoring proteins on a surface, one approach is to functionalize the surface with specific chemicals that can be activated through external energy excitation (e.g., chemical (241), photon (242) or electron (230,243)). After the surface functionalization, biotin/biotinylated compounds can be attached to these activated surfaces. Streptavidin/avidin is added as an intermediate binding layer on top of the biotin/biotinylated compounds. Then the proteins that are modified with biotin (or so called biotinylated proteins) can be attached to this streptavidin/avidin intermediate layer to achieve specific binding (230,243,244). For example, Christman et al. have developed a technique based on optical lithography to generate two-dimensional protein patterns utilizing photo- and pH-responsive polymers. The activation of the polymer generated aldehyde functional groups, which can subsequently be used to attach proteins through biotin/streptavidin interactions (242,245) (see Figure 15).

Along the same vein, chemical functionalized surfaces have been utilized for the patterning of cytoskeleton and motor proteins via streptavidin and biotin interactions. For example, Romet-Lemonne et al. have devised a method to pattern kinesin motor molecules on the sidewall of a microfabricated chamber for the end goal of mimicking cellular mitotic processes (241). In their approach, gold metal lines were patterned on the sidewalls of a channel. Self-assembled monolayers of chemical functionalized thiols were deposited on the gold metal lines and subsequently functionalized with biotin. Multi-layers of proteins (e.g., bovine serum albumin) were then attached to the functionalized surface through a series of streptavidin and biotin interactions as discussed. These intermediate layers of proteins were added to enhance the motor functions. Finally, biotinylated kinesins were attached to these intermediate layers of proteins. The kinesins were proven to support the transportation of microtubules along the sidewall of the microfabricated chamber after these patterning steps.

In the above examples, although the physical locations of the proteins are specifically defined, the orientations of the proteins cannot be precisely controlled. As discussed, certain proteins, such as actin and tubulin, have functional polarities and the ability to define their orientation as well as their physical location on a surface ensures the desired directional assembly. Fortunately, those proteins, such as actin, have associative proteins (i.e., actin-binding proteins) that can be used to define their functional orientation. By patterning these associative proteins, the functional orientation of the respective proteins can be controlled accordingly. For example, Huang et al. (244), and Brough and Christman et al. (230) have individually demonstrated patterned growth of F-actin with controlled functional polarity through the use of gelsolin on the microscale and nanoscale domains, respectively. In the work of Huang et al. (244), a self-assembled monolayer of methyl-terminated 1-octadecanethiol and amineterminated cysteamine was deposited onto a thin layer of gold-covered glass through microcontact printing, which was subsequently treated with biotinylated compounds. The biotinylated gelsolinactin complexes were then bound to the microscale patterned surface through an intermediate streptavidin layer. Using a different surface functionalization scheme via the use of electron beam lithography, Brough and Christman et al. have demonstrated controlled growth of F-actin down to the single filament level on a nanopatterned surface (230) (see Figure 16). Together with the ability to pattern cytoskeleton proteins in two-dimensional space, the above demonstrations have moved one step closer to the possibility of building true three-dimensional structures utilizing cytoskeleton proteins.

4.3.2.2. Patterning of Multiple Types of Proteins on Surfaces: For the examples discussed thus far, only one type of protein can be patterned on a surface. The ability to pattern multiple functional proteins on a surface at the cellular or sub-cellular length scale allows different biological or mechanical properties to be explored (246). For example, two types of motor proteins within the same motor family that are patterned in close proximity, may be exploited for higher ordered mechanical functions (e.g., bidirectional transportation) (247,248). Lithography technologies, such as optical lithography (249,250), dip-pen lithography (251), and soft lithography (252), have been utilized to define two or more types of proteins (or the same protein with different fluorescent labels) on the micro and nanoscale.

Clearly, it will be advantageous if we can make use of the conventional MEMS/nanofabrication technologies (e.g., optical lithography and electron beam lithography) to pattern multiple proteins in the same way as done for silicon based processing. To achieve this purpose, understanding the biocompatibility of the chemicals used in conventional MEMS/nanofabrication is paramount. In particular, Verma et al. have carried out systematic studies on the effects of conventional micro- and nanofabrication processing chemicals and resists on the functionality of casein, kinesin, and microtubules through motility assays (253). They found that casein and kinesin are tolerant to most of the processing chemicals examined (e.g., organic solvents: isopropanol alcohol (IPA) and acetone; developers: methyl isobutyl ketone (MIBK)

and tetramethylammonium hydroxide (TMAH)), while microtubules are only stable in diluted organic solvents. Additionally, they found that UV light exposure (source: mercury lamp, power output density: 12mW/cm^2) for 10 min or shorter does not affect the functionality of the kinesin motors. However, more thorough investigations are required before we can utilize conventional MEMS/nanofabrication technologies to pattern multiple types of cytoskeleton and motor proteins on a surface.

The use of a non-lithographic approach to achieve multiple protein patterning has recently been investigated as well. A new technique called diffusion-limited patterning (DLP) (254) has demonstrated the concept of patterning multiple proteins inside a confined nanofluidic environment through molecular diffusion. Before we continue the discussion on this specific type of patterning technology, the fundamentals of diffusion is presented to gain better insight. From the molecular viewpoint of diffusion, each individual molecule in solution has a certain amount of thermal energy (i.e., kT) which translates into kinetic motion. In a solution where the solute and solvent molecules co-exist, the thermal agitation causes the solute molecules bombarding constantly by the surrounding solvent molecules, resulting in irregular and random motion known as Brownian motion. The diffusion path for a molecule traveling due to this random motion can be represented by (255),

$$\Delta^2 = 2D\tau \tag{11}$$

where Δ is the square root of the mean of the square of the displacement of the molecule, D is the diffusion coefficient, and τ is the time for which the molecule has traveled.

DLP technology (254) exploits the time-controlled diffusion of molecular species, which subsequently react and attach on the functionalized surfaces of a fluidic channel. The molecules can only access the surface/substrate through the entrance of the channels and the reaction between the molecules and the surface is irreversible (e.g., streptavidin-biotin interactions) such that once the molecules are bound to the surface, they will not be detached. For example, assume that there are three types of molecules, A, B and C, that have been functionalized in a way such that they will bind specifically to the functionalized surface of micro/nanofluidic channels. First, molecule A is allowed to diffuse into the channel due to the established concentration gradient which results in it coating the surface. By monitoring the time of diffusion (see Equation 11), the total coverage of molecule A can be controlled. Molecule B is then allowed to diffuse into the same channel. Since the entrance portion of the channel is already coated with molecule A, molecule B cannot interact with the surface and consequently, molecule B must be allowed to diffuse further downstream until it finds a location where surface functionalization can occur. This process is then repeated for molecule C. By doing so, multiple molecular components can be patterned on the side walls of the channel and on the solid substrate (see Figure 17).

Unlike the simple diffusion of molecules, the diffusion constant (see Equation 11) for this type of diffusion-reaction system is a function of the channel geometry, surface density of the binding molecules, and the concentration and diffusion constants of the diffusing molecular species. In addition, the resolution of the DLP technique can be controlled by channel geometry, association rate constant of the binding reaction, diffusivity of the molecules, and the surface binding density. Karnik et al. achieved patterning resolution of ~1μm in a nanofluidic channel (~35nm high, 3.5μm wide and 120μm long) using this DLP technique (254). The time scale of the DLP is a function of the diffusion constant of the molecules, the channel geometries, surface binding density, and concentration of the molecules at the entrance of the channel. According to the experimental data provided by Karnik et al., the time scale required to pattern 1mg/ml of streptavidin into ~25μm of a nanofluidic channel is ~30min. This technology can

potentially be useful for the patterning of multiple cytoskeleton and motor proteins in a confined area.

So far we have discussed how natural molecular components can be immobilized on a surface with high specificity through either physical confinement or chemical binding. As discussed earlier in Section 2, the self-assembly process of these natural molecular components are dictated by shortrange forces whose effective ranges are less than 100nm. In order to initiate any form of self assembly process on a binding surface, these molecular components need to be transported from a farfield region to a region close to the binding surface for the short-range forces to take over. In the next section, we will discuss the technologies that are capable to transport the molecules from the bulk fluid to the surface binding area for the initiation of self-assembling process.

5 Technologies for Fluidic Manipulation and Molecular Transportation

Effective construction of molecular components at pre-defined locations relies on the active transport of molecular components from a bulk fluid to a desired specific binding location on a solid surface. In the previous section, we have discussed some of the available technologies for the patterning of molecular components on a solid surface. Now we are ready to study how molecular components can be transported and spatially distributed in an active and controlled manner. Specifically, we will study two different types of transportation mechanisms: namely bulk molecular transportation through electrokinetic forces and single molecular transportation through the use of cytoskeleton and motor proteins.

5.1 Bulk Molecular Transport by Electrokinetic Forces

Bulk molecular transport by pure diffusion is unidirectional (i.e., from high concentration to low concentration) which means it will be difficult to manipulate and maintain the spatial distribution of the molecules (or local concentration) inside a liquid medium. The control of the spatial distribution of molecules is beneficial in guiding the self-assembly process to occur at pre-defined locations. However, diffusion alone will not be optimally effective in achieving this purpose. On the other hand, electrokinetic force fields have been shown to have the ability to generate short range forces (for particle manipulation) and long range forces (for bulk fluidic manipulation) by simply changing the operating parameters of the electric fields. Consequently, their abilities to control the spatial distribution of molecules in bulk fluids have been widely employed in various micro/nano engineering systems. In the following section, we will briefly review the theoretical background for some of these electrokinetic forces, followed by samples of recent developments utilizing these force fields for engineering applications.

5.1.1 DC Electrokinetics

5.1.1.1. Electrophoresis and Electroosmosis -Theory: Electrokinetic-based manipulation can be broadly categorized into DC electrokinetics and AC electrokinetics. Electrophoresis and electro-osmosis are examples of DC electrokinetics. The physical phenomenon known as electrophoresis occurs when a DC electric potential is applied, causing charged molecules to move, according to their polarity, in the direction of the electric field. The force, $\vec{F}_e$, exerted on the charged molecules under the influence of the electric field, $\vec{E}$, can be expressed as,

$$\vec{F}_e = q\vec{E} \tag{12}$$

where q is the charge of the molecules. Equation (12) indicates that the force generated on positively-charged molecules will be in the same direction as the applied electric field, which

means that these molecules will migrate towards the negative electrode. On the other hand, electroosmosis is the physical phenomenon where charged molecules at the solid-liquid interface move under the influence of an electric field. This results in the translation of neutral molecules (or solvent molecules) by viscous drag and initiates bulk fluid motion. The formation of the charged molecules at the solid-liquid interface, or so called diffuse electric double layer, is therefore the driving force behind this physical phenomenon. This electric double layer can be formed through the ionization or dissociation of surface chemical groups (e.g., at the proper pH of the medium, the following reactions will occur on the surface of glass immersed in water, $\text{Si-O-H} \rightarrow \text{Si-O}^- + \text{H}^+$ or $\text{Si} - \text{OH} + \text{H}^+ \rightarrow \text{SiOH}_2^+$) and the absorption of ions from the solution. The characteristic length, or so called Debye length (λ), of this double layer can be expressed as (16, 256),

$$\kappa = \frac{1}{\lambda} = \sqrt{\sum_i \frac{\rho_{\infty i} q_e^2 z_i^2}{\varepsilon \varepsilon_0 k T}} \tag{13}$$

where $\rho_{\infty i}$ is the ionic concentration of ions, i, in the bulk, q_e is the electron charge, and z_i is the valency of the ions. Notice that the Debye length varies inversely to the ionic concentration of the medium (i.e., Debye length increases with decreasing ionic concentration). Normally the range of the Debye length is on the order of 1nm up to 100nm depending on the ionic concentration of solution. On the other hand, it is important to know the relationship between the electroosmotic velocity of the bulk flow and the applied electric field. This can be represented by the Helmholtz- Smoluchowski equation (256),

$$V_{\text{HS}} = -\frac{\zeta \varepsilon \varepsilon_0}{\nu} E_x \tag{14}$$

where V_{HS} is the electroosmotic velocity, E_x is the one-dimensional electric field, ν is the viscosity of the fluid, and ξ is the zeta potential which is a function of the charge distribution in the diffuse electric double layer. The creation of this electroosmotic bulk flow can move the embedded molecules depending on the direction of the electric field.

5.1.1.2. Electrophoresis and Electroosmosis – Engineering Applications: The use of electrophoretic and electro-osmotic force fields to separate molecules and particles in capillary channels has developed into an important analytical technology in the fields of chemistry and biology since its first perception in the early 1980s (257). Pioneering work for the implementation of capillary electrophoresis in microfluidic channels in the early 1990s (258) has sparked the interest of scientific communities to push the technology towards further maturation and closer to the realization of micro-total-analysis-systems (259–266).

The use of these types of electrokinetic mechanisms exploits the different mobility of molecular species or particles under the influence of electric fields in a fluid medium for the purpose of molecular separation (see Equation 14). The molecules/particles can be well separated into sub-populations based on their own electrophoretic mobility, which can then be transported or manipulated into different regions of the fluidic channels (see Figure 18). The use of these electrokinetic force fields in microfluidic channels can achieve high resolution size specificity, high speed, and high throughput separation. For example, earlier work on DNA sequencing (267, 268) has shown that DNA fragments of 70 to 1000bp can be separated in 120 seconds in a microfluidic channel measuring 3.5cm long and ~100μm wide (267). Besides DNA molecules, molecular species such as peptides and proteins (269) and biological particles such as viruses, bacteria, and eukaryotic cells (270) have been successfully transported and analyzed

in these systems. Since this subject matter is relatively well-studied, interested readers can refer to review articles by Bousse et al. (271) and Erickson and Li (272) for the recent developments.

In addition to the use of electrophoresis and electroosmosis in a microfluidic channel for bulk molecular transport, researchers have recently investigated the use of electrokinetics in a nanofluidic channel for the transport of molecular species. In an ionic medium inside a microfluidic channel, charged ions accumulate on the surface while leaving the overall charge in the bulk to be neutral (since the channel dimension is much greater than the Debye length). In this case, electric field manipulation of the ionic species can only be effective on the surface. However, when one of the channel dimensions is comparable to the Debye length (i.e., 1 – 100nm depending on the ionic conditions of the medium), the electric field can now be effective not only on the surface, but also in the bulk (within the channel), which allows direct electric manipulation of the ionic species. Specifically, Karnik et al. has exploited this length scale matching of Debye length (see Equation 13) and the characteristic length of the nanofluidic channel to create a new type of transportation mechanism, which was termed as a nanofluidic transistor (273, 274).

In the work of Karnik et al. (273), two types of nanofluidic confinements, namely two-dimensional silicon dioxide nanochannels (30–40nm height and 1μm wide) and one-dimensional silicon dioxide nanotubes (10–100nm internal diameter), have been fabricated to exploit the concept of a nanofluidic transistor. Analogous to a conventional semiconductor transistor, the nanofluidic device consists of source, gate, and drain components where the source and drain components are the microchannel reservoirs for the molecular/ionic species and the gate component consists of the nanofluidic confinements with external bias control through the silicon dioxide dielectric layer. Without a bias voltage, the transportation of the molecules is highly contingent on the ionic concentration due to its influence on the Debye length (see Equation 13). For example, when a negatively charged dye was introduced into the confinement, the fluorescence intensity at low salt concentrations was one-tenth of that at high salt concentrations (owing to the pH insensitivity of the dye, there is a direct correlation between the amount of dye molecules to fluorescence intensity). With the appropriate bias voltages (both on the gate, source and drain), molecules such as ions and 30-base ssDNA can successfully pass through the confinement at a controlled concentration.

Upon the successful demonstration of electrostatic control of ions and DNA molecules using the nanofluidic transistor, the same research group has recently achieved the transport of proteins (i.e., avidin) using a modified nanofluidic transistor (274) (See Figure 19). Together, the nanofluidic transistor will be a useful technology to regulate and transport molecular components to the desired region on a substrate with high temporal and spatial control.

5.1.2 AC Electrokinetics

5.1.2.1. Dielectrophoresis – Theory: Thus far we have discussed the manipulation of charged molecules by DC electric fields in a liquid medium through electrophoresis and the induction of one dimensional bulk fluid flow through electroosmosis. Similar effects can be obtained by using AC electric fields. For instance, instead of being restricted to only moving charged molecules, neutral molecules in a liquid medium can be manipulated through dielectrophoresis. Simply put, dielectrophoresis is the movement of polarizable molecules under inhomogeneous electric fields (275). According to this definition, the effect of dielectrophoresis can be applied to both AC and DC electric fields as long as the electric field is spatially non-uniformly distributed. The dielectrophoretic (DEP) force, $\vec{F}_{\mathrm{DEP}}$, acting on a molecule can be represented by the following equation,

$$\vec{F}_{\text{DEP}}=(\vec{P}\cdot\nabla)\vec{E} \tag{15}$$

where $\vec{P}$ is the dipole moment of the molecule and ∇ is the gradient operator. If the molecule is spherically shaped, with radius *a*,Equation (15) can be further expressed into the following equation,

$$\vec{F}_{\text{DEP}}=2\pi a^3\varepsilon_2 Re[K(\omega)]\nabla\left|\vec{E}\right|^2 \tag{16}$$

where $Re[K(\omega)]$ is the real part of the frequency dependent Clausius-Mossotti factor, $K(\omega)=\frac{\varepsilon_1-\varepsilon_2}{\varepsilon_1+2\varepsilon_2}$, where ε_1 and ε_2 are the permittivities of the molecule and the medium, respectively. $Re[K(\omega)]$ lies between 1 and −0.5 for spherical particles (276). From Equation (16), it is obvious that the dielectrophoretic force is frequency and volume dependent; the latter caused by the fact that the force scales with the cube of the characteristic body length.

5.1.2.2. Dielectrophoresis –Engineering Applications: Depending on the applied AC frequency and the dielectric properties of the embedded particles and the fluid medium, the DEP force acting on particles can be either positive (i.e., particles get attracted to high electric field gradient) or negative (i.e., particles get repelled from high electric field gradient). If the particles are close to the electrode, positive DEP force results in their immobilization on the electrode edge. On the other hand, negative DEP force results in specific confinement of particles in a region away from the electrode edge. DEP manipulation has shown to be applicable for a wide range of particle sizes, from around 10μm down to sub-20nm. For example, microscale entities, such as cells (277–279), or nanoscale entities, such as carbon nanotubes (CNT) (280–285), proteins (286,287), DNA (288), and viruses (289) have been immobilized on the edges of electrodes by positive DEP force or through the use of electric potential traps made with negative DEP force. Length scale matching between electrode and particles is the key to dictating the quantity of particles collected. For example, the use of microelectrodes generally results in the collection of bundles of nanoscale entities (283), whereas the use of nanoscale electrodes ensures the collection of single nanoscale entities (282,286,290). As a note, the lower limit for the particle size that can be manipulated by DEP force is dictated by the thermal randomization energy, *kT*. However, the effectiveness of DEP on the particle size limit is still under experimental investigation (291).

Apart from utilizing positive or negative DEP individually, they can be used together for particle separation. A celebrated example is the separation of metallic single-walled CNT from the ones with semi-conducting properties in a suspension performed by Krupke et al. (292). Incidentally, this work solves a long standing problem that stems from the inability to separate different types of CNT during their synthesis. The concept is to exploit the “crossover” AC frequency where positive and negative DEP forces act on the individual CNT with different dielectric properties. In the work of Krupke et al., a drop of CNT suspension with both semi-conducting and metallic CNT was deposited on a chip featuring an interdigitated electrode array operating at an AC voltage of 10V peak-to-peak at 10MHz. The metallic CNT, which experiences positive DEP forces, is attracted towards the electrode leaving the semi-conducting CNT, which experiences negative DEP forces, in the liquid suspension.

In addition, the combinatorial use of microfluidics and DEP can achieve sorting and separation of particles in the bulk fluid. A technique called dielectrophoresis field-flow-fractionation (DEP-FFF) exploits the nature of DEP on dielectric particles in conjunction with microfluidic flow, to achieve particle separation (293). In a fluidic channel with planar electrodes on the

surface, DEP-FFF utilizes the fact that particles with different dielectric properties experience different amounts of DEP force. This results in different levitation heights of the particles along the vertical direction of the channel, enabling the particles to be moved at different velocities due to the parabolic flow profile that develops in a pressuredriven flow inside the channel. This technique has been successfully applied for cell separation applications (294) and more recently on the separation of metallic and semi-conducting single-walled CNT (295).

Instead of using “physical” electrodes to generate inhomogeneous electric fields, Chiou et al. have recently developed a novel particle manipulation and transportation technology, termed optoelectronic tweezers (OET) (296). Through the use of a photoconductive material, light-induced DEP results by creating “virtual” electrodes on the surface (296) (see Figure 20). Conventionally, microfluidic chips with integrated electrodes have fixed the locations where inhomogeneous electric fields can be generated (i.e., where the electrodes are located). OET technology allows the “virtual” electrodes to be actively placed and altered anywhere on a substrate for the generation of inhomogeneous electric fields to achieve particle manipulation. Since the technology relies on optical image projection to activate the photoconductive surface, the ultimate resolution of the virtual electrodes is dictated by the optical diffraction limit. The power consumption of the OET system is 100,000 times lower than that used in optical tweezers. In addition, creation of 15,000 DEP traps across an area of $1.3 \times 1.0 mm^2$ for single particle (diameter~4.5μm) manipulation was demonstrated (see Figure 20). With such a high resolution (i.e., 1.52μm/pixel for the system demonstrated) and high throughput, this technology will be an attractive tool for parallel manipulation of microfabricated structures for device integration.

5.1.2.3. AC Electroomosis – Theory: In addition to manipulating particles by AC electric fields, bulk fluidic motion can also be induced. Similar to the induction of one-dimensional fluid flow by electroosmosis, three-dimensional bulk fluid motion can be induced in a similar fashion by using AC electric fields, or so called AC electroosmosis. Although AC electroosmosis is a newly identified phenomenon, recent theoretical and experimental studies have deepened the understanding of its physical origin (276,297–301). In AC electroosmosis, the charging of the electrode surface is a dynamic process, where the polarity of the double layer formation alternates with the frequency of the applied electric potential (which is known as electrode polarization). The process of electrode polarization and its interaction with the electric field is the fundamental driving force behind this phenomenon. To understand how AC electroosmosis can generate bulk fluidic motion, consider the moment when an electric potential $\pm V$ is applied on two separate planar electrodes. At this point in time, an electric field will be generated instantaneously and the tangential components of the electric field near the electrode surfaces will impart electrophoretic forces (Equation 12) on the ions present in the electric double layers, causing them to move in the corresponding directions. When the polarity of the electric potential is reversed, the tangential components of the electric field will be reversed. However, now the charges present on the electrode surface are of the opposite polarity and therefore the electrophoretic forces imparted on these ions will remain in the same direction. This gives rise to a tangential fluid velocity on the surface and results in a global fluidic motion (see Figure 21b). The time averaged AC electroosmotic velocity, V_{ac}, is given by (297),

$$V_{\mathrm{ac}} = \frac{\varepsilon \varepsilon_0 V^2 \Omega^2}{8 \nu z (1+\Omega^2)^2} \tag{17}$$

where Ω is given by,

$$\Omega=\omega\frac{\varepsilon\varepsilon_0}{\sigma}\frac{\pi}{2}z\kappa \tag{18}$$

where V is the amplitude of the AC potential, z is the position, σ is conductivity of the fluid medium, and κ is defined in Equation (13). Equation (17) indicates that the time averaged AC electroosmotic velocity has a square dependency with the applied AC potential. AC electroosmosis occurs at a lower frequency regime (i.e., up to 500kHz) compared to that of DEP (i.e., on the order of MHz) while still having a larger effective range (276).

5.1.2.4. AC Electroomosis – Engineering Applications: The bulk fluid motion generated by AC electroosmosis transports the embedded particles from the far-field region to the surface of the electrode. With specifically designed electrode geometries, AC electroosmosis has been exploited to concentrate particles within a localized region (277,302). Wong et al. has demonstrated a combination of a circular central electrode together with a circular ring outer electrode (see Figure 21a) to generate AC electroosmotic flow to transport bacteria (~ 1 – 2μm) and ssDNA fragments (~20 bases) to the surface of the electrode. Once there, electrophoretic and dielectrophoretic forces trap the particles on the surface (277) (see Figure 21). Detailed numerical and experimental analysis on this particular type of concentrator has recently been carried out by Bown and Meinhart (303).

Here we have briefly reviewed the most common types of electrokinetic forces for particle (i.e., electrophoresis and DEP) and fluidic (i.e., DC and AC electroosmosis) manipulation. In general, electrokinetic effects are a non-trivial phenomenon. Most of the time, the resultant particle/fluidic manipulations originate from a combined effect of AC and DC electrokinetics (277,302,304,305). More in-depth studies on the fundamentals of electrokinetics phenomenon can be referred to an excellent book by Morgan and Green (306) and review articles by Ramos et al. (276) and Hughes (307). For the current development of electrokinetics for engineering applications, readers can refer to recent review articles by Wong et al. (308), Burke (291), and Voldman (309).

5.2 Single Molecular Transport by Cytoskeleton and Motor Proteins

Shifting focus away from bulk molecular transport through electrokinetic forces, we now look into a new class of transportation mechanism which exploits cytoskeleton and motor proteins as the active transportation facilitator. This recently developed technology has garnered attention in the field of MEMS and nanotechnology for a few reasons. Firstly, motor proteins, such as kinesin and myosin, can move with a step size on the order of 10nm, which means transportation on the molecular scale is feasible. Secondly, these molecular motors are powered using ATP in solution as an energy source, which makes them an attractive choice within micro/nano-total-analysis-systems. Thirdly, well-established surface chemistry and genetic engineering allows the modification of cytoskeleton and motor proteins as well as the working solid substrate for specific patterning of biological entities. Finally, the structures and the functionalities of some of the cytoskeleton and motor proteins are relatively well-studied, which allows for their utilization for different types of mechanical tasks. In the following, we will briefly review the recent development of the active transportation of molecular species using this newly developed approach.

Early research on the mechanical properties of cytoskeleton filamentous structures inside microfabricated channel (135) have pioneered the use of microfabrication technologies to confine or pattern the cytoskeleton and motor proteins for active transportation of substances. The grand vision is to utilize those biological entities to load, transport, deliver and eventually assemble the molecular components in specific locations (310). To achieve this goal, a few

hurdles need to be addressed. Primary to these challenges is the orientation control of the microfilaments to achieve directional transportation of cargo, patterning, and integration of the cytoskeleton and motor proteins. Also, external control of the motor proteins to eventually achieve an automated nanoscale transportation system remains critical. In the following, we will sample through some of the recent developments on this subject matter.

5.2.1 Cytoskeleton Proteins as "Molecular Railways"—Utilizing cytoskeleton and motor proteins as an active transportation method can commonly be approached in three different ways. The first approach is to immobilize the microfilament structures on the substrate so that the motor molecules can "walk" on these "molecular railways" (311). The second approach is to immobilize the motor proteins onto a substrate and then allow the microfilament structures to be transported over the motor proteins (232,310,312–314). The last approach is an extension of the second approach, where the microfilament structures are further immobilized on the motor proteins by cross-linking agents or irradiation. Additional motor proteins that carry the cargo can then "walk" along the immobilized tracks (315).

5.2.2 Controlling the Trajectory of Motor Protein Motion—Generally speaking, unidirectional transportation is not guaranteed in these mechanisms due to the randomly scattered functional polarities of the microfilament structures on the surface. To ensure transport unidirectionality, Yokokawa et al. has shown that using microfluidic pulse injection in conjunction with continuous flow of ATP, can align randomly oriented microtubules on kinesin along the flow direction at a yield of about 95% (315). After the re-orientation of the microtubules, a cross-linking agent, such as glutaraldehyde, was added to the kinesins and microtubules to fix the orientation of the microtubules to become fixed. Beads coated with kinesin molecular motors were then moved along these re-orientated microtubules unidirectionally (i.e., the 3^{rd}approach). The re-orientation technique has proven to work in both simple flow cells and PDMS microfluidic channels.

Along that same vein, directed movement of the microfilament structures can be passively dictated by microfluidic channel geometries (314) or actively controlled by external force fields (232,316). In these studies, microtubules were exploited as "molecular shuttles" that were propelled by underlying, surface-bound kinesin molecular motors (i.e., the 2^{nd}approach). For instance, Clemmens et al. designed three different types of microfluidic channel geometries (i.e., crossing junctions, reflector junctions, and spiral) to study the motion of "molecular shuttles" (314). In general, microtubules follow the guided pathway of the channel sidewalls (314,317). Without the effect of the sidewalls, microtubules will tend to transport along their original pathway without deviating from their original path (i.e., laterally deviation of ~.25μm for 5μm traveling distance (314,317)). Specifically, in a reflector junction (i.e., short segment of closed-ended channel), microtubules will bend and reverse their path of motion completely. This demonstrated directional control of the microtubules since regardless of the initial polarity of the microtubules, all will eventually move in the same direction after being "reflected" by the junction (similar effects can be obtained for arrow-shape microchannel structures (316, 318)).

On the other hand, controlling the motion pathways of microfilament structures through external force fields has been studied. Specifically, electric fields have been exploited to actively steer the motion of microtubules (232,316). The concept exploits the charged nature of microtubules under physiological conditions (e.g., charges $\sim 12 \pm 2e^{-}$ per tubulin dimer was estimated in the experiments performed by van den Heuvel et al., (232)). When the leading end of a microtubule is not bound to a kinesin motor, it will only be influenced by Brownian motion and therefore receptive to an electric field that can dictate its movement. The degree of the bending of the leading end is an interplay between the local electric field strength and the local flexural rigidity of the microtubules. As mentioned earlier in Section 3.3, the flexural

rigidity of microtubules is length dependent (up to a certain length) due to its material anisotropy. By controlling the surface density of the kinesin motors, the local flexural rigidity of the microtubules can be adjusted. With an optimal surface density of kinesin motors and external electric field strength, the leading end of the microtubule can be bent accordingly for the next kinesin motor to "grab" and change its path of motion (232,316).

5.2.3 Switching Motor Proteins "On" and "Off"—To realize an automated nanoscale transportation system, the strategy to switch "on" and "off" motor molecules is required. In the work of Yokokawa et al., an approach was devised to achieve such switching of molecules (231). Since these molecular motors are driven by ATP hydrolysis, they can be activated/deactivated by the addition of a chemical that can quench ATP. In their experiments, hexokinase was used to convert ATP and glucose into ADP and glucose-6-phosphate, which resulted in the deactivation of the motor molecules. To reactivate the motor molecules, excess ATP was added. The response time between the "on" and "off" states were optimized by controlling the concentrations of the ATP and hexokinase, respectively. On the other hand, light-controlled activation of the motor proteins has been demonstrated by Hess et al. (312). The concept utilizes a caged-compound to release ATP upon the exposure of photon energy. Once the ATP is released, kinesin motors will be activated. At the same time, an ATP-consuming enzyme (e.g., hexokinease) will consume ATP molecules inside the solution and halt the molecular movement of the kinesin. In this sense, light controlled activation of molecular motors can be achieved.

5.2.4 Cytoskeleton and Motor Proteins for Engineering Functions—While the previous examples have shown how we can transport molecular cargo using cytoskeleton and motor proteins, higher ordered functions, such as stretching individual DNA molecules *in vitro*, have also been demonstrated. Stretching a DNA molecule to its full length generally requires an applied force on the order of 10pN (44). Accordingly, this task cannot be performed by either single kinesin or myosin motors whose maximum force outputs are ~5pN. Diez et al. provided a solution by simply utilizing arrays of kinesin molecular motors functionalized on a surface to generate collective forces for the stretching (313). In their work, a simple flow cell was constructed in which the glass surface was coated with casein to prevent the denaturation of kinesin, and to prevent the sticking of the microtubules to the surface. The kinesin was coated on the surface, followed by the addition of microtubules with bound DNA through biotin-streptavidin interactions (see Figure 22). By lowering the pH to 6.0, one side of the DNA molecule was anchored on the surface (i.e., the bond between the DNA and the surface can withstand ~160pN (319)), resulting in the stretching of the DNA molecule upon the movement of the microtubules. In addition to stretching single DNA molecules, the path of movement for the microtubules can be influenced as depicted in Figure 22. This is an important demonstration showing the utilization of cytoskeleton and motor proteins *in vitro* to perform an engineering task such as DNA stretching.

Thus far, we have presented the properties of natural molecular components and the technologies to transport and pattern these molecules specifically on a solid surface. In the next section, we will look into some specific examples on how some of these molecular components can be utilized and incorporated into top-down fabricated structures to perform engineering tasks.

6 Examples of Functional Micro and Nano Devices from Top-down and Bottom-up Approaches

Propelling static structures with precise mechanical motion requires actuators of matching length scales for efficient energy coupling (320,321). Macroscale actuators enable us to build

and move structures on the order of meters to kilometers. On the microscale domain, the maturity of MEMS technology has enabled us to manipulate objects from the millimeter scale down to the micrometer scale through a variety of actuation mechanisms (308,322–324). On the other hand, the development of nanoscale actuators for nanoscale machinery is still in its infancy stage. Currently, the smallest man-made functional actuator through top-down approaches is on the order of ~300nm (i.e., CNT-based electrostatic motor) (325). Therefore, actuating structures on an even smaller scale (e.g., sub-100nm domain) with precise control still remains a tremendous engineering challenge.

Instead of pushing the manufacturing limit to produce even smaller engineered actuators, a potentially more fruitful option would involve the utilization of the already optimized molecular toolbox that has long existed in the nature. For instance, cells, analogous to microscale factories, contain nanoscale sensors and actuators that drive our everyday life processes (e.g., cytoskeleton and motor proteins, in Section 3.3). As we have seen, each individual biological actuator is on the order of 10nm and can perform a variety of linear and rotary motions. Taking advantage of these biological actuators and incorporating them into top-down fabricated structures results in a new top-down and bottom-up hybrid manufacturing paradigm of micro/nano-machineries.

6.1 Propulsion and Transportation of Microscale Structures by Single Natural Molecular Motors

Broadly speaking, there are two different types of biological molecular motors that operate on the intra-cellular level, namely linear and rotary motors. As we have described earlier, linear motors such as kinesin and myosin act as “molecular transporters” for organelles or transmit forces through microfilament structures, such as F-actin or microtubules. An example of rotary motors, such as F_0F_1-adenosine triphosphate synthase (F_0F_1-ATPase), which is the “molecular power generator” that synthesizes ATP needed to sustain normal metabolic functions and can be found in the mitochondria and chloroplasts of animal and plant cells (326). Through genetic engineering and manipulation of surface chemistry (327), these tiny biological entities can be utilized to propel top-down/bottom-up fabricated micro/nanoscale structures (328).

Apart from moving molecular components, cytoskeleton and motor proteins have proven to be able to transport top-down fabricated objects that are thousands of times larger than the motor molecules themselves. In earlier work performed by Limberis and Stewart (311), silicon microchips ($10 \times 10 \times 5 \mu m^3$) were fabricated and subsequently surface functionalized with kinesin motors (with an estimated maximum packing density of 10^5 motors per μm). These microchips were then transported (at a speed of 800nm/s in saturating ATP) on an amino-silanized glass substrate with randomly distributed microtubules.

In order to confine the motility range of the motor molecules (or the transported objects) to achieve directed transportation, it is necessary to define specifically the “molecular railways” on the substrate. As mentioned earlier in Section 4.3, microtubules or F-actin can be patterned specifically using microfluidic patterning (231) or the parylene lift-off technique (235,329). In the work of Yokokawa et al. (231), microbeads (diameter ~ 320nm) and microstructures ($2 \times 3 \times 2 \mu m^3$) were successfully transported by kinesin on patterned microtubules (through microfluidic patterning) at a speed of 476 ± 56nm/s and 308nm/s, respectively (See Figure 23).

6.2 Microfluidic Pumping by the Synergetic Effects of Bacterial Flagellar Motors

Swimming in low Reynolds number ($Re \ll 1$) conditions requires different types of mechanisms than what we have perceived in the macroscopic world (330). A well-known example is *Escherichia coli* (which is also known as *E. coli*, whose size is ~1μm diameter by 2μm long (331)), whose swimming motion is supported by asymmetric rotational movement of its

flagellar filaments which are attached to its base (3,330,332). The engine that powers the movement of the filaments is the so-called bacterial flagellar motor (BFM). The BFM is one of the most powerful rotary biological entities known in nature (in terms of torque generation) (331). With the radius of the rotor being ~40nm, it is able to generate 4000pN·nm of torque near stall and can spin clockwise or counterclockwise at speeds on the order of 100Hz (331, 333). The motor is powered through proton movement in an electrochemical gradient (331, 333). Since all microfluidics and nanofluidics systems are driven in low Reynolds number regimes, the use of these natural "swimmers" for some engineering applications in micro/nanofluidics systems appears like a natural fit. This approach has recently been addressed by Tung and Kim (334) who have explored the possibility of using arrays of flagellated bacteria (i.e., *E. coli*) as the driving source for the induction of fluidic motion inside microfluidic channel.

In the work of Tung and Kim (334), the *E. coli* is genetically engineered to feature counterclockwise flagella rotation while the flagellar filaments can also be bound to the glass surface through non-specific binding. These modifications ensure the *E. coli* can be tethered on a glass surface and rotated in a clockwise sense. The mutated *E. coli* are then assembled inside a microfluidic glass channel fabricated by thermal fusion bonding. To synchronize the flagellar rotation, hydrodynamic loading (i.e., controlling the flow rate of the fluid inside the channel) was employed. Under specific loading, the authors found that the *E. coli* can be aligned to the flow direction momentarily and then be synchronized upon the removal of the hydrodynamic loading. It has been estimated that stopping the flagellar rotation requires hydrodynamic torque of 3000pN·nm, which was determined through a numerical simulation. They have also estimated that the microfluidic device, based on this hybrid integration, can produce flow rate up to 0.25nL/min in synchronized operation of the cells rotating at 10rps.

6.3 Actuation of Micro-cantilever by Synergetic Effects of Nanoscale Synthetic Molecular Motors

In addition to using natural molecular motors for actuation, synthetic chemists have created a new class of mechanically interlocked synthetic molecules, such as rotaxanes, which can be used to mimic the behavior of natural muscle (335). Rotaxanes consist of a dumbbell-shaped component, which features one or more recognition sites along the rod section and is terminated by bulky "stopper"-like structures (22). In between the stoppers, there are one or more ring-shaped components encircling the recognition sites. The ring-shaped components can be controllably switched back and forth from one recognition site to the other through chemical, electrochemical, or photochemical stimulus in solution (22), or electrical (336) or photon (337) excitation on a solid substrate. The molecule has proven to be able to perform mechanical switching in either a solution phase (22) or in a condensed form on a solid substrate (338, 339). The latter proof is a pre-requisite for the realization of any solid-state devices utilizing these synthetic molecules (336,340). In particular, the mechanical properties of [2]rotaxane molecules have recently been studied through single molecule force spectroscopy. The results revealed that the repulsive electrostatic interaction energy responsible for the molecular actuation is ~65kcal/mol (or ~0.45nN·nm per molecule) (341). With the actuation distance of ~1.4nm (335), a constant average actuation force of ~320pN is calculated. While this number is only a crude estimation, it remains two orders of magnitude higher than the maximum actuation force generated by natural molecular motors (e.g., the stall forces that myosin and kinesin can generate are ~5pN). The high controllability and impressive mechanical actuation force output are one of the reasons why rotaxane molecules have garnered recent attention for micro/nanomechanical systems.

Utilizing synthetic molecules to perform macroscale work (337) or actuate microscale structures (340) has only recently been demonstrated. For example, Huang et al. recently

demonstrated a self-assembled monolayer of [3]rotaxane molecules can be used to actuate a top-down fabricated micro-cantilever beam (500μm × 100μm × 1μm) (340). The [3]ro-taxane molecule used had two ring-shaped components encircling a single dumbbell featuring two pairs of recognition sites. Each ring-shaped component featured the ability to switch back and forth from one recognition site to the other while covalently bound to the upper surface of the cantilever (see Figure 24A). The dimensions of a [3]rotaxane molecule is ~1nm × 8.5nm × 1nm with a center-to-center distance in-between the recognition sites of 4.2nm, assuming the molecule is fully stretched (335). During the actuation, the inter-ring distance can shorten from 4.2nm to 1.4nm (335). The actuation distance is 35% of the length of the molecule. The control of the ring movement within the molecules was triggered by oxidation and reduction reactions. For example, in the presence of an oxidizing environment, the rings will move towards each other creating stress on the upper cantilever surface (which corresponds to upward beam bending). When returned to a neutral state through the introduction of a reducing agent, the rings move back to their ground state (corresponding to the beam relaxed state). The device was able to reversibly bend for 25 cycles with a maximum initial bending amplitude of 35nm (340) (see Figure 24B). This demonstrated that the cumulative effects of nanoscale motion by synthetic molecules can be used to propel microscale structures.

In addition to rotaxanes, other types of synthetic molecules exist which can potentially be used in a variety of micro/nanotechnology applications. For the detailed accounts of these synthetic molecules, readers can refer to review articles provided by Balzani et al. (22,23). In addition, readers can refer to Browne and Feringa (342) for the most recent development of synthetic molecular machines for engineering applications.

Thus far, we have seen how molecular and cellular entities (either natural or synthetic) can be exploited singly or cooperatively to drive top-down fabricated micro/nano structures. On the other hand, the human body has proven to be a long-lived machine (e.g., the life cycles of skeletal muscle > 10^9, which is the longest lasting actuation material known (343)). This is a performance level that engineered systems have yet to achieve. Incorporating these natural tissues into engineered structures may provide another dimension for a long-lived propulsion mechanism.

6.4 Micro Actuators Powered by Muscle Fibers

Recently, Xi et al. has demonstrated the bottom-up integration of cardiomyocytes (single cells of heart muscle) onto a simple microfabricated structure to perform mechanical motion (344) (see Figure 25). The main contributions from their work are the establishment of a protocol to selectively grow and sustain viable muscle cells on predefined locations on a microfabricated device and at the same time, ensure strong binding between the muscle cells and the microstructure for efficient mechanical energy transmission.

In their device, the MEMS structure was first fabricated through the single-crystal reactive etching and metallization (SCREAM) process (345) followed by its immersion into a solution of poly-N-isopropylacrylamide (PNIPAAm) in ethanol. PNIPAAm, which is a thermal responsive polymer, serves as a negative and sacrificial material to induce selective growth of muscle cells and in later steps serves as a release layer for the hybrid integrated structure. Once dried, the resulting thin layer of PNIPAAm (16 – 20μm) was then patterned through a shadow mask followed by subsequent deposition of Cr and Au layers on the MEMS structure. Taking advantage of the selective growth of muscle cells on the gold surface as opposed to the PNIPAAm polymer, the muscle cells can be self-assembled onto the patterned gold surfaces selectively. To ensure an efficient energy coupling from the muscle cells to the micro-structure, a Cr adhesion layer was used which provides a tight interconnect between the SiO_2 (top layer of the micro-structure) and the gold surface (where the muscle cell is attached).

Upon the release of the structures, the movement of the structures is powered by the continuous contraction and relaxation of the muscle bundles in the presence of glucose in a physiological liquid medium (see Figure 25). The device was composed of two legs with dimensions of 138μm long and 40μm wide. The average stepping frequency of the device was 1.8Hz with average maximum step size of 25μm. The measured maximum speed was 38μm/s. This proof-of-concept demonstration has laid down a significant foundation for hybrid integration of muscle cells into MEMS structures and serves as a novel actuation mechanism on the microscale domain.

7 Conclusions

With the advancement of MEMS and nanotechnology, we are able to manipulate, pattern, and transport molecules with the precise spatial control necessary to operate in single molecule regimes (346). In addition, we have benefited from scientific studies, both early and recent, which focused on some of the intricate, natural molecular components that now allow us to utilize them in a variety of engineering systems. In this review, we have discussed the properties of a few natural molecular components, the technologies used to guide molecular growth, and those used to manipulate molecular components in bulk or as single entities. In addition, we have presented a few examples of constructing functional mechanical devices which combined top-down and bottom-up fabrication approaches. Despite the fact that these hybrid integrated mechanical devices are relatively primitive when compared to nature's functional structures, the concepts behind their construction constitute an important demonstration as to the use of molecular components, through guided self-assembly processes in cooperation with top-down fabricated structures, to perform useful work.

Early work that first observed cell motility and mitosis noted the necessity of highly regulated temporal and spatial control of cytoskeleton protein assembly, which has provided insights into the system's complex and adaptive device construction. With the ability to regulate the control mechanisms of molecular component assembly, hybrid integrated devices with higher-order functionalities are expected. To exert such exacting control in both the spatial and temporal domains, creative and combinatorial use of molecular transport, patterning, and self-assembling technologies appear to be necessary. In addition, nature has shown us that the cooperative effects of molecular components are required to sustain a variety of cellular processes. While some research efforts have focused on utilizing different molecular components within the same system for collective work (247,248), this approach for device construction has yet to be explored. This remains an interesting and potentially fruitful area of study towards complex system creation.

As a final note, nature continues to amaze through the use of simple molecules that form simple components. More impressive however is that when these components interact together, they eventually produce an adaptive complex system with emergent properties (e.g., Simple Molecules → Cells → Tissues → Organs → Human). While much work must be done before we fully understand the intricate details of these highly nonlinear systems (347), this will not and should not prohibit the construction of adaptive complex devices. Recently, engineers have demonstrated the combinatorial use of bio-nano-information technology to drive cell activity without a complete comprehension of the complicated network of signal pathways responsible for driving the cellular system (348–350). Similar approaches therefore may allow for the creation of adaptive functional complex devices despite relative ignorance of the overriding system parameters. Now that we have the technology to manipulate entities on a multitude of length scales (i.e., from nanometer-scale to meter-scale), we have moved a step closer to achieving one of the eventual goals of building functional devices that match the complexity and functionality of naturally evolved systems.

Acknowledgments

This work is supported by Center for Scalable and Integrated Nanomanufacturing (SINAM) under National Science Foundation (award number: DMI – 0327077) and Center for Cell Control (PN2 EY018228) through the NIH Roadmap for Nanomedicine. Tak-Sing Wong is supported by the INTEL foundation Ph.D. fellowship.

In addition, the authors would like to thank Dr. Karen Christman, Dan Garcia, Gauvain Haulot, Robert Lam, Peter Lillihoj, Chien Sun, Winny Tan, Hideaki Tsutsui, Takane Usui, Dr. Fang Wei, Ieong Wong of UCLA, Prof. Adam Po-Hao Huang of University of Arkansas, Prof. A. Senthil Kumar of National University of Singapore, Prof. Pak Kin Wong of University of Arizona for the help and valuable comments on the manuscript. We would like to specially thank Dr. Kuan Wang, Dr. Jeff Forbes, and Gustavo Gutierrez-Cruz of National Institutes of Health and Prof. Heather Maynard of UCLA for the close collaborations.

References

1. Horne RW, Wildy P. Virology 1961;15:348–373. [PubMed: 14448959]
2. Aizenberg J, Tkachenko A, Weiner S, Addadi L, Hendler G. Nature 2001;412:819–822. [PubMed: 11518966]
3. McMahon, TA.; Bonner, JT. On size and life. New York: Scientific American Library : Distributed by W.H. Freeman; 1983.
4. Mann, S. Biomineralization : principles and concepts in bioinorganic materials chemistry. New York: University Press, Oxford; 2001.
5. Mann S. Journal of the Chemical Society-Dalton Transactions 1997:3953–3961.
6. Aizenberg J, Weaver JC, Thanawala MS, Sundar VC, Morse DE, Fratzl P. Science 2005;309:275–278. [PubMed: 16002612]
7. Hartwell LH, Culotti J, Pringle JR, Reid BJ. Science 1974;183:46–51. [PubMed: 4587263]
8. Bray, D. Cell movements : from molecules to motility. New York: Garland Pub; 2001.
9. Mitchison TJ, Cramer LP. Cell 1996;84:371–379. [PubMed: 8608590]
10. Watson JD, Crick FHC. Nature 1953;171:737–738. [PubMed: 13054692]
11. Hartwell LH, Hopfield JJ, Leibler S, Murray AW. Nature 1999;402:C47–C52. [PubMed: 10591225]
12. Weng GZ, Bhalla US, Iyengar R. Science 1999;284:92–96. [PubMed: 10102825]
13. Anderson PW. Science 1972;177:393–396. [PubMed: 17796623]
14. Ottino JM. AICHE Journal 2003;49:292–299.
15. Ottino JM. Nature 2004;427:399–399. [PubMed: 14749808]
16. Israelachvili, JN. Intermolecular and surface forces. Boston: Academic Press, Amsterdam; 1992.
17. Lide, DR. CRC handbook of chemistry and physics. Boca Raton, FL: CRC Press; 1994.
18. London F. Transactions of the Faraday Society 1937;33:8–26.
19. Lennard-Jones JE. Proceedings of the Physical Society 1931;43:461–482.
20. Joesten, MD.; Schaad, LJ. Hydrogen bonding. New York: M. Dekker; 1974.
21. Howard, J. Mechanics of motor proteins and the cytoskeleton. Sunderland, Mass: Sinauer Associates Publishers; 2001.
22. Balzani V, Gomez-Lopez M, Stoddart JF. Accounts of Chemical Research 1998;31:405–414.
23. Balzani V, Credi A, Raymo FM, Stoddart JF. Angewandte Chemie-International Edition 2000;39:3349–3391.
24. Mann S, Ozin GA. Nature 1996;382:313–318.
25. Aizenberg J. Advanced Materials 2004;16:1295–1302.
26. Langer JS. Reviews of Modern Physics 1980;52:1–28.
27. Falini G, Albeck S, Weiner S, Addadi L. Science 1996;271:67–69.
28. Belcher AM, Wu XH, Christensen RJ, Hansma PK, Stucky GD, Morse DE. Nature 1996;381:56–58.
29. Aizenberg J, Black AJ, Whitesides GM. Nature 1999;398:495–498.
30. Peterson KE. Proceedings of the IEEE 1982;70:420–457.
31. Brantley WA. Journal of Applied Physics 1973;44:534–535.
32. Curry JD. Proceedings of Royal Society of London. Series B 1977;196:443–463.

33. Jackson AP, Vincent JFV, Turner KL. Proceedings of Royal Society of London. Series B 1988;234:415–440.
34. Meldrum FC. International Materials Reviews 2003;48:187–224.
35. Schaffer TE, IonescuZanetti C, Proksch R, Fritz M, Walters DA, Almqvist N, Zaremba CM, Belcher AM, Smith BL, Stucky GD, Morse DE, Hansma PK. Chemistry of Materials 1997;9:1731–1740.
36. Song F, Soh AK, Bai YL. Bio-materials 2003;24:3623–3631.
37. Nukala PKVV, Simunovic S. Physical Review E 2005;72:041919.
38. Song J, Malathong V, Bertozzi CR. Journal of the American Chemical Society 2005;127:3366–3372. [PubMed: 15755154]
39. Murphy WL, Mooney DJ. Nature Biotechnology 2002;20:30–31.
40. Bergerhoff G, Hundt R, Sievers R, Brown ID. Journal of Chemical Information and Computer Sciences 1983;23:66–69.
41. Available on web: http://icsd.ill.fr/icsd/index.html
42. Piana S, Reyhani M, Gale JD. Nature 2005;438:70–73. [PubMed: 16267550]
43. Lodish, HF. Molecular cell biology. New York: W.H. Freeman and Company; 2004.
44. Rief M, Clausen-Schaumann H, Gaub HE. Nature Structural Biology 1999;6:346–349.
45. Essevaz-Roulet B, Bockelmann U, Hes-lot F. Proceedings of the National Academy of Sciences of the United States of America 1997;94:11935–11940. [PubMed: 9342340]
46. Wang JC. Proceedings of the National Academy of Sciences of the United States of America 1979;76:200–203. [PubMed: 284332]
47. Rhodes D, Klug A. Nature 1980;286:573–578. [PubMed: 7402337]
48. Simmel FC, Dittmer WU. Small 2005;1:284–299. [PubMed: 17193445]
49. Smith SB, Cui YJ, Bustamante C. Science 1996;271:795–799. [PubMed: 8628994]
50. Bryant Z, Stone MD, Gore J, Smith SB, Cozzarelli NR, Bustamante C. Nature 2003;424:338–341. [PubMed: 12867987]
51. Bustamante C, Bryant Z, Smith SB. Nature 2003;421:423–427. [PubMed: 12540915]
52. Wang MD. Current Opinion in Biotechnology 1999;10:81–86. [PubMed: 10047511]
53. Baumann CG, Smith SB, Bloomfield VA, Bustamante C. Proceedings of the National Academy of Sciences of the United States of America 1997;94:6185–6190. [PubMed: 9177192]
54. Wang MD, Yin H, Landick R, Gelles J, Block SM. Biophysical Journal 1997;72:1335–1346. [PubMed: 9138579]
55. Hagerman PJ. Annual Review of Biophysics and Biophysical Chemistry 1988;17:265–286.
56. Gere, JM. Mechanics of materials. Pacific Grove, CA: Brooks/Cole; 2001.
57. Strick TR, Allemand JF, Bensimon D, Bensimon A, Croquette V. Science 1996;271:1835–1837. [PubMed: 8596951]
58. Gore J, Bryant Z, Nollmann M, Le MU, Cozzarelli NR, Bustamante C. Nature 2006;442:836–839. [PubMed: 16862122]
59. Olson WK, Gorin AA, Lu XJ, Hock LM, Zhurkin VB. Proceedings of the National Academy of Sciences of the United States of America 1998;95:11163–11168. [PubMed: 9736707]
60. Bustamante C, Smith SB, Liphardt J, Smith D. Current Opinion in Structural Biology 2000;10:279–285. [PubMed: 10851197]
61. Vinograd J, Lebowitz J, Radloff R, Watson R, Laipis P. Proceedings of the National Academy of Sciences of the United States of America 1965;53:1104–1111. [PubMed: 4287964]
62. Shlomai J, Friedmann A, Becker Y. Virology 1976;69:647–659. [PubMed: 176788]
63. Boehmer PE, Lehman IR. Annual Review of Biochemistry 1997;66:347–384.
64. Holliday R. Genetical Research 1964;5:282–304.
65. Ortiz-Lombardia M, Gonzalez A, Eritja R, Aymami J, Azorin F, Coll M. Nature Structural Biology 1999;6:913–917.
66. Kallenbach NR, Ma RI, Seeman NC. Nature 1983;305:829–831.
67. Seeman NC. Annual Review of Biophysics and Biomolecular Structure 1998;27:225–248.
68. Seeman NC, Lukeman PS. Reports on Progress in Physics 2005;68:237–270.

69. Chen JH, Seeman NC. Nature 1991;350:631–633. [PubMed: 2017259]
70. Zhang YW, Seeman NC. Journal of the American Chemical Society 1994;116:1661–1669.
71. Chen JH, Kallenbach NR, Seeman NC. Journal of the American Chemical Society 1989;111:6402–6407.
72. Mao CD, Sun WQ, Seeman NC. Nature 1997;386:137–138. [PubMed: 9062186]
73. Qi J, Li XJ, Yang XP, Seeman NC. Journal of the American Chemical Society 1996;118:6121–6130.
74. Yang XP, Wenzler LA, Qi J, Li XJ, Seeman NC. Journal of the American Chemical Society 1998;120:9779–9786.
75. Winfree E, Liu FR, Wenzler LA, Seeman NC. Nature 1998;394:539–544. [PubMed: 9707114]
76. Shih WM, Quispe JD, Joyce GF. Nature 2004;427:618–621. [PubMed: 14961116]
77. Rothemund PWK. Nature 2006;440:297–302. [PubMed: 16541064]
78. Mao CD, Sun WQ, Shen ZY, See-man NC. Nature 1999;397:144–146. [PubMed: 9923675]
79. Yin P, Yan H, Daniell XG, Turberfield AJ, Reif JH. Angewandte Chemie-International Edition 2004;43:4906–4911.
80. Sherman WB, Seeman NC. Nano Letters 2004;4:1203–1207.
81. Yurke B, Turberfield AJ, Mills AP, Simmel FC, Neumann JL. Nature 2000;406:605–608. [PubMed: 10949296]
82. Simmel FC, Yurke B. Physical Review E 2001;63:041913.
83. Li XJ, Yang XP, Qi J, Seeman NC. Journal of the American Chemical Society 1996;118:6131–6140.
84. Liu DS, Balasubramanian S. Angewandte Chemie-International Edition 2003;42:5734–5736.
85. Seeman NC. Trends in Biochemical Sciences 2005;30:119–125. [PubMed: 15752983]
86. Huxley HE. Science 1969;164:1356–1366. [PubMed: 4181952]
87. Waters JC, Cole RW, Rieder CL. Journal of Cell Biology 1993;122:361–372. [PubMed: 8320259]
88. Sharp DJ, Rogers GC, Scholey JM. Nature 2000;407:41–47. [PubMed: 10993066]
89. Kreis, T.; Vale, R. Guidebook to the cytoskeletal and motor proteins. New York: Oxford University Press, Oxford; 1999.
90. Cleveland DW, Sullivan KF. Annual Review of Biochemistry 1985;54:331–365.
91. Vale RD, Fletterick RJ. Annual Review of Cell and Developmental Biology 1997;13:745–777.
92. Vale RD. Cell 2003;112:467–480. [PubMed: 12600311]
93. Pollard TD, Cooper JA. Annual Review of Biochemistry 1986;55:987–1035.
94. Warrick HM, Spudich JA. Annual Review of Cell Biology 1987;3:379–421.
95. Pantaloni D, Le Clainche C, Carlier MF. Science 2001;292:1502–1506. [PubMed: 11379633]
96. Korn ED. Physiological Reviews 1982;62:672–737. [PubMed: 6280220]
97. Korn ED, Carlier MF, Pantaloni D. Science 1987;238:638–644. [PubMed: 3672117]
98. Kabsch W, Mannherz HG, Suck D, Pai EF, Holmes KC. Nature 1990;347:37–44. [PubMed: 2395459]
99. Kishino A, Yanagida T. Nature 1988;334:74–76. [PubMed: 3386748]
100. Tsuda Y, Yasutake H, Ishijima A, Yanagida T. Proceedings of the National Academy of Sciences of the United States of America 1996;93:12937–12942. [PubMed: 8917522]
101. Moy VT, Florin EL, Gaub HE. Science 1994;266:257–259. [PubMed: 7939660]
102. Frieden C. Proceedings of the National Academy of Sciences of the United States of America-Biological Sciences 1983;80:6513–6517.
103. Pollard TD. Journal of Cell Biology 1986;103:2747–2754. [PubMed: 3793756]
104. Schafer DA, Cooper JA. Annual Review of Cell and Developmental Biology 1995;11:497–518.
105. Fujiwara I, Takahashi S, Tadakuma H, Funatsu T, Ishiwata S. Nature Cell Biology 2002;4:666–673.
106. Dabiri GA, Sanger JM, Portnoy DA, Southwick FS. Proceedings of the National Academy of Sciences of the United States of America 1990;87:6068–6072. [PubMed: 2117270]
107. Theriot JA, Mitchison TJ, Tilney LG, Portnoy DA. Nature 1992;357:257–260. [PubMed: 1589024]
108. Nishizaka T, Yagi T, Tanaka Y, Ishi-wata S. Nature 1993;361:269–271. [PubMed: 8423853]
109. Yasuda R, Miyata H, Kinosita K. Journal of Molecular Biology 1996;263:227–236. [PubMed: 8913303]

110. Gittes F, Mickey B, Nettleton J, Howard J. Journal of Cell Biology 1993;120:923–934. [PubMed: 8432732]
111. Yanagida T, Nakase M, Nishiyama K, Oosawa F. Nature 1984;307:58–60. [PubMed: 6537825]
112. Dupuis DE, Guilford WH, Wu J, Warshaw DM. Journal of Muscle Research and Cell Motility 1997;18:17–30. [PubMed: 9147990]
113. Matsudaira P, Mandelkow E, Renner W, Hesterberg LK, Weber K. Nature 1983;301:209–214. [PubMed: 6823301]
114. Hanein D, Volkmann N, Goldsmith S, Michon AM, Lehman W, Craig R, DeRosier D, Almo S, Matsudaira P. Nature Structural Biology 1998;5:787–792.
115. Volkmann N, DeRosier D, Matsudaira P, Hanein D. Journal of Cell Biology 2001;153:947–956. [PubMed: 11381081]
116. Imamura M, Endo T, Kuroda M, Tanaka T, Masaki T. Journal of Biological Chemistry 1988;263:7800–7805. [PubMed: 3286641]
117. Blanchard A, Ohanian V, Critchley D. Journal of Muscle Research and Cell Motility 1989;10:280–289. [PubMed: 2671039]
118. Pelletier O, Pokidysheva E, Hirst LS, Bouxsein N, Li Y, Safinya CR. Physical Review Letters 2003;91:148102. [PubMed: 14611558]
119. Tyler JM, Anderson JM, Branton D. Journal of Cell Biology 1980;85:489–495. [PubMed: 6768755]
120. Mcgough AM, Josephs R. Proceedings of the National Academy of Sciences of the United States of America 1990;87:5208–5212. [PubMed: 2367532]
121. Wang K. Biochemistry 1977;16:1857–1865. [PubMed: 139917]
122. Mullins RD, Heuser JA, Pollard TD. Proceedings of the National Academy of Sciences of the United States of America 1998;95:6181–6186. [PubMed: 9600938]
123. Pollard TD, Borisy GG. Cell 2003;112:453–465. [PubMed: 12600310]
124. Didry D, Carlier MF, Pantaloni D. Journal of Biological Chemistry 1998;273:25602–25611. [PubMed: 9748225]
125. Pantaloni D, Carlier MF. Cell 1993;75:1007–1014. [PubMed: 8252614]
126. Lal AA, Brenner SL, Korn ED. Journal of Biological Chemistry 1984;259:3061–3065.
127. Yin HL, Stossel TP. Nature 1979;281:583–586. [PubMed: 492320]
128. Allen PG, Janmey PA. Journal of Biological Chemistry 1994;269:32916–32923. [PubMed: 7806519]
129. Erickson HP. Trends in Cell Biology 1998;8:133–137. [PubMed: 9695825]
130. Wade RH, Chretien D. Journal of Structural Biology 1993;110:1–27. [PubMed: 8494670]
131. Nogales E, Whittaker M, Milligan RA, Downing KH. Cell 1999;96:79–88. [PubMed: 9989499]
132. Nogales E, Wolf SG, Downing KH. Nature 1998;391:199–203. [PubMed: 9428769]
133. Mickey B, Howard J. Journal of Cell Biology 1995;130:909–917. [PubMed: 7642706]
134. Kurachi M, Hoshi M, Tashiro H. Cell Motility and the Cytoskeleton 1995;30:221–228. [PubMed: 7758138]
135. Dogterom M, Yurke B. Science 1997;278:856–860. [PubMed: 9346483]
136. Felgner H, Frank R, Schliwa M. Journal of Cell Science 1996;109:509–516. [PubMed: 8838674]
137. Janson ME, Dogterom M. Biophysical Journal 2004;87:2723–2736. [PubMed: 15454464]
138. Pampaloni F, Lattanzi G, Jonas A, Surrey T, Frey E, Florin EL. Proceedings of the National Academy of Sciences of the United States of America 2006;103:10248–10253. [PubMed: 16801537]
139. Kikumoto M, Kurachi M, Tosa V, Tashiro H. Biophysical Journal 2006;90:1687–1696. [PubMed: 16339879]
140. Takasone T, Juodkazis S, Kawagishi Y, Yamaguchi A, Matsuo S, Sakakibara H, Nakayama H, Misawa H. Japanese Journal of Applied Physics Part 1-Regular Papers Short Notes & Review Papers 2002;41:3015–3019.
141. Howard J, Hyman AA. Nature 2003;422:753–758. [PubMed: 12700769]
142. Schiff PB, Fant J, Horwitz SB. Nature 1979;277:665–667. [PubMed: 423966]

143. Hill TL. Proceedings of the National Academy of Sciences of the United States of America 1985;82:4404–4408. [PubMed: 3859869]
144. Peskin CS, Odell GM, Oster GF. Biophysical Journal 1993;65:316–324. [PubMed: 8369439]
145. Inoue S, Salmon ED. Molecular Biology of the Cell 1995;6:1619–1640. [PubMed: 8590794]
146. van Doorn GS, Tanase C, Mulder BM, Dogterom M. European Biophysics Journal with Biophysics Letters 2000;29:2–6. [PubMed: 10826773]
147. Kolomeisky AB, Fisher ME. Biophysical Journal 2001;80:149–154. [PubMed: 11159390]
148. Rayment I. Structure 1996;4:501–504. [PubMed: 8736548]
149. Vale RD. Annual Review of Cell Biology 1987;3:347–378.
150. Howard J. Annual Review of Physiology 1996;58:703–729.
151. Rice S, Lin AW, Safer D, Hart CL, Naber N, Carragher BO, Cain SM, Pechatnikova E, Wilson-Kubalek EM, Whittaker M, Pate E, Cooke R, Taylor EW, Milligan RA, Vale RD. Nature 1999;402:778–784. [PubMed: 10617199]
152. Toyoshima YY, Kron SJ, Mcnally EM, Niebling KR, Toyoshima C, Spudich JA. Nature 1987;328:536–539. [PubMed: 2956522]
153. Spudich JA. Nature Reviews Molecular Cell Biology 2001;2:387–392.
154. Rayment I, Rypniewski WR, Schmidtbase K, Smith R, Tomchick DR, Benning MM, Winkelmann DA, Wesenberg G, Holden HM. Science 1993;261:50–58. [PubMed: 8316857]
155. Shih WM, Gryczynski Z, Lakowicz JR, Spudich JA. Cell 2000;102:683–694. [PubMed: 11007486]
156. Kendrick-Jones, J.; Hodge, TP.; Lister, IMB.; Roberts, RC.; Buss, F. available on web: http://www.mrc-lmb.cam.ac.uk/myosin/Review/Reviewframeset.html)
157. Foth BJ, Goedecke MC, Soldati D. Proceedings of the National Academy of Sciences of the United States of America 2006;103:3681–3686. [PubMed: 16505385]
158. Brenner B. Journal of Muscle Research and Cell Motility 2006;27:173–187. [PubMed: 16470332]
159. Cheney RE, Oshea MK, Heuser JE, Coelho MV, Wolenski JS, Espreafico EM, Forscher P, Larson RE, Mooseker MS. Cell 1993;75:13–23. [PubMed: 8402892]
160. Yildiz A, Forkey JN, McKinney SA, Ha T, Goldman YE, Selvin PR. Science 2003;300:2061–2065. [PubMed: 12791999]
161. Walker ML, Burgess SA, Sellers JR, Wang F, Hammer JA, Trinick J, Knight PJ. Nature 2000;405:804–807. [PubMed: 10866203]
162. Kitamura K, Tokunaga M, Iwane AH, Yanagida T. Nature 1999;397:129–134. [PubMed: 9923673]
163. Yanagida T, Iwane AH. Proceedings of the National Academy of Sciences of the United States of America 2000;97:9357–9359. [PubMed: 10944206]
164. Toyoshima YY, Kron SJ, Spudich JA. Proceedings of the National Academy of Sciences of the United States of America 1990;87:7130–7134. [PubMed: 2144900]
165. Finer JT, Simmons RM, Spudich JA. Nature 1994;368:113–119. [PubMed: 8139653]
166. Kull FJ, Sablin EP, Lau R, Fletterick RJ, Vale RD. Nature 1996;380:550–555. [PubMed: 8606779]
167. Yildiz A, Tomishige M, Vale RD, Selvin PR. Science 2004;303:676–678. [PubMed: 14684828]
168. Asbury CL, Fehr AN, Block SM. Science 2003;302:2130–2134. [PubMed: 14657506]
169. Ray S, Meyhofer E, Milligan RA, Howard J. Journal of Cell Biology 1993;121:1083–1093. [PubMed: 8099076]
170. Rock RS, Rice SE, Wells AL, Purcell TJ, Spudich JA, Sweeney HL. Proceedings of the National Academy of Sciences of the United States of America 2001;98:13655–13659. [PubMed: 11707568]
171. Alberty RA, Goldberg RN. Biochemistry 1992;31:10610–10615. [PubMed: 1420176]
172. Cross RA. Current Biology 1997;7:R631–R633. [PubMed: 9368744]
173. Ishijima A, Kojima H, Funatsu T, Tokunaga M, Higuchi H, Tanaka H, Yanagida T. Cell 1998;92:161–171. [PubMed: 9458041]
174. Young EC, Mahtani HK, Gelles J. Biochemistry 1998;37:3467–3479. [PubMed: 9521668]
175. Howard J, Hudspeth AJ, Vale RD. Nature 1989;342:154–158. [PubMed: 2530455]
176. Vale RD, Funatsu T, Pierce DW, Romberg L, Harada Y, Yanagida T. Nature 1996;380:451–453. [PubMed: 8602245]

177. Svoboda K, Block SM. Cell 1994;77:773–784. [PubMed: 8205624]
178. Kojima H, Muto E, Higuchi H, Yanagida T. Biophysical Journal 1997;73:2012–2022. [PubMed: 9336196]
179. Coppin CM, Pierce DW, Hsu L, Vale RD. Proceedings of National Academy of Sciences of the United States of America 1997;94:8539–8544.
180. Mehta AD, Rock RS, Rief M, Spudich JA, Mooseker MS, Cheney RE. Nature 1999;400:590–593. [PubMed: 10448864]
181. Marden JH, Allen LR. Proceedings of the National Academy of Sciences of the United States of America 2002;99:4161–4166. [PubMed: 11917097]
182. Schnitzer MJ, Block SM. Nature 1997;388:386–390. [PubMed: 9237757]
183. Coy DL, Wagenbach M, Howard J. Journal of Biological Chemistry 1999;274:3667–3671. [PubMed: 9920916]
184. Xia YN, Whitesides GM. Angewandte Chemie-International Edition 1998;37:551–575.
185. Xia YN, Rogers JA, Paul KE, Whitesides GM. Chemical Reviews 1999;99:1823–1848. [PubMed: 11849012]
186. Harriott LR. Proceedings of the IEEE 2001;89:366–374.
187. Chen Y, Pepin A. Electrophoresis 2001;22:187–207. [PubMed: 11288885]
188. Garcia R, Martinez RV, Martinez J. Chemical Society Reviews 2006;35:29–38. [PubMed: 16365640]
189. Bratton D, Yang D, Dai JY, Ober CK. Polymers for Advanced Technologies 2006;17:94–103.
190. Vieu C, Carcenac F, Pepin A, Chen Y, Mejias M, Lebib A, Manin-Ferlazzo L, Couraud L, Launois H. Applied Surface Science 2000;164:111–117.
191. Kramer S, Fuierer RR, Gorman CB. Chemical Reviews 2003;103:4367–4418. [PubMed: 14611266]
192. Tseng AA, Notargiacomo A, Chen TP. Journal of Vacuum Science & Technology B 2005;23:877–894.
193. Qin D, Xia YN, Xu B, Yang H, Zhu C, Whitesides GM. Advanced Materials 1999;11:1433–1437.
194. Suh KY, Khademhosseini A, Eng G, Langer R. Langmuir 2004;20:6080–6084. [PubMed: 15248685]
195. Zhong ZY, Gates B, Xia YN, Qin D. Langmuir 2000;16:10369–10375.
196. Wong, TS.; Brough, B.; Christman, KL.; Kolodziej, CM.; Huang, A.; Lam, R.; Forbes, JG.; Wang, K.; Maynard, HD.; Ho, CM. IEEE 7th International Conference on Nanotechnology; Hong Kong SAR. 2007. p. 126-130.
197. Barton JE, Odom TW. Nano Letters 2004;4:1525–1528.
198. Brinker CJ, Lu YF, Sellinger A, Fan HY. Advanced Materials 1999;11:579–585.
199. Vlasov YA, Bo XZ, Sturm JC, Norris DJ. Nature 2001;414:289–293. [PubMed: 11713524]
200. Narayanan S, Wang J, Lin XM. Physical Review Letters 2004;93:135503. [PubMed: 15524734]
201. Landau EM, Levanon M, Leiserowitz L, Lahav M, Sagiv J. Nature 1985;318:353–356.
202. Mann S. Nature 1988;332:119–124.
203. Mann S, Heywood BR, Rajam S, Birchall JD. Nature 1988;334:692–695.
204. Feng S, Bein T. Nature 1994;368:834–836.
205. Heller MJ. Annual Review of Biomedical Engineering 2002;4:129–153.
206. Chi PY, Lin HY, Liu CH, Chen CD. Nanotechnology 2006;17:4854–4858.
207. Kim E, Xia YN, Whitesides GM. Journal of the American Chemical Society 1996;118:5722–5731.
208. Bystrenova E, Facchini M, Cavallini M, Cacace MG, Biscarini F. Angewandte Chemie-International Edition 2006;45:4779–4782.
209. Zhang G, Yan X, Hou XL, Lu G, Yang B, Wu LX, Shen JC. Langmuir 2003;19:9850–9854.
210. Bensimon A, Simon A, Chiffaudel A, Croquette V, Heslot F, Bensimon D. Science 1994;265:2096–2098. [PubMed: 7522347]
211. Bensimon D, Simon AJ, Croquette V, Bensimon A. Physical Review Letters 1995;74:4754–4757. [PubMed: 10058590]
212. Petit CAP, Carbeck JD. Nano Letters 2003;3:1141–1146.

213. Bjork P, Holmstrom S, Inganas O. Small 2006;2:1068–1074. [PubMed: 17193170]
214. Demers LM, Ginger DS, Park SJ, Li Z, Chung SW, Mirkin CA. Science 2002;296:1836–1838. [PubMed: 12052950]
215. Zhang GJ, Tanii T, Funatsu T, Ohdomari I. Chemical Communications 2004:786–787. [PubMed: 15045063]
216. Hu WC, Sarveswaran K, Lieberman M, Bernstein GH. IEEE Transactions on Nanotechnology 2005;4:312–316.
217. Matsumoto F, Harada M, Nishio K, Masuda H. Advanced Materials 2005;17:1609–1612.
218. Chen MS, Dulcey CS, Chrisey LA, Dressick WJ. Advanced Functional Materials 2006;16:774–783.
219. Stadler BM, Huwiler CB, Voros J, Grandin HM. IEEE Transactions on Nanobioscience 2006;5:215–219. [PubMed: 16999248]
220. Kannan B, Kulkarni RP, Majumdar A. Nano Letters 2004;4:1521–1524.
221. Chandra RA, Douglas ES, Mathies RA, Bertozzi CR, Francis MB. Angewandte Chemie-International Edition 2006;45:896–901.
222. Lynch M, Mosher C, Huff J, Nettikadan S, Johnson J, Henderson E. Proteomics 2004;4:1695–1702. [PubMed: 15174138]
223. Christman KL, Enriquez-Rios VD, Maynard HD. Soft Matter 2006;2:928–939.
224. Blawas AS, Reichert WM. Biomaterials 1998;19:595–609. [PubMed: 9663732]
225. Kane RS, Takayama S, Ostuni E, Ingber DE, Whitesides GM. Biomaterials 1999;20:2363–2376. [PubMed: 10614942]
226. Harris, JM. Poly(ethylene glycol) chemistry : biotechnical and biomedical applications. New York: Plenum Press; 1992.
227. Suh KY, Kim YS, Lee HH. Advanced Materials 2001;13:1386–1389.
228. Wong, I.; Ho, CM. Proceedings of 19th Annual IEEE International Conference on Micro Electro Mechanical Systems; Istanbul, Turkey. 2006. p. 558-561.
229. Brough, B. Ph.D dissertation, Mechanical and Aerospace Engineering Department. Los Angeles: University of California; 2006.
230. Brough B, Christman KL, Wong TS, Kolodziej CM, Forbes JG, Wang K, Maynard HD, Ho CM. Soft Matter 2007;3:541–546.
231. Yokokawa R, Takeuchi S, Kon T, Nishiura M, Ohkura R, Sutoh K, Fujita H. Journal of Microelectromechanical Systems 2004;13:612–619.
232. van den Heuvel MGL, De Graaff MP, Dekker C. Science 2006;312:910–914. [PubMed: 16690866]
233. Atsuta K, Noji H, Takeuchi S. Lab on a Chip 2004;4:333–336. [PubMed: 15269800]
234. Jo BH, Van Lerberghe LM, Motsegood KM, Beebe DJ. Journal of Microelectromechanical Systems 2000;9:76–81.
235. Yoshida, Y.; Yokokawa, R.; Suzuki, H.; At-suta, K.; Fujita, H.; Takeuchi, S. Proceedings of 18th Annual IEEE International Conference on Micro Electro; Florida, USA: Mechanical Systems, Miami Beach; 2005. p. 750-753.
236. Florin EL, Moy VT, Gaub HE. Science 1994;264:415–417. [PubMed: 8153628]
237. Merkel R, Nassoy P, Leung A, Ritchie K, Evans E. Nature 1999;397:50–53. [PubMed: 9892352]
238. Schmidt JJ, Jiang XQ, Montemagno CD. Nano Letters 2002;2:1229–1233.
239. Weber PC, Ohlendorf DH, Wendoloski JJ, Salemme FR. Science 1989;243:85–88. [PubMed: 2911722]
240. Grubmuller H, Heymann B, Tavan P. Science 1996;271:997–999. [PubMed: 8584939]
241. Romet-Lemonne G, VanDuijn M, Dogterom M. Nano Letters 2005;5:2350–2354. [PubMed: 16351176]
242. Christman KL, Maynard HD. Langmuir 2005;21:8389–8393. [PubMed: 16114947]
243. Zhang GJ, Tanii T, Zako T, Hosaka T, Miyake T, Kanari Y, Funatsu TW, Ohdomari I. Small 2005;1:833–837. [PubMed: 17193534]
244. Huang L, Manandhar P, Byun KE, Chase PB, Hong S. Langmuir 2006;22:8635–8638. [PubMed: 17014097]

245. Christman KL, Requa MV, Enriquez-Rios VD, Ward SC, Bradley KA, Turner KL, Maynard HD. Langmuir 2006;22:7444–7450. [PubMed: 16893251]
246. Doh J, Irvine DJ. Proceedings of the National Academy of Sciences of the United States of America 2006;103:5700–5705. [PubMed: 16585528]
247. Badoual M, Julicher F, Prost J. Proceedings of the National Academy of Sciences of the United States of America 2002;99:6696–6701. [PubMed: 12011432]
248. Mallik R, Gross SP. Current Biology 2004;14:R971–R982. [PubMed: 15556858]
249. Douvas A, Argitis P, Misiakos K, Dimotikali D, Petrou PS, Kakabakos SE. Biosensors & Bioelectronics 2002;17:269–278. [PubMed: 11849922]
250. Doh J, Irvine DJ. Journal of the American Chemical Society 2004;126:9170–9171. [PubMed: 15281792]
251. Lee KB, Lim JH, Mirkin CA. Journal of the American Chemical Society 2003;125:5588–5589. [PubMed: 12733870]
252. Tien J, Nelson CM, Chen CS. Proceedings of the National Academy of Sciences of the United States of America 2002;99:1758–1762. [PubMed: 11842197]
253. Verma V, Hancock WO, Catchmark JM. IEEE Transactions on Advanced Packaging 2005;28:584–593.
254. Karnik R, Castelino K, Duan CH, Majumdar A. Nano Letters 2006;6:1735–1740. [PubMed: 16895365]
255. Einstein, A.; Fèurth, R.; Cowper, AD. Investigations on the theory of the Brownian movement. New York: Dover Publications; 1956.
256. Probstein, RF. Physicochemical hydrodynamics : an introduction. New York: Wiley; 1994.
257. Terabe S, Otsuka K, Ichikawa K, Tsuchiya A, Ando T. Analytical Chemistry 1984;56:111–113.
258. Harrison DJ, Fluri K, Seiler K, Fan ZH, Effenhauser CS, Manz A. Science 1993;261:895–897. [PubMed: 17783736]
259. Manz A, Effenhauser CS, Burggraf N, Harrison DJ, Seiler K, Fluri K. Journal of Micromechanics and Microengineering 1994;4:257–265.
260. McKnight TE, Culbertson CT, Jacobson SC, Ramsey JM. Analytical Chemistry 2001;73:4045–4049. [PubMed: 11534734]
261. Molho JI, Herr AE, Mosier BP, Santiago JG, Kenny TW, Brennen RA, Gordon GB, Mohammadi B. Analytical Chemistry 2001;73:1350–1360.
262. Fu LM, Yang RJ, Lee GB, Liu HH. Analytical Chemistry 2002;74:5084–5091. [PubMed: 12380834]
263. Fu LM, Yang RJ. Electrophoresis 2003;24:1253–1260. [PubMed: 12707919]
264. Seiler K, Fan ZHH, Fluri K, Harrison DJ. Analytical Chemistry 1994;66:3485–3491.
265. Lin CH, Lee GB, Chen SH, Chang GL. Sensors and Actuators a-Physical 2003;107:125–131.
266. Guzman KAD, Karnik RN, Newman JS, Majumdar A. Journal of Microelectromechanical Systems 2006;15:237–245.
267. Woolley AT, Mathies RA. Proceedings of the National Academy of Sciences of the United States of America 1994;91:11348–11352. [PubMed: 7972062]
268. Woolley AT, Mathies RA. Analytical Chemistry 1995;67:3676–3680. [PubMed: 8644919]
269. Li Y, Xiang R, Wilkins JA, Honrath C. Electrophoresis 2004;25:2242–2256. [PubMed: 15274008]
270. Kremser L, Blaas D, Kenndler E. Electrophoresis 2004;25:2282–2291. [PubMed: 15274010]
271. Bousse L, Cohen C, Nikiforov T, Chow A, Kopf-Sill AR, Dubrow R, Parce JW. Annual Review of Biophysics and Biomolecular Structure 2000;29:155–181.
272. Erickson D, Li DQ. Analytica Chimica Acta 2004;507:11–26.
273. Karnik R, Fan R, Yue M, Li DY, Yang PD, Majumdar A. Nano Letters 2005;5:943–948. [PubMed: 15884899]
274. Karnik R, Castelino K, Majumdar A. Applied Physics Letters 2006;88:123114.
275. Pohl, HA. Dielectrophoresis : the behavior of neutral matter in nonuniform electric fields. Cambridge, New York: Cambridge University Press; 1978.
276. Ramos A, Morgan H, Green NG, Castellanos A. Journal of Physics D-Applied Physics 1998;31:2338–2353.

277. Wong PK, Chen CY, Wang TH, Ho CM. Analytical Chemistry 2004;76:6908–6914. [PubMed: 15571340]
278. Albrecht DR, Tsang VL, Sah RL, Bhatia SN. Lab on a Chip 2005;5:111–118. [PubMed: 15616749]
279. Gray DS, Tan JL, Voldman J, Chen CS. Biosensors & Bioelectronics 2004;19:1765–1774. [PubMed: 15198083]
280. Yamamoto K, Akita S, Nakayama Y. Journal of Physics D-Applied Physics 1998;31:L34–L36.
281. Diehl MR, Yaliraki SN, Beckman RA, Barahona M, Heath JR. Angewandte Chemie 2002;114:363–366.
282. Nagahara LA, Amlani I, Lewenstein J, Tsui RK. Applied Physics Letters 2002;80:3826–3828.
283. Fung CMKM, Wong VTS, Chan RHM, Li WJ. IEEE Transactions on Nanotechnology 2004;3:395–403.
284. Chan RHM, Fung CKM, Li WJ. Nanotechnology 2004;15:S672–S677.
285. Li JQ, Zhang Q, Peng N, Zhu Q. Applied Physics Letters 2005;86:153116.
286. Holzel R, Calander N, Chiragwandi Z, Willander M, Bier FF. Physical Review Letters 2005;95:128102. [PubMed: 16197115]
287. Asokan SB, Jawerth L, Carroll RL, Cheney RE, Washburn S, Superfine R. Nano Letters 2003;3:431–437.
288. Washizu M, Kurosawa O. IEEE Transactions on Industry Applications 1990;26:1165–1172.
289. Hughes MP, Morgan H. Journal of Physics D-Applied Physics 1998;31:2205–2210.
290. Bezryadin A, Dekker C, Schmid G. Applied Physics Letters 1997;71:1273–1275.
291. Burke, PJ. Encyclopedia of Nanoscience and Nanotechnology. Nalwa, HS., editor. Vol. Vol. 6. American Scientific Publishers; 2004. p. 623-642.
292. Krupke R, Hennrich F, von Lohneysen H, Kappes MM. Science 2003;301:344–347. [PubMed: 12829788]
293. Huang Y, Wang XB, Becker FF, Gascoyne PRC. Biophysical Journal 1997;73:1118–1129. [PubMed: 9251828]
294. Wang XB, Yang J, Huang Y, Vykoukal J, Becker FF, Gascoyne PRC. Analytical Chemistry 2000;72:832–839. [PubMed: 10701270]
295. Peng HQ, Alvarez NT, Kittrell C, Hauge RH, Schmidt HK. Journal of the American Chemical Society 2006;128:8396–8397. [PubMed: 16802794]
296. Chiou PY, Ohta AT, Wu MC. Nature 2005;436:370–372. [PubMed: 16034413]
297. Ramos A, Morgan H, Green NG, Castellanos A. Journal of Colloid and Interface Science 1999;217:420–422. [PubMed: 10469552]
298. Scott M, Kaler KVIS, Paul R. Journal of Colloid and Interface Science 2001;238:449–451. [PubMed: 11374941]
299. Green NG, Ramos A, Gonzalez A, Morgan H, Castellanos A. Physical Review E 2000;61:4011–4018.
300. Gonzalez A, Ramos A, Green NG, Castellanos A, Morgan H. Physical Review E 2000;61:4019–4028.
301. Green NG, Ramos A, Gonzalez A, Morgan H, Castellanos A. Physical Review 2002;E 66:026305. [PubMed: 12241283]
302. Zhou H, White LR, Tilton RD. Journal of Colloid and Interface Science 2005;285:179–191. [PubMed: 15797412]
303. Bown MR, Meinhart CD. Microfluidics and Nanofluidics 2006;2:513–523.
304. Huang Y, Ewalt KL, Tirado M, Haigis TR, Forster A, Ackley D, Heller MJ, O'Connell JP, Krihak M. Analytical Chemistry 2001;73:1549–1559. [PubMed: 11321308]
305. Cheng J, Sheldon EL, Wu L, Uribe A, Gerrue LO, Carrino J, Heller MJ, O'Connell JP. Nature Biotechnology 1998;16:541–546.
306. Morgan, H.; Green, NG. AC electrokinetics : colloids and nanoparticles. Philadelphia, PA: Research Studies Press; 2003.
307. Hughes MP. Nanotechnology 2000;11:124–132.

308. Wong PK, Wang TH, Deval JH, Ho CM. IEEE-ASME Transactions on Mechatronics 2004;9:366–376.
309. Voldman J. Annual Review of Biomedical Engineering 2006;8:425–454.
310. Hess H, Matzke CM, Doot RK, Clemmens J, Bachand GD, Bunker BC, Vogel V. Nano Letters 2003;3:1651–1655.
311. Limberis L, Stewart RJ. Nanotechnology 2000;11:47–51.
312. Hess H, Clemmens J, Qin D, Howard J, Vogel V. Nano Letters 2001;1:235–239.
313. Diez S, Reuther C, Dinu C, Seidel R, Mertig M, Pompe W, Howard J. Nano Letters 2003;3:1251–1254.
314. Clemmens J, Hess H, Doot R, Matzke CM, Bachand GD, Vogel V. Lab on a Chip 2004;4:83–86. [PubMed: 15052344]
315. Yokokawa R, Takeuchi S, Kon T, Nishiura M, Sutoh K, Fujita H. Nano Letters 2004;4:2265–2270.
316. Jia LL, Moorjani SG, Jackson TN, Hancock WO. Biomedical Microdevices 2004;6:67–74. [PubMed: 15307447]
317. Clemmens J, Hess H, Howard J, Vogel V. Langmuir 2003;19:1738–1744.
318. Hiratsuka Y, Tada T, Oiwa K, Kanayama T, Uyeda TQP. Biophysical Journal 2001;81:1555–1561. [PubMed: 11509368]
319. Allemand JF, Bensimon D, Jullien L, Bensimon A, Croquette V. Biophysical Journal 1997;73:2064–2070. [PubMed: 9336201]
320. Ho CM, Tai YC. Annual Review of Fluid Mechanics 1998;30:579–612.
321. Ho, CM. Proceedings of 14th Annual IEEE International Conference on Micro Electro Mechanical Systems; Switzerland: Interlaken; 2001. p. 375-384.
322. Kim CJ, Pisano AP, Muller RS. Journal of Microelectromechanical Systems 1992;1:31–36.
323. Zhou JWL, Chan HY, To TKH, Lai KWC, Li WJ. IEEE-ASME Transactions on Mechatronics 2004;9:334–342.
324. Lu YW, Kim CJ. Applied Physics Letters 2006;89:164101.
325. Fennimore AM, Yuzvinsky TD, Han WQ, Fuhrer MS, Cumings J, Zettl A. Nature 2003;424:408–410. [PubMed: 12879064]
326. Fillingame RH. Science 1999;286:1687–1688. [PubMed: 10610565]
327. Hess H, Bachand GD, Vogel V. Chemistry-a European Journal 2004;10:2110–2116.
328. Soong RK, Bachand GD, Neves HP, Olkhovets AG, Craighead HG, Mon-temagno CD. Science 2000;290:1555–1558. [PubMed: 11090349]
329. Yoshida, Y.; Shimozawa, T.; Nishizaka, T.; Ishiwata, S.; Takeuchi, S. Proceedings of 19th IEEE International Conference on Micro Electro Mechanical Systems; Turkey: Istanbul; 2006. p. 134-137.
330. Purcell EM. American Journal of Physics 1977;45:3–11.
331. Berg HC. Annual Review of Biochemistry 2003;72:19–54.
332. Silverma M, Simon M. Nature 1974;249:73–74. [PubMed: 4598030]
333. Oster G, Wang HY. Trends in Cell Biology 2003;13:114–121. [PubMed: 12628343]
334. Tung S, Kim JW. IEEE Transactions on Automation Science and Engineering 2006;3:260–263.
335. Liu Y, Flood AH, Bonvallett PA, Vignon SA, Northrop BH, Tseng HR, Jeppesen JO, Huang TJ, Brough B, Baller M, Magonov S, Solares SD, God-dard WA, Ho CM, Stoddart JF. Journal of the American Chemical Society 2005;127:9745–9759. [PubMed: 15998079]
336. Collier CP, Wong EW, Belohradsky M, Raymo FM, Stoddart JF, Kuekes PJ, Williams RS, Heath JR. Science 1999;285:391–394. [PubMed: 10411498]
337. Berna J, Leigh DA, Lubomska M, Mendoza SM, Perez EM, Rudolf P, Teobaldi G, Zerbetto F. Nature Materials 2005;4:704–710.
338. Tseng HR, Wu DM, Fang NXL, Zhang X, Stoddart JF. Chemphyschem 2004;5:111–116. [PubMed: 14999851]
339. Huang TJ, Tseng HR, Sha L, Lu WX, Brough B, Flood AH, Yu BD, Celestre PC, Chang JP, Stoddart JF, Ho CM. Nano Letters 2004;4:2065–2071.

340. Huang TJ, Brough B, Ho CM, Liu Y, Flood AH, Bonvallet PA, Tseng HR, Stoddart JF, Baller M, Magonov S. Applied Physics Letters 2004;85:5391–5393.

341. Brough B, Northrop BH, Schmidt JJ, Tseng HR, Houk KN, Stoddart JF, Ho CM. Proceedings of the National Academy of Sciences of the United States of America 2006;103:8583–8588. [PubMed: 16735470]

342. Browne WR, Feringa BL. Nature Nanotechnology 2006;1:25–35.

343. Hunter, IW.; Lafontaine, S. Technical Digest of Solid-State Sensor and Actuator Workshop. South Carolina, USA: Hiton Head Island; 1992. p. 178-185.

344. Xi JZ, Schmidt JJ, Montemagno CD. Nature Materials 2005;4:180–184.

345. Shaw KA, Zhang ZL, Macdonald NC. Sensors and Actuators a-Physical 1994;40:63–70.

346. Eigler DM, Schweizer EK. Nature 1990;344:524–526.

347. Karsenti E. Nature Reviews Molecular Cell Biology 2008;9:255–262.

348. Wong, PK. Ph.D dissertation, Mechanical and Aerospace Engineering Department. Los Angeles: University of California; 2005.

349. Ho D, Garcia D, Ho CM. Journal of Nanoscience and Nanotechnology 2006;6:875–891. [PubMed: 16736745]

350. Wong PK, Yu F, Shahangian A, Cheng G, Sun R, Ho CM. Proceedings of National Academy of Sciences of the United States of America 2008;105:5105–5110.

351. Klein MG, Shi WX, Ramagopal U, Tseng Y, Wirtz D, Kovar DR, Staiger CJ, Almo SC. Structure 2004;12:999–1013. [PubMed: 15274920]

352. Mclaughlin PJ, Gooch JT, Mannherz HG, Weeds AG. Nature 1993;364:685–692. [PubMed: 8395021]

353. Burtnick LD, Koepf EK, Grimes J, Jones EY, Stuart DI, McLaughlin PJ, Robinson RC. Cell 1997;90:661–670. [PubMed: 9288746]

354. Robinson RC, Turbedsky K, Kaiser DA, Marchand JB, Higgs HN, Choe S, Pollard TD. Science 2001;294:1679–1684. [PubMed: 11721045]

355. Ott A, Magnasco M, Simon A, Libchaber A. Physical Review E 1993;48:R1642–R1645.

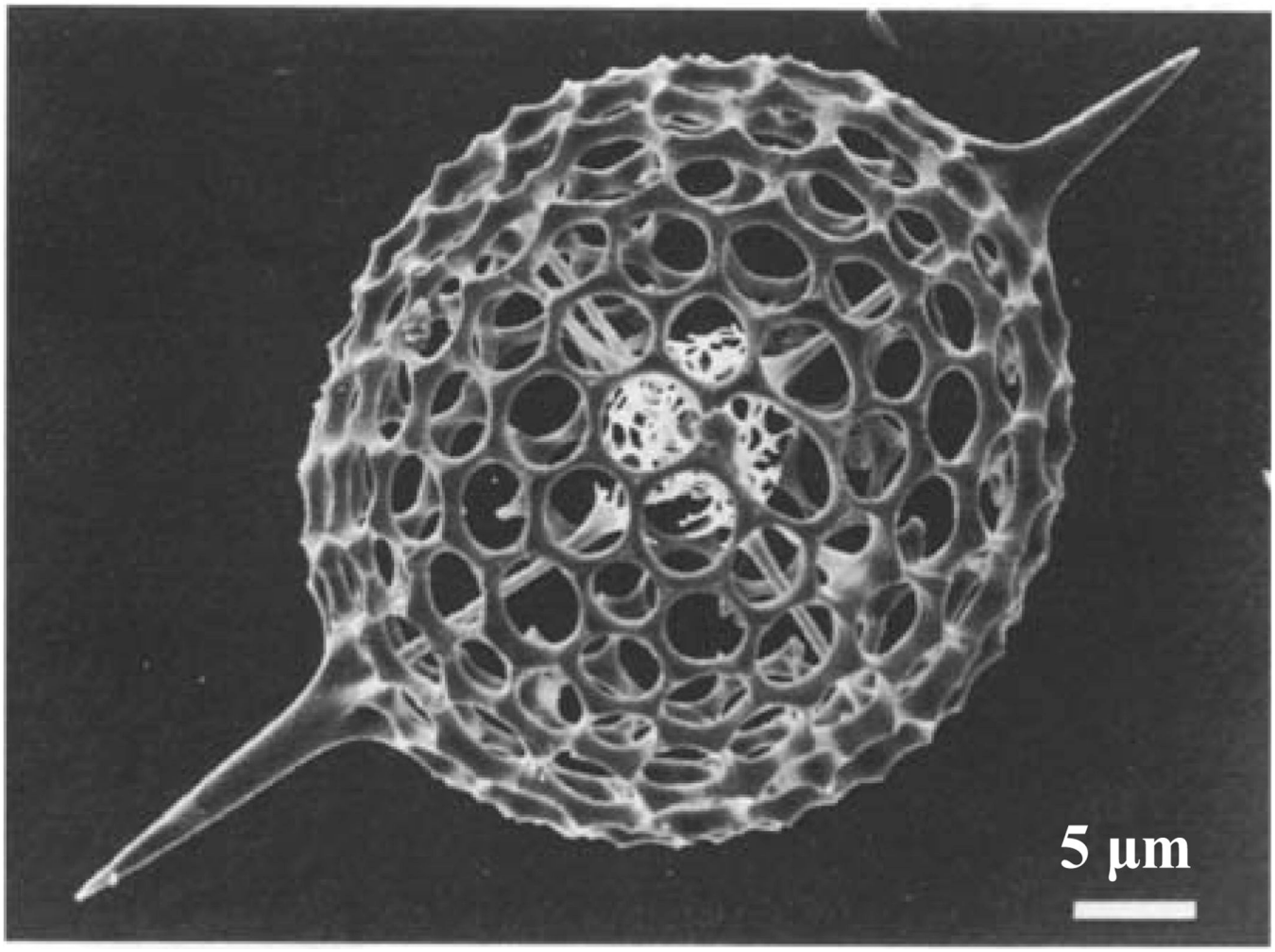

Figure 1.
A radiolarian micro-skeleton with single porous shell and large centrally organized radial spines. (Reprinted with permission from Oxford University Press and courtesy of Prof. Stephen Mann, University of Bristol, UK)

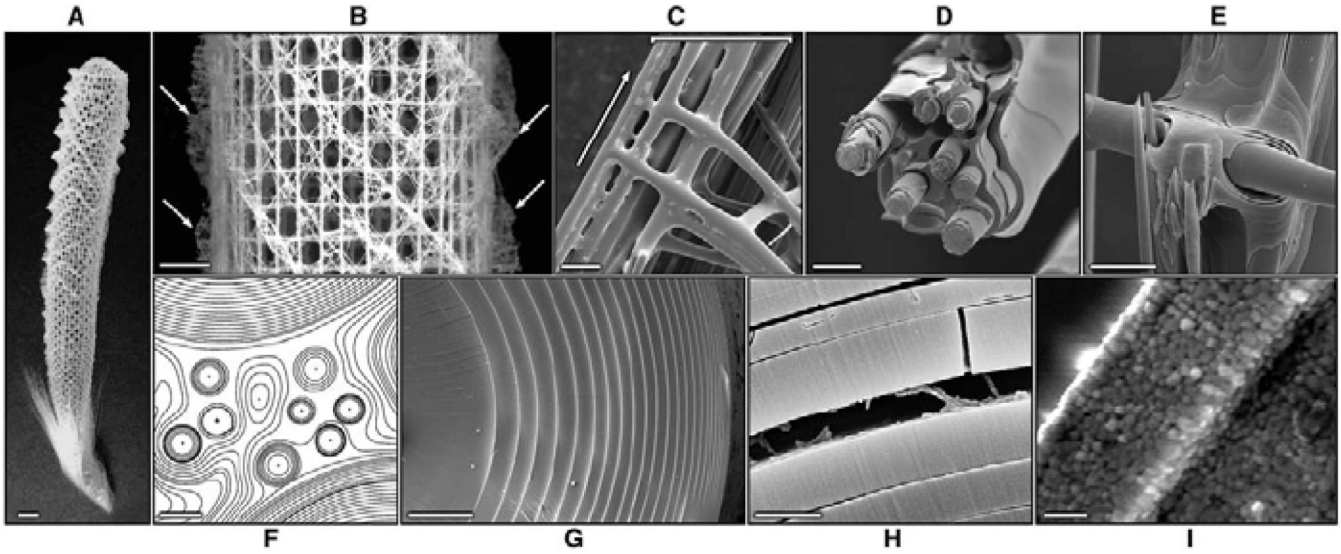

Figure 2.
Sectioning of the skeleton of Euplectella sp showing the structural hierarchy from nanoscale (I) to macroscale domain (A–B). Scale bar, A: 1cm, B: 5mm, C: 100μm, D:20μm, E:25μm, F: 10μm, G:5μm, H:1μm, I:500nm. (Reprinted with permission from Aizenberg et al., Science, 2005, 309: 275–278, Copyright 2005, AAAS)

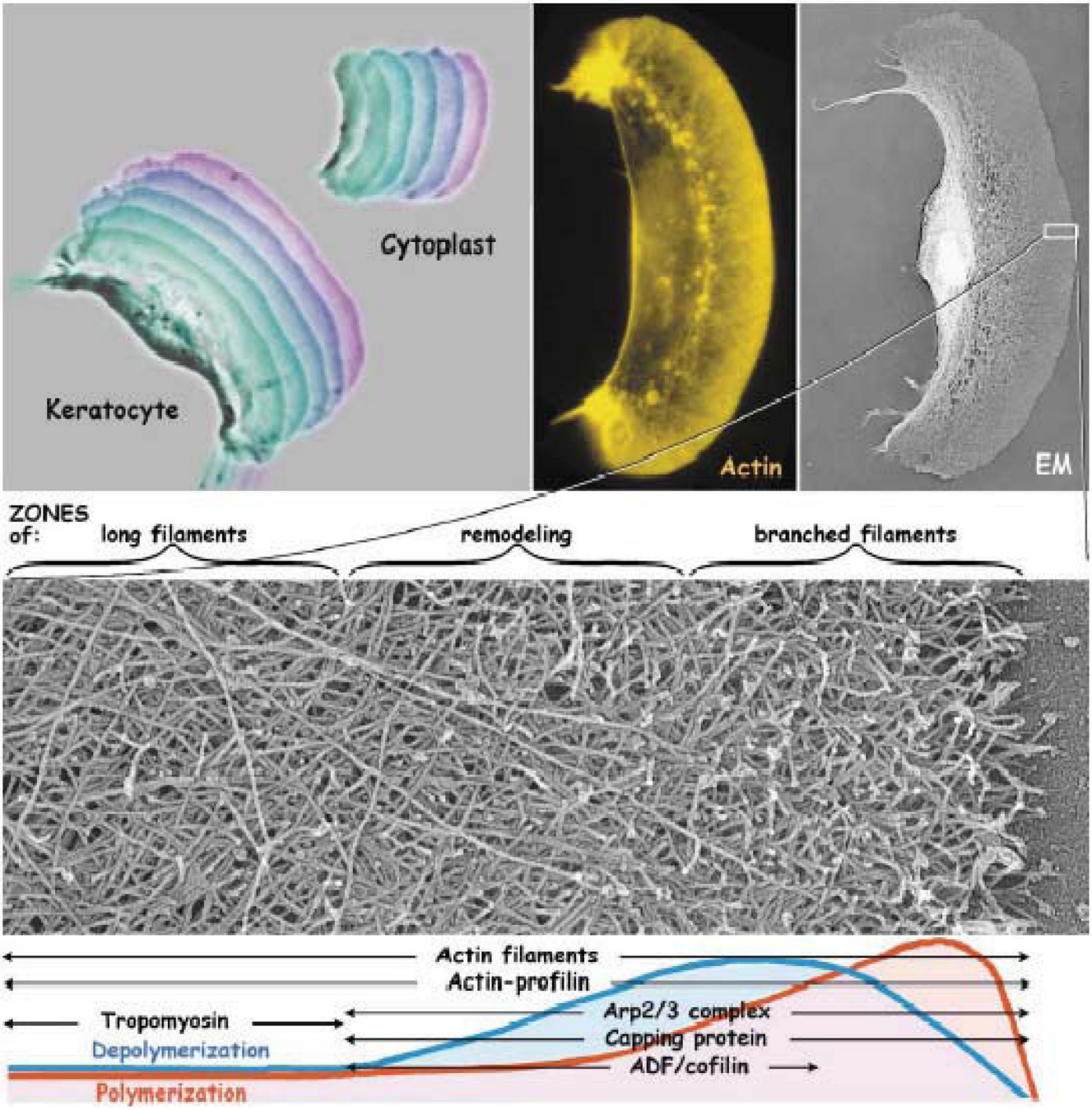

Figure 3.

Cell movement is originated from the spatially and temporally controlled assembly and disassembly of molecular proteins. (Top left) Overlays of phase contrast micrographs (in 15 sec intervals) showing the motility of a keratocyte and a keratocyte cytoplast. (Top middle) Fluorescently labeled actin filaments and (Top right and bottom) the corresponding electron micrographs (Reprinted with permission from Pollard and Borisy, Cell, 2003, 112:453–465, copyright 2003, Elsevier)

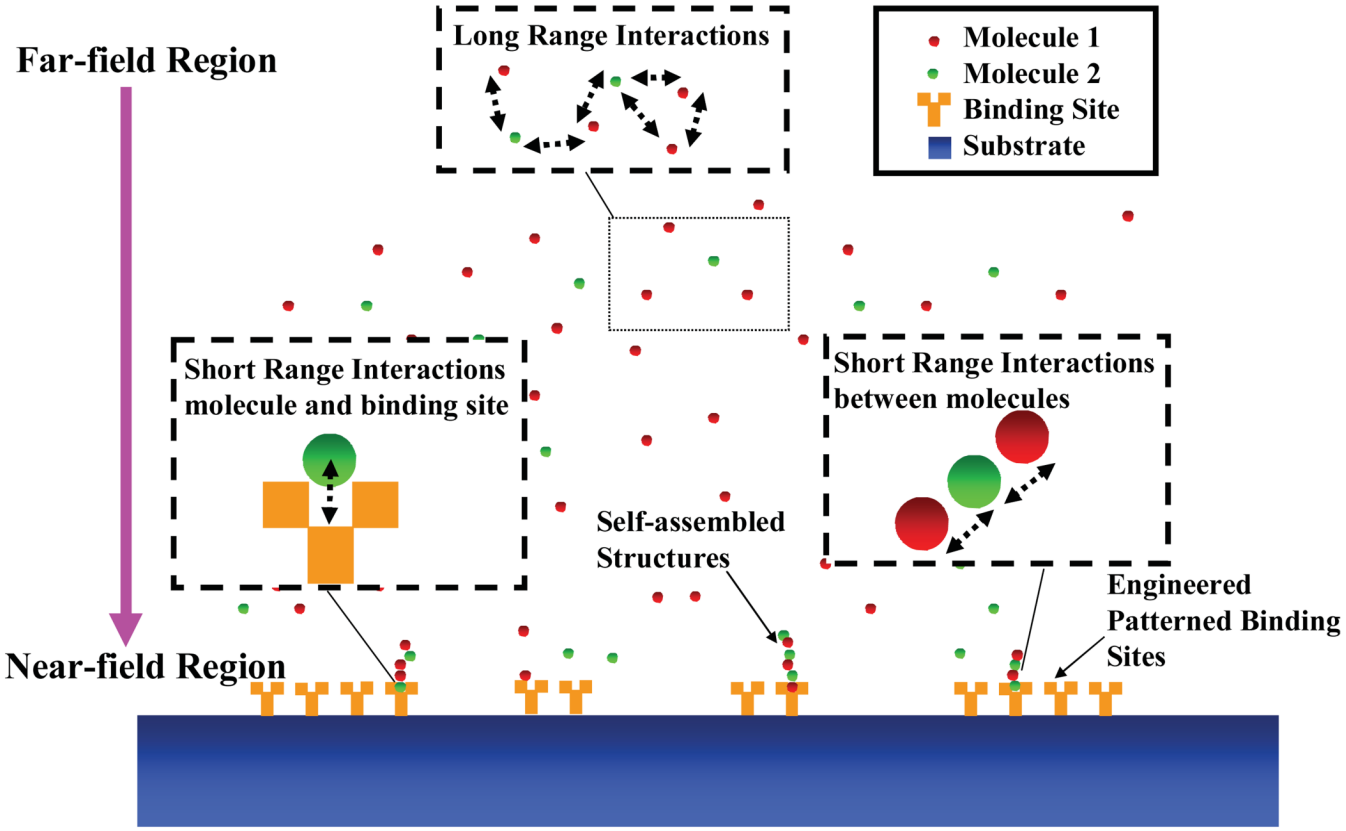

Figure 4.
Conceptual representation of intermolecular interactions involved in a guided self-assembled system utilizing top-down and bottom-up fabrication schemes

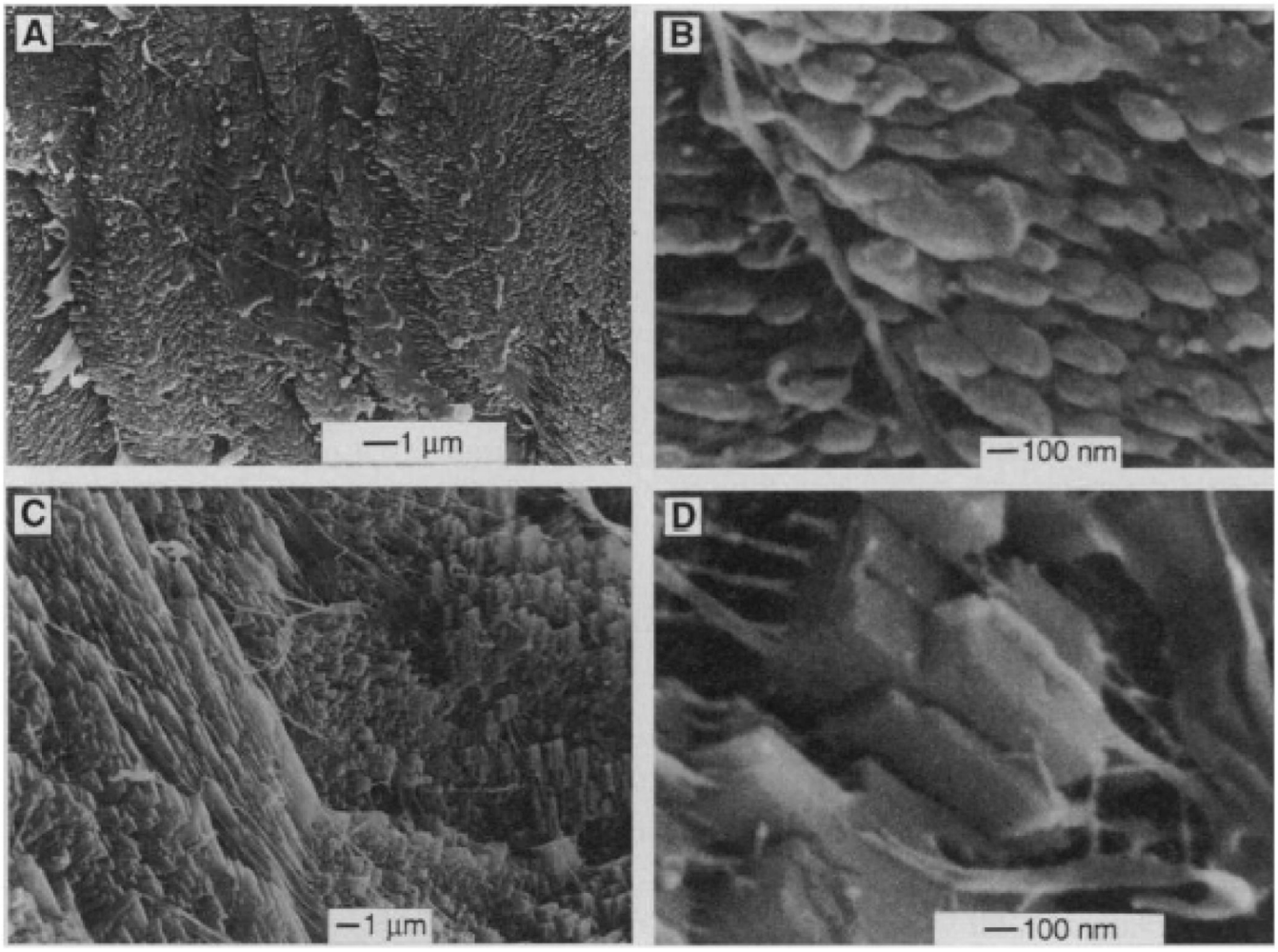

Figure 5.
The formation of aragonite and calcite crystals induced by protein macromolecules. (A and B) Aragonite induced by the soluble glycoproteins extracted from the aragonitic layer of the shell of *Elliptio sp.* (C and D) Calcite induced from the soluble glycoproteins extracted from the calcitic shell of *M. californianus*. (Reprinted with permission from Falini et al., Science, 1996, 271: 67–69 Copyright 1996, AAAS)

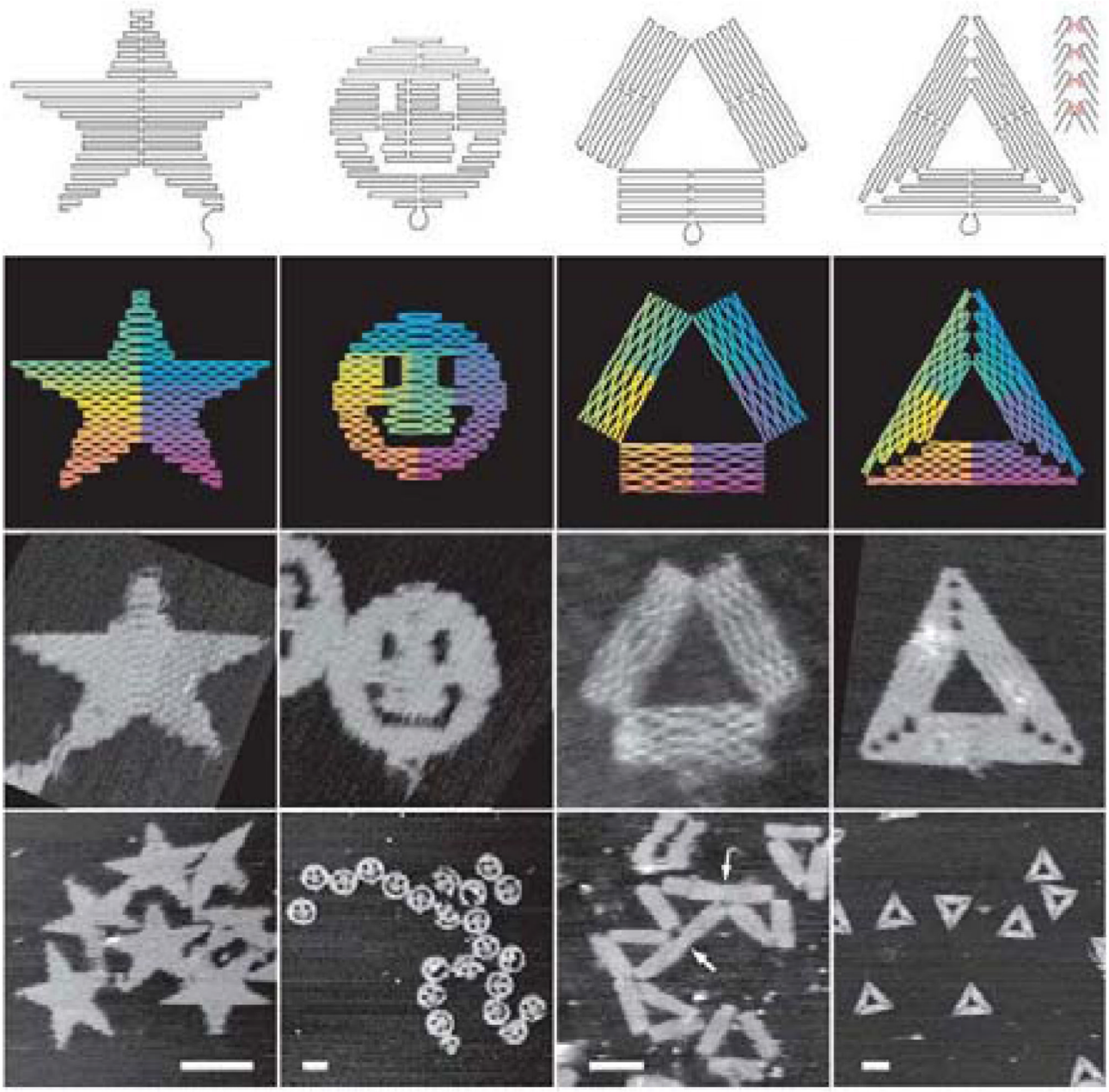

Figure 6.
Pattern formation by nanoscale self-assembly of DNA. Scale bar, 100nm. (Reprinted by permission from Macmillian Publishers Ltd: P.W.K. Rothermund, Nature, 2006, 440: 297–302, copyright 2006)

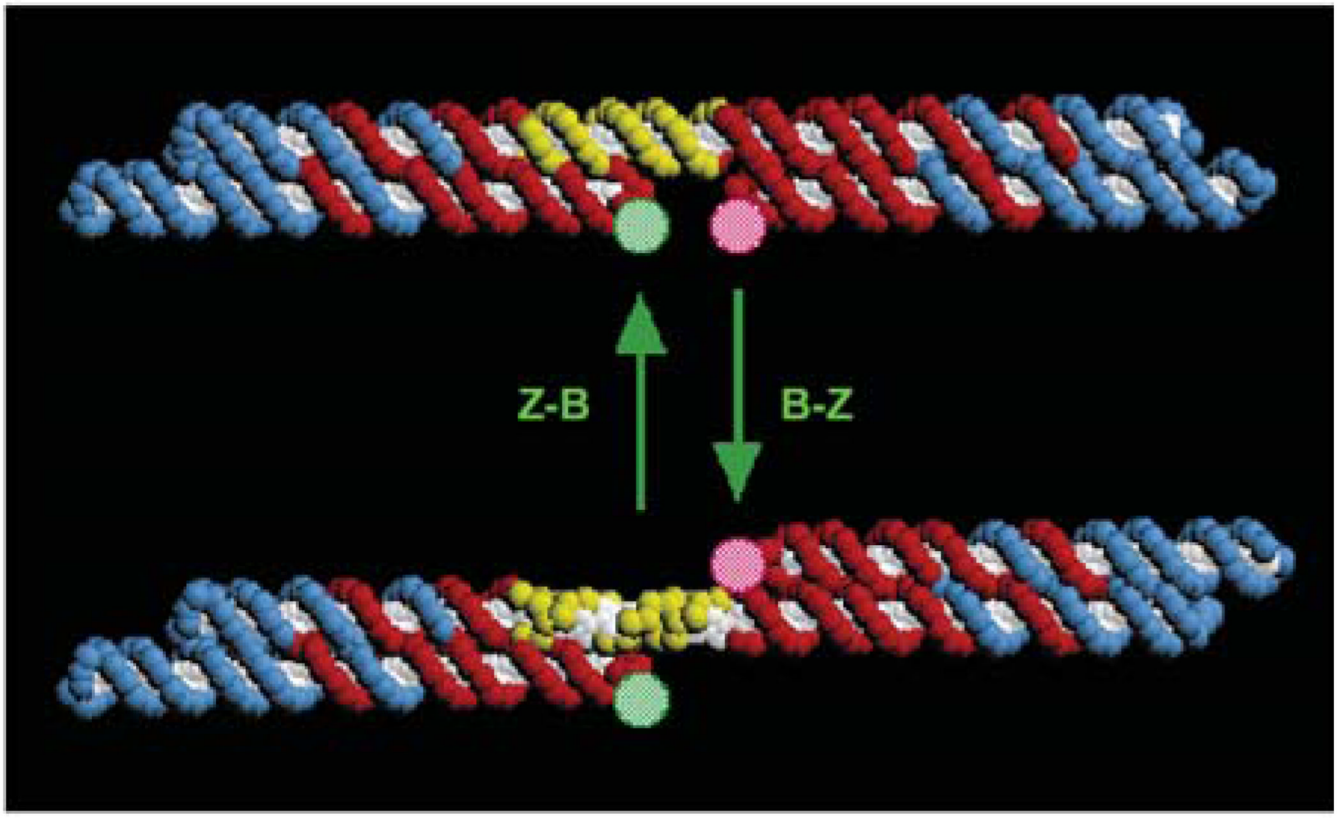

Figure 7.
A DNA nanomechanical rotary device based on B-form and Z-form DNA conformational changes. (Reprinted by permission from Macmillian Publishers Ltd: Mao et al., Nature, 1999, 397:144–146, copyright 1999)

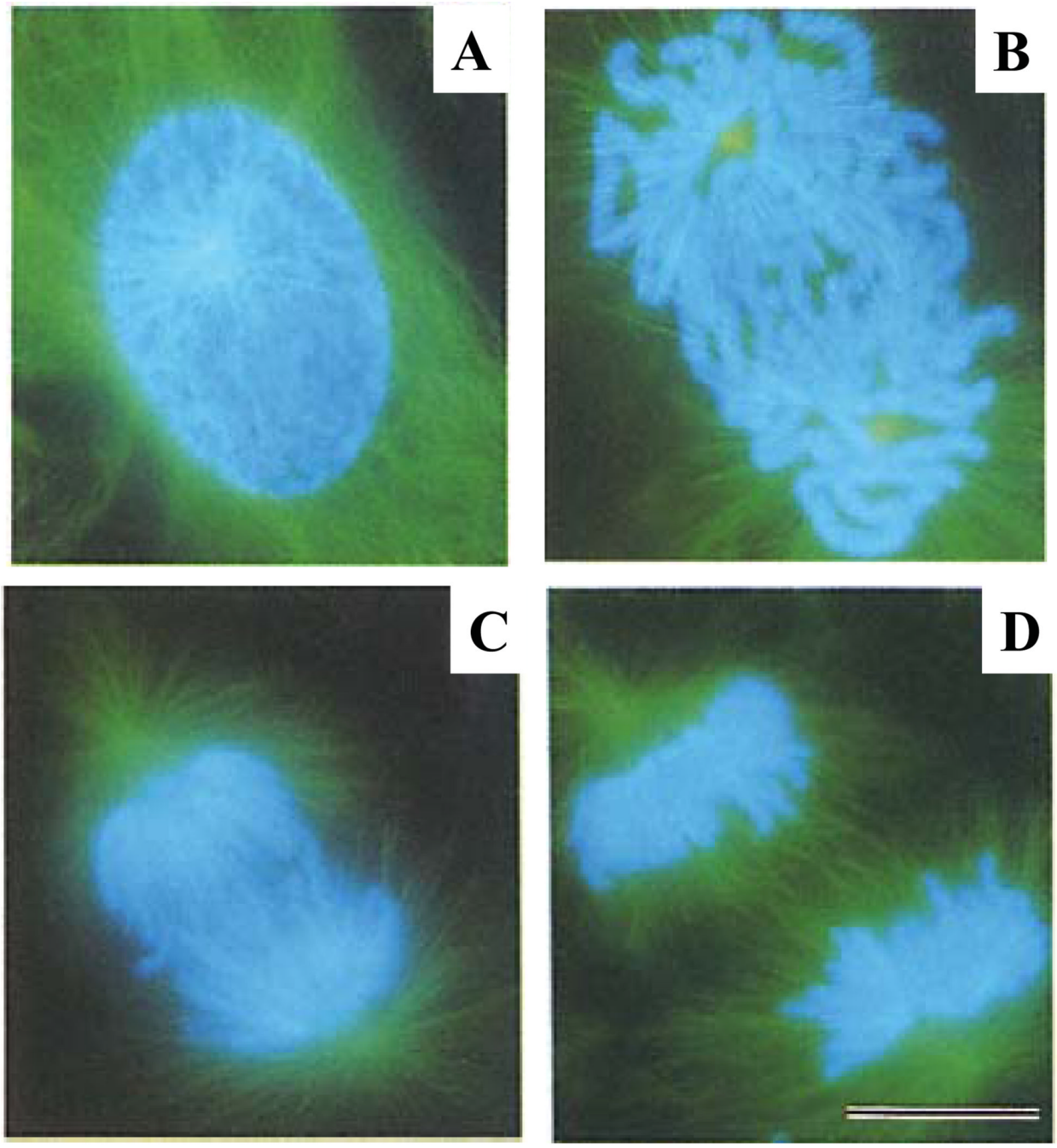

Figure 8.
Fluorescent image sequences showing the spatial distribution of chromosomes (shown in blue) and microtubules (shown in green) at 4 different stages of the mitosis process (from A – D). Scale bar, 20μm. (Reproduced by permission from The Journal of Cell Biology, 1993, 122: 361 – 372. Copyright 1993 The Rockefeller University Press)

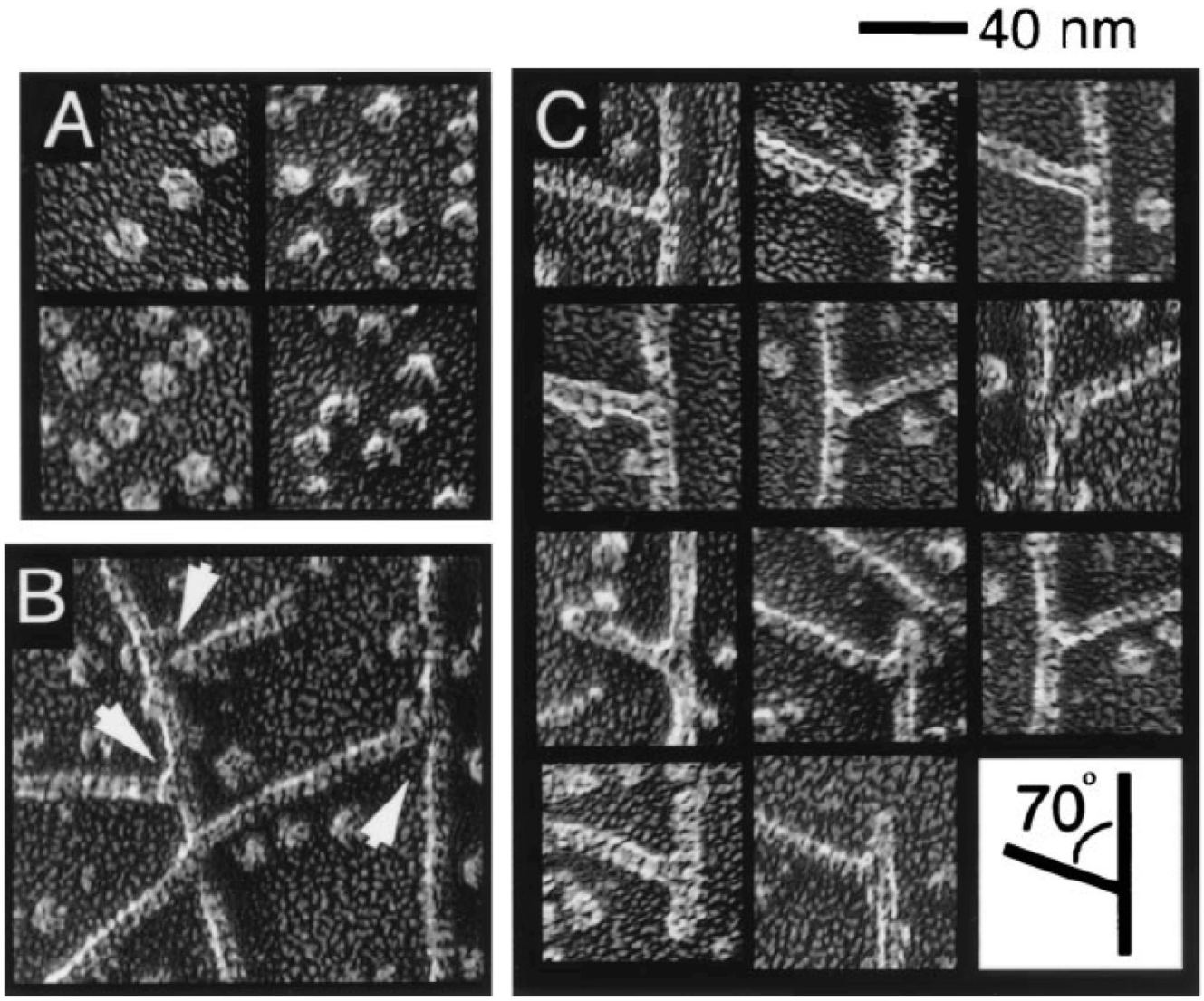

Figure 9.

Electron micrograph showing the branching structures formed by Arp2/3 and F-actin. (A) Arp2/3 complex. (B) F-actin forms branched structures with the presence of Arp2/3. (C) The side-branching structures are at 70° with respect to the main F-actin. (Reproduced from Proceedings of National Academy of Sciences, USA, 1998, 95: 6181 – 6186. Copyright 1998 The National Academy of Sciences, USA)

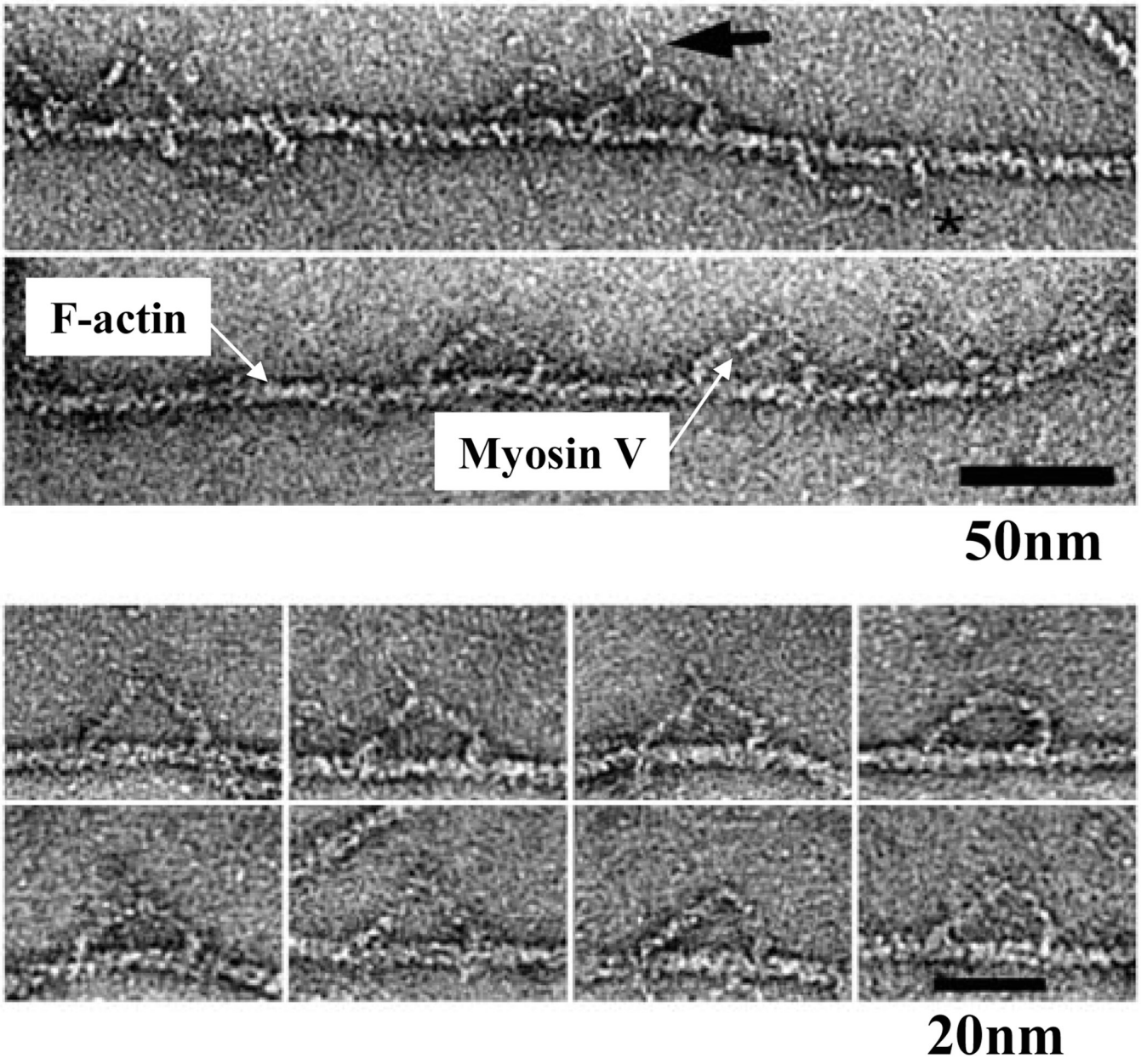

Figure 10.
Electron micrograph showing the structure of myosin V bound to an actin filament. (Lower panel) Myosin V spans a distance of 13 actin subunits. (Reprinted by permission from Macmillian Publishers Ltd: Walker et al., Nature, 2000, 405: 804–807, copyright 2000)

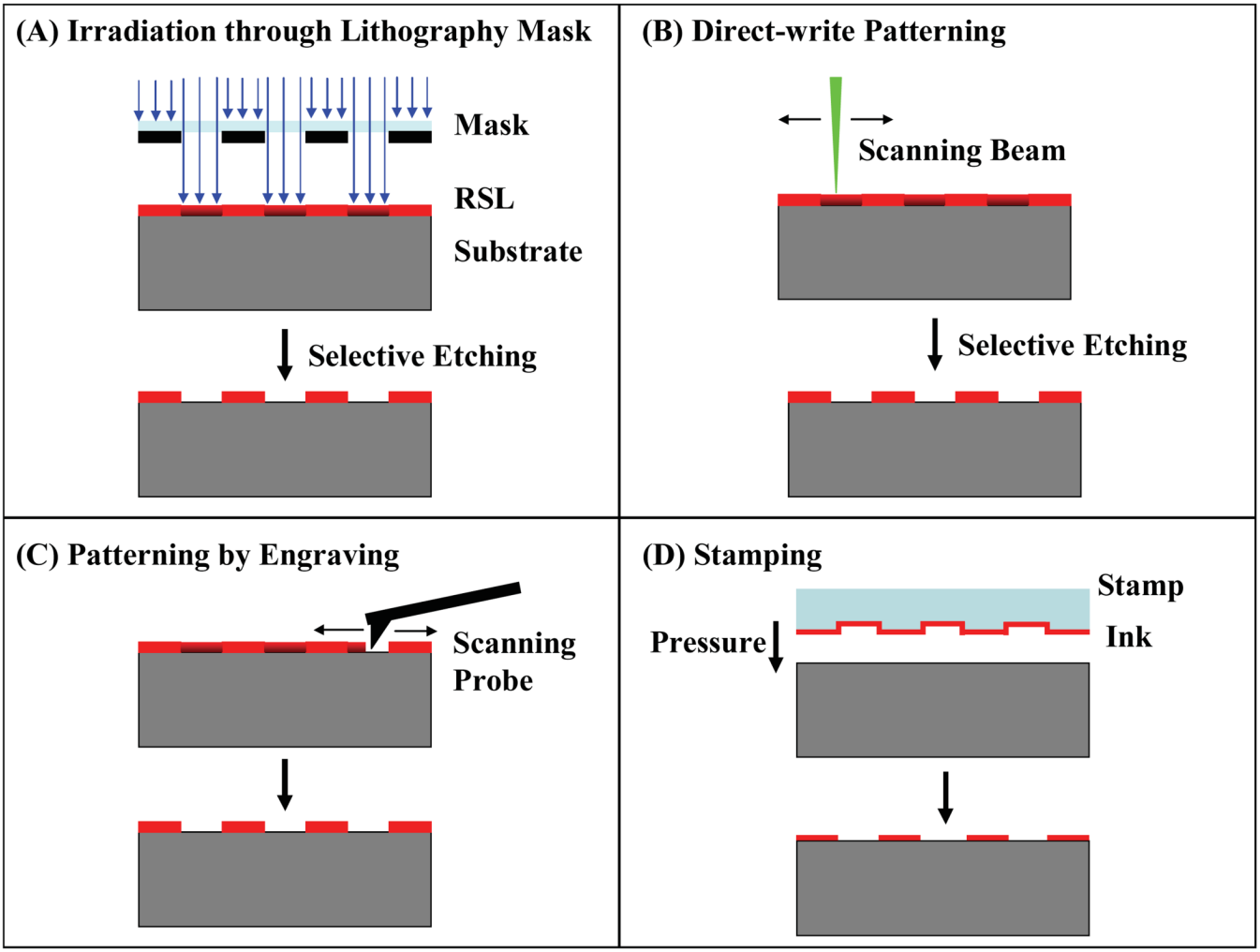

Figure 11.
Concepts of selected lithography technologies

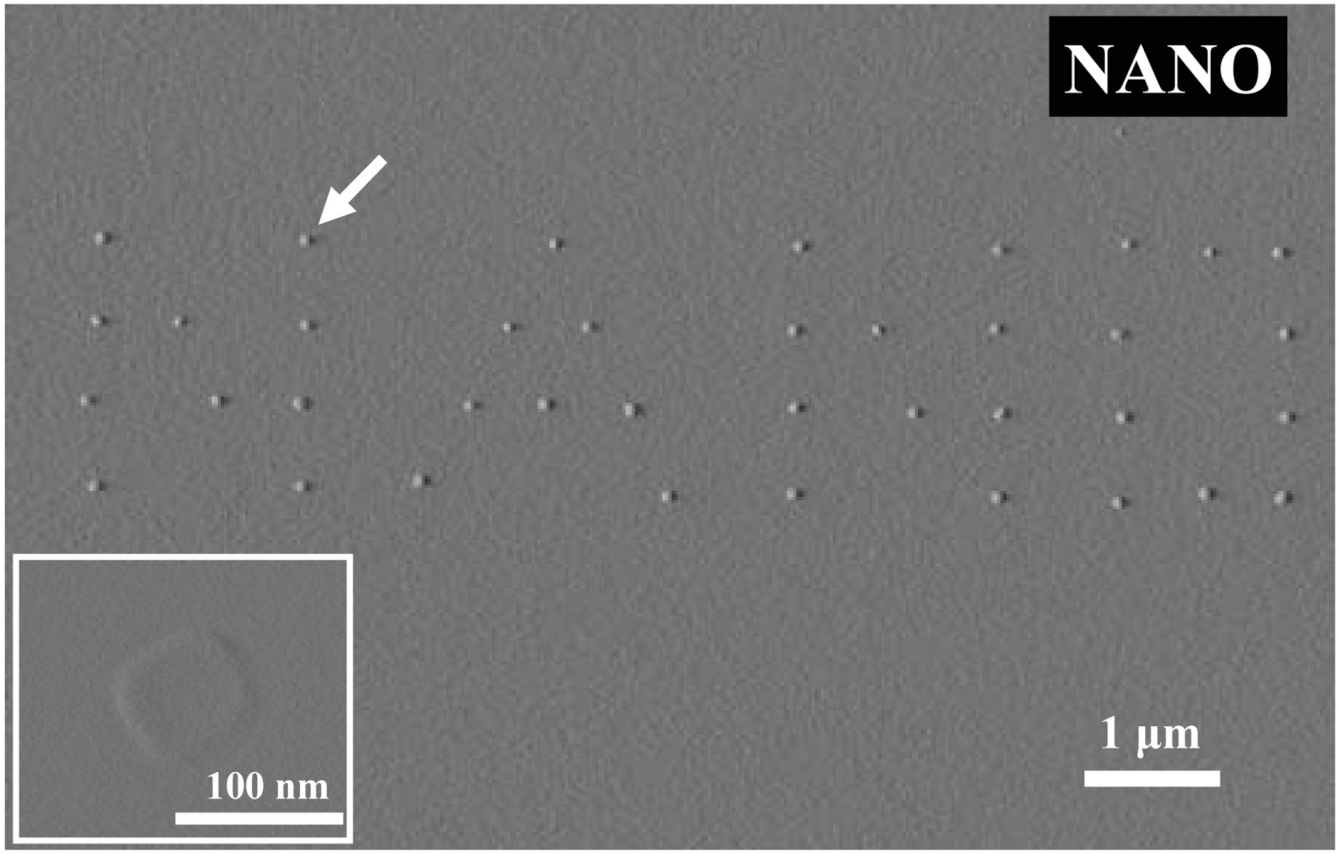

Figure 12.
Synthesis of KCl nanocrystals on predetermined locations through wetting/dewetting of droplets on electron beam lithography defined patterns (196)

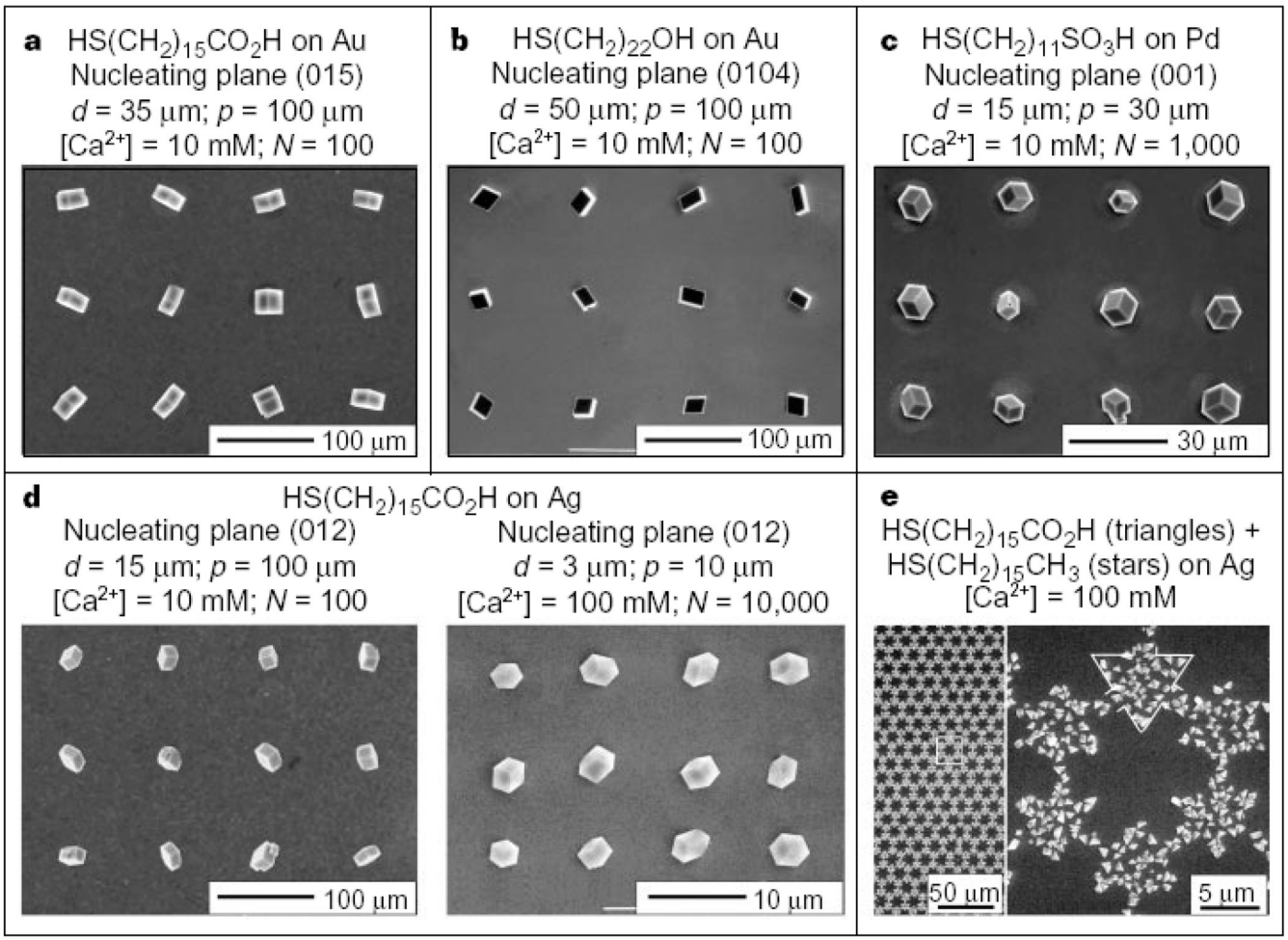

Figure 13.

Control of crystallographic orientation of CaCO3 crystals by using a self-assembled monolayer at pre-determined locations of a surface (Reprinted by permission from Macmillian Publishers Ltd: Aizenberg et al., Nature, 1999, 398: 495–498, copyright 1999)

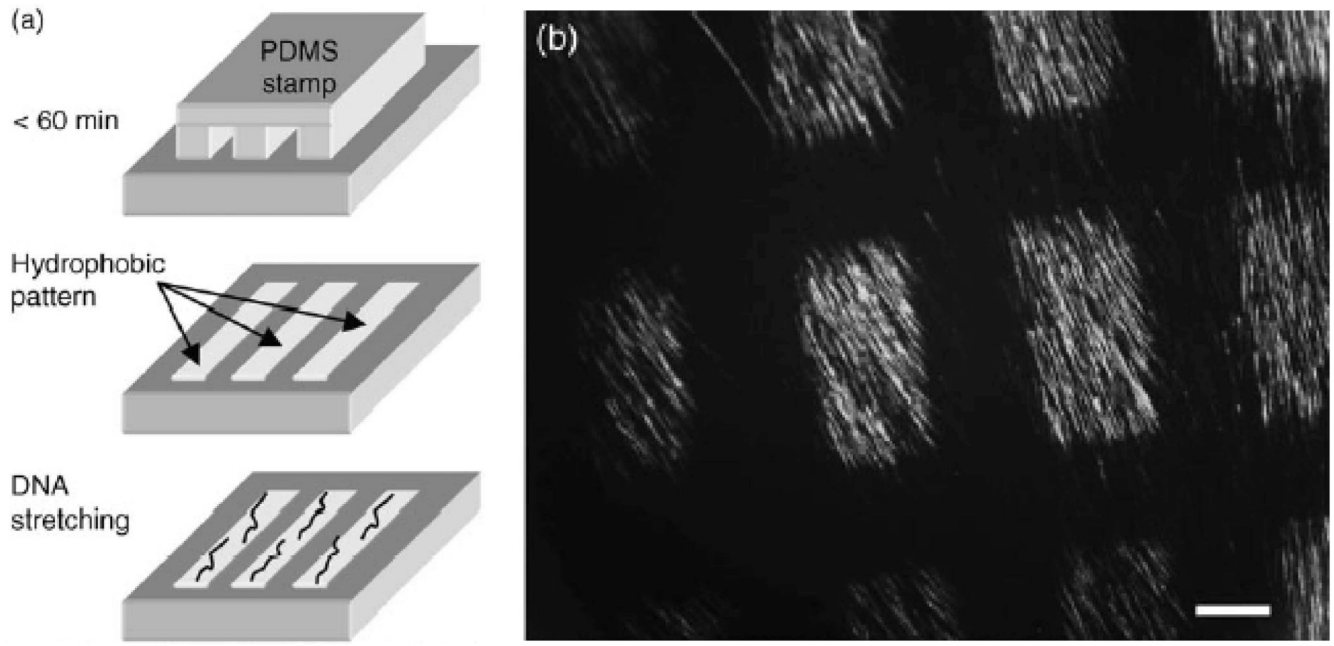

Figure 14.
DNA patterning through soft lithography and molecular combing. Scale bar, 25μm. (Reprinted by permission from Wiley InterScience: Björk et al., Small, 2006, 2:1068–1074, copyright 2006)

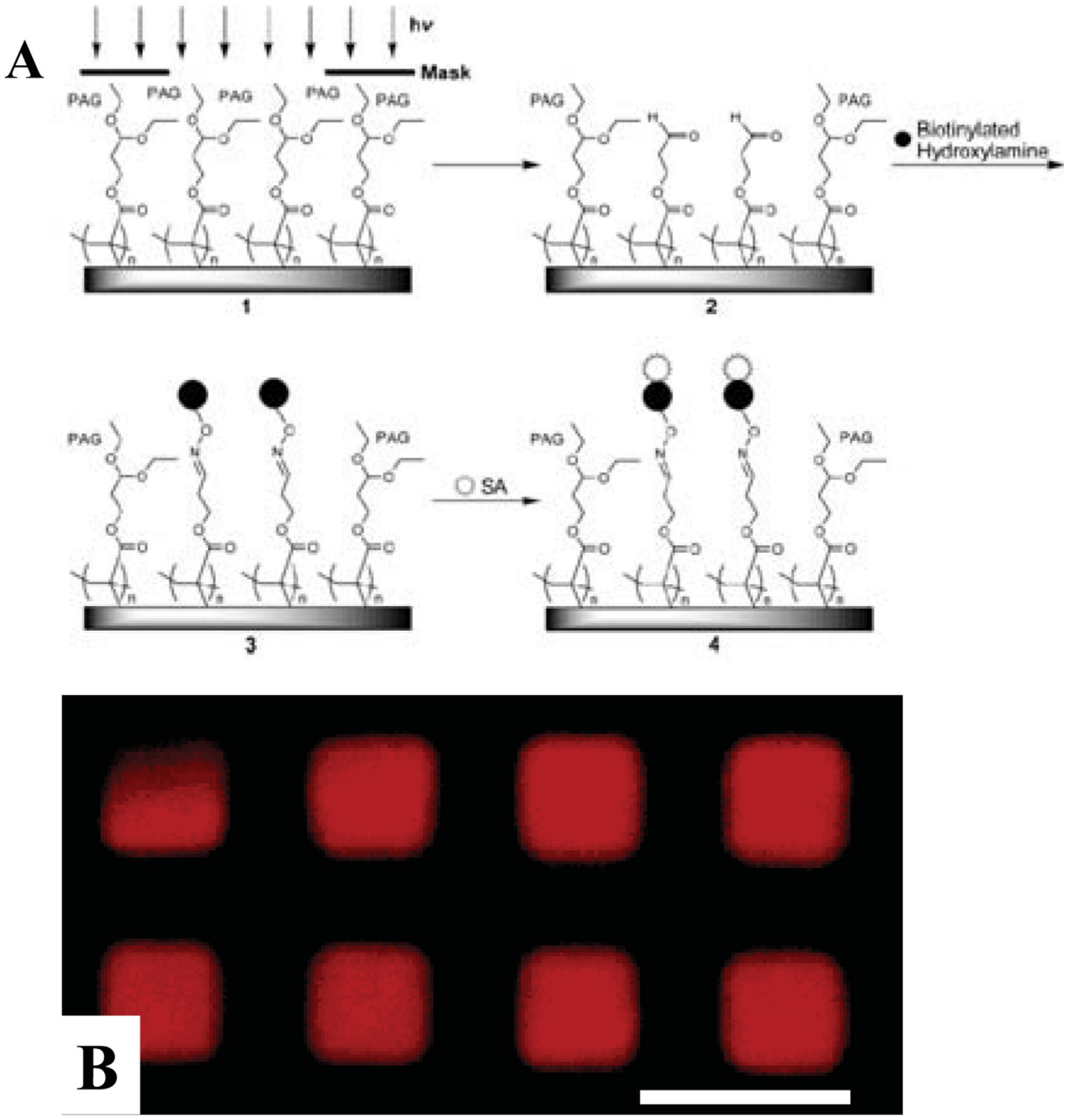

Figure 15.

2D protein patterning through optical lithography. (A) Process flow showing the surface functional groups activation by deep UV light and the subsequent protein attachment. (B) Red fluorescent streptavidin was patterned to locations of UV exposure after incubation of a biotinylated aldehyde reactive probe. Scale bar, 25μm. (Reprinted by permission from American Chemical Society: K.L. Christman & H.D. Maynard, Langmuir, 2005, 21:8389–8393, copyright 2005)

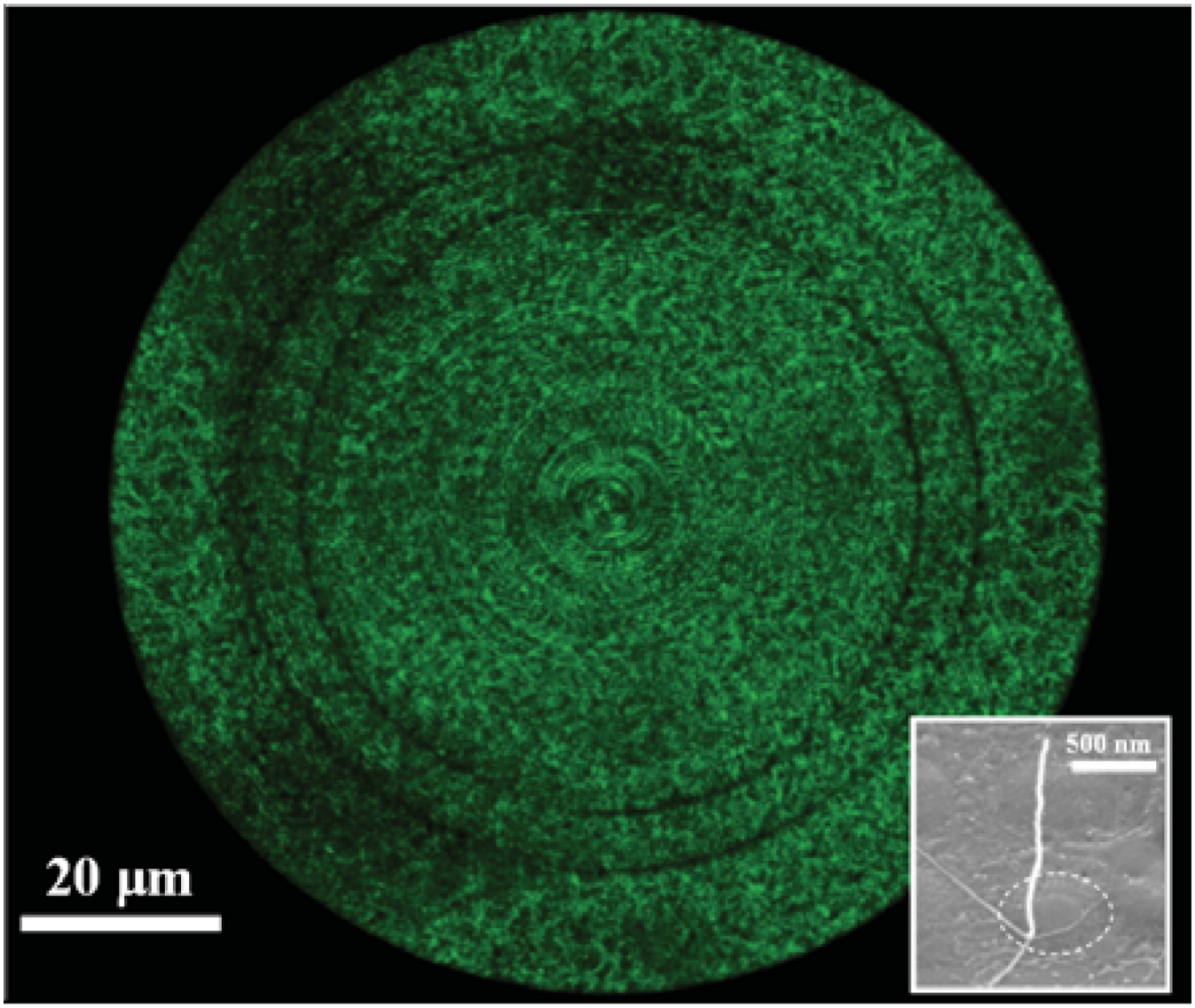

Figure 16.
Optical fluorescence image showing the surface-initiated growth of F-actin from electron beam lithography defined nanoscale patterns (i.e., concentric circles). Inset showing a SEM image of a free-standing surface-initiated growth of single F-actin. Scale bar, 500nm (229, 230)

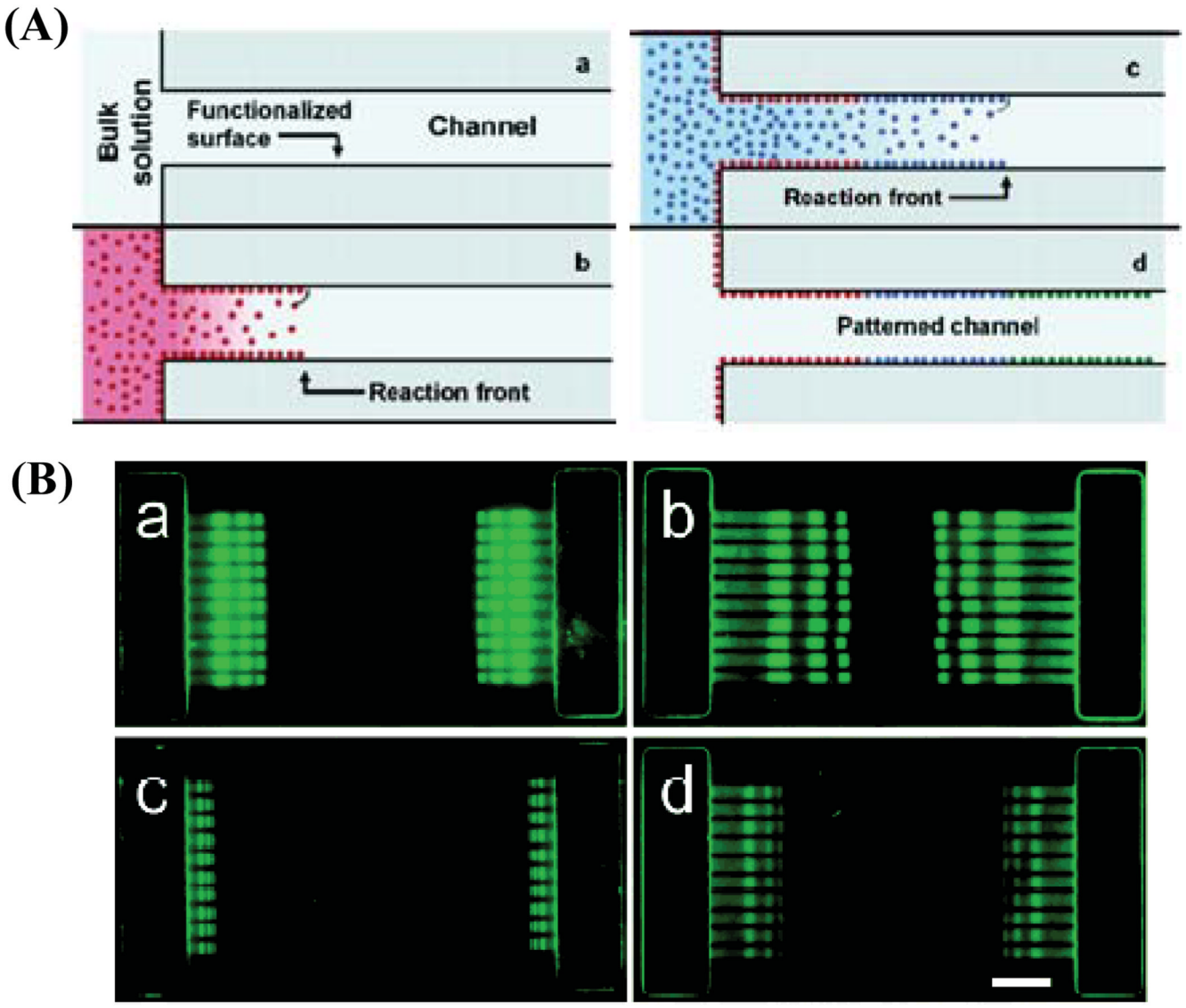

Figure 17.
Diffusion limited patterning inside nanofluidic channels. (A) Schematic showing the concept of DLP. (B) DLP with unlabeled and fluorescently labeled streptavidin. Channel design, concentrations of the streptavidin and time durations for each step are as follows: (a) channel design I, 1mg/ml, 5 min (b) channel design II, 1mg/ml, 2 min, (c) channel design I, 100μg/ml, 10min, (d) channel design II, 100μg/ml, 10min. Scale bar, 20μm. (Reprinted by permission from American Chemical Society: Karnik et al., Nano Lett., 2006, 6: 1735–1740, copyright 2006)

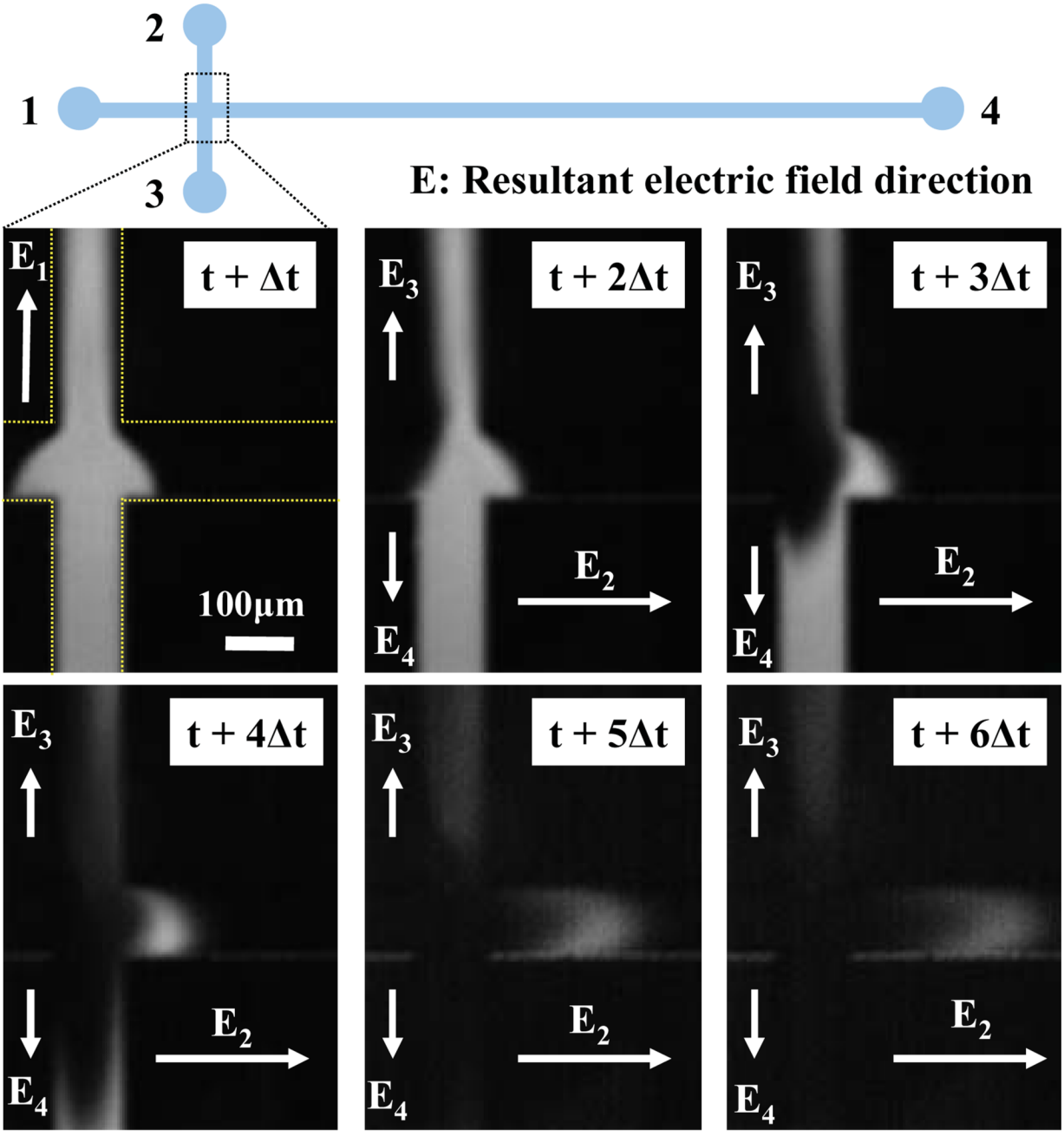

Figure 18.
Capillary electrophoretic movement of fluorescently-tagged DNA molecules inside a microfluidic channel

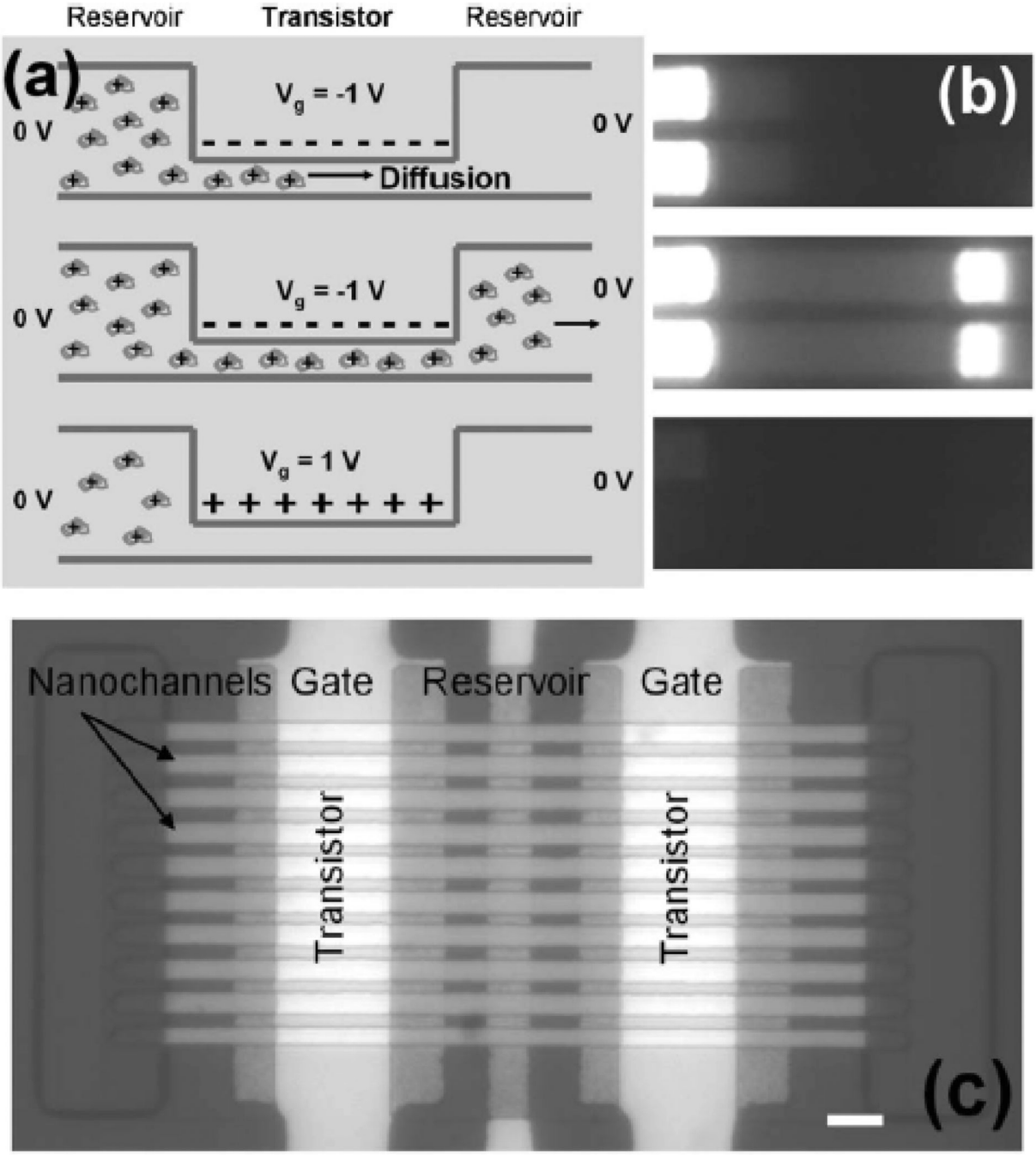

Figure 19.

A nanofluidic transistor for molecular transport. (a) Schematic showing the diffusion of the avidin when the transistor is switched on without bias between the microchannels. (b) Fluorescence images corresponding to (a). (c) Micrograph of a nanofluidic transistor. Scale bar, 10μm. (Reprinted with permission from Karnik et al., Appl. Phy. Lett., 2006, 88:123114, Copyright 2006, American Institute of Physics)

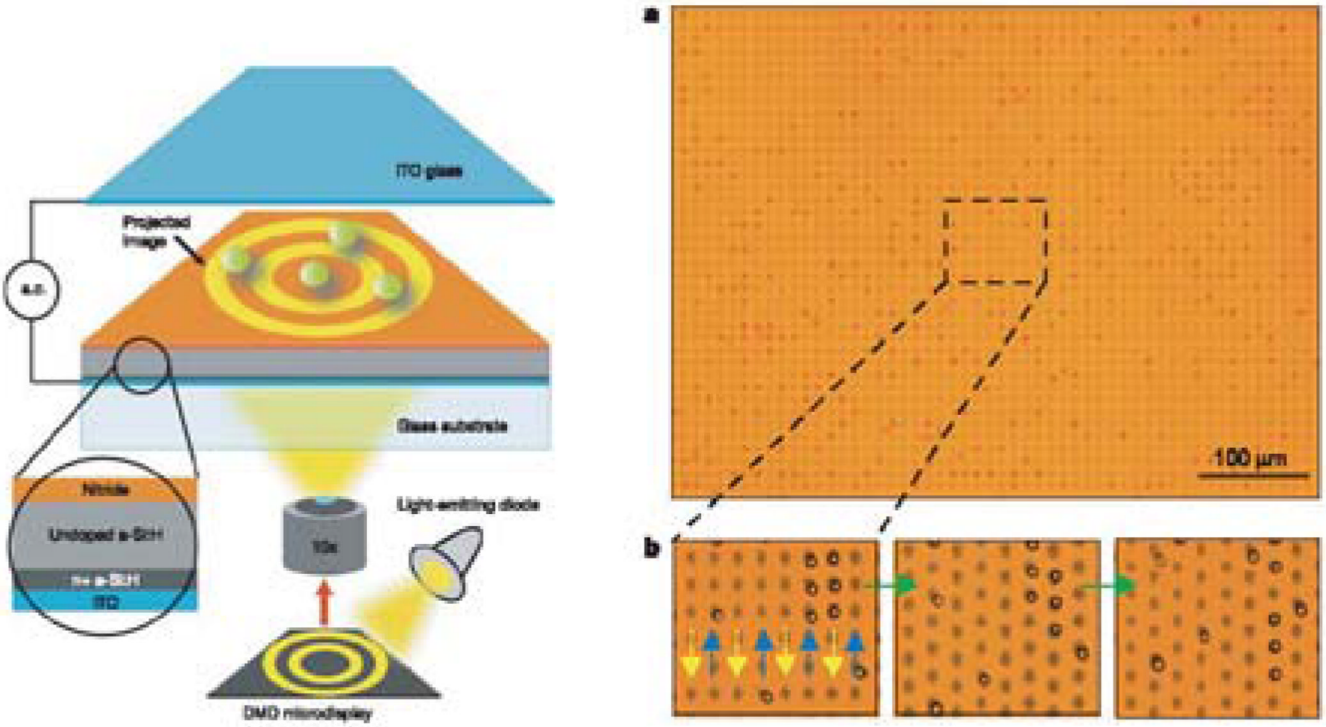

Figure 20.
Particle manipulation and transportation by optoelectronic tweezers (OET). (Reprinted by permission from Macmillian Publishers Ltd: Chiou et al., Nature, 2005, 436: 370–372, copyright 2005)

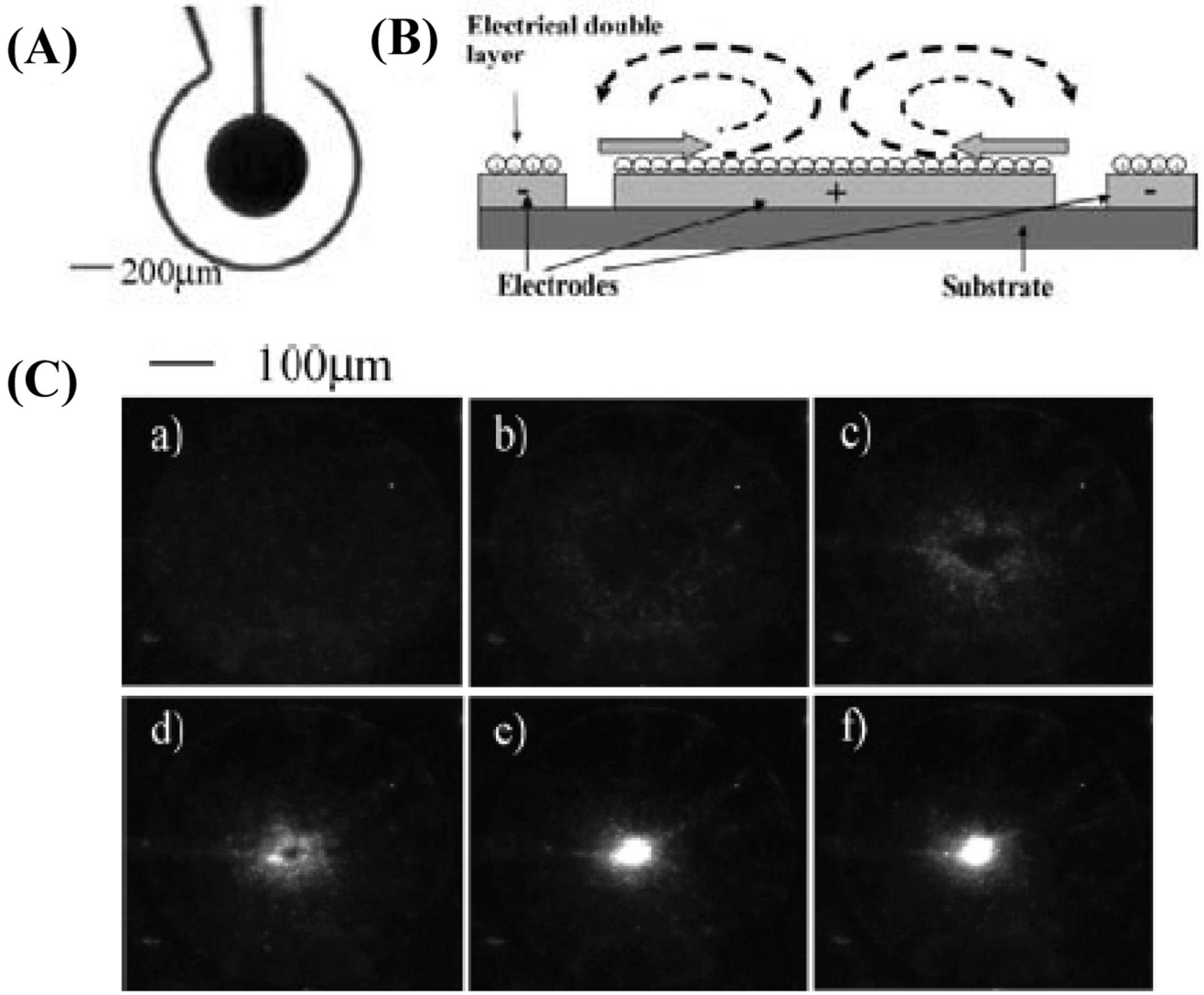

Figure 21.
AC electroosmotic focusing of biomolecules. (A) Design of the electrodes. (B) Schematic showing the formation of AC electroosmotic flow. (C) Time sequence images (in 10s interval, a–f) showing the concentration of 200nm fluorescence particles on the central electrode. (Reprinted by permission from American Chemical Society: Wong et al., Anal. Chem., 2004, 76: 6908–6914, copyright 2004)

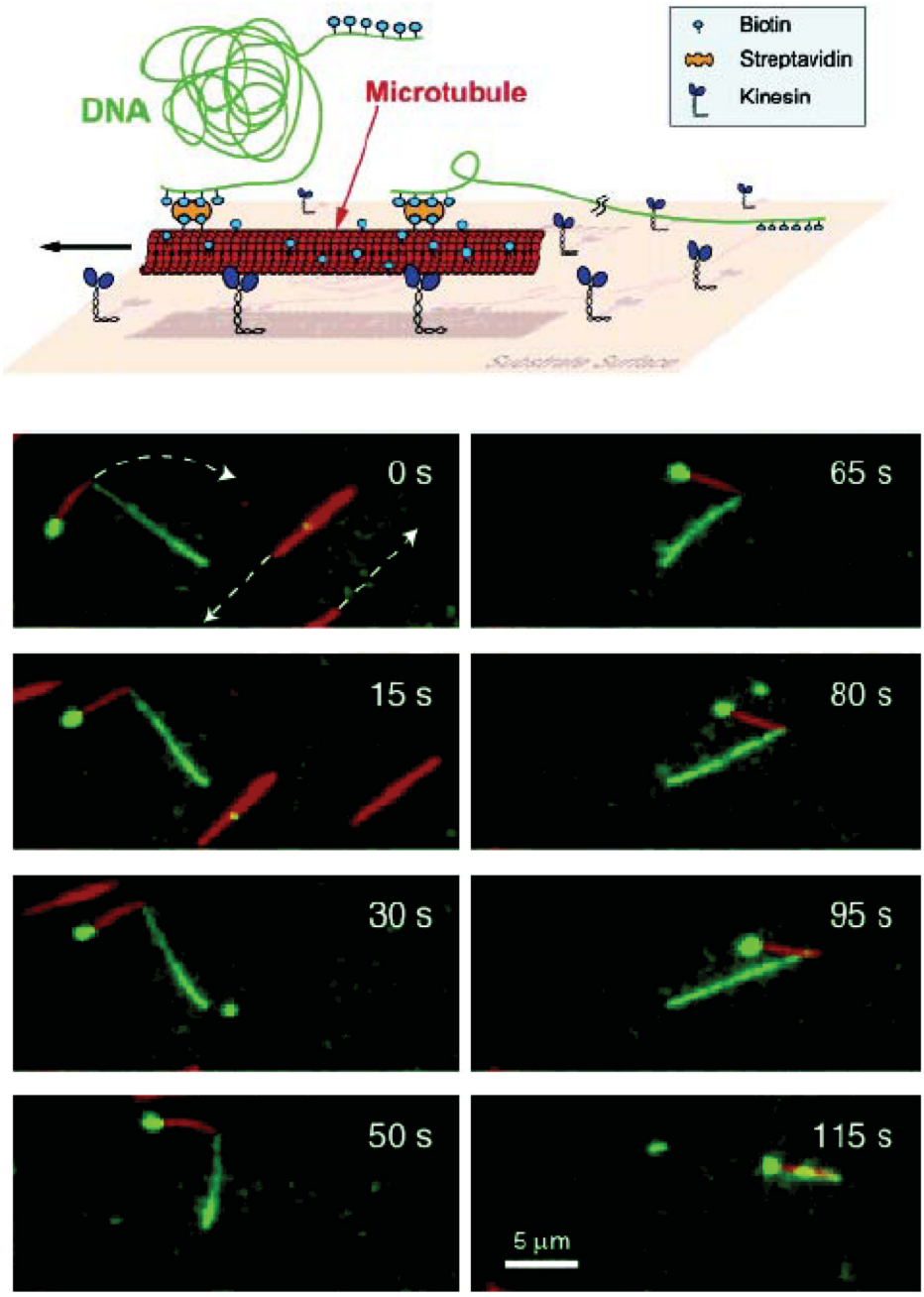

Figure 22.
Manipulation of DNA by the inter-cooperative motion of microtubules and the kinesin. (Reprinted by permission from American Chemical Society: Diez et al., Nano Lett. 2003, 3:1251–1254, copyright 2003)

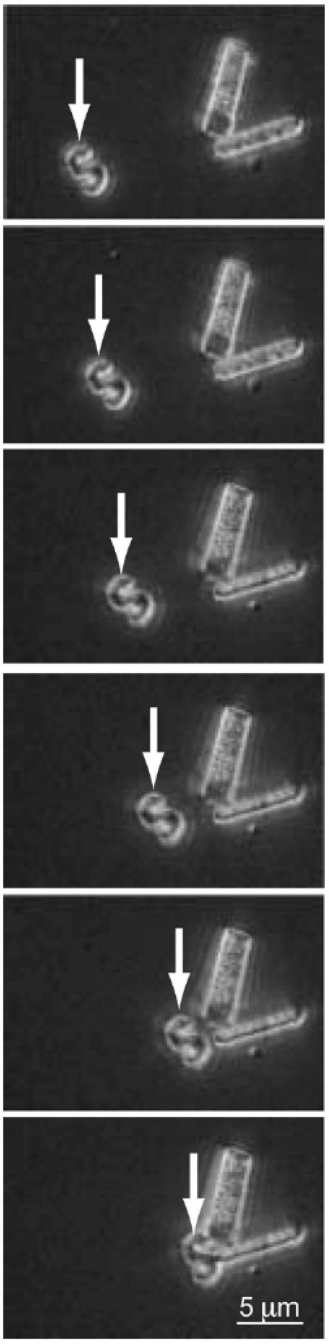

Figure 23.
Sequences of images (in 10s interval) showing the transportation of a micromachined S structure with microtubule-kinesin system. (Reprinted with permission from Yokokawa et al., JMEMS, 2004, 13: 612–619, Copyright 2004, IEEE)

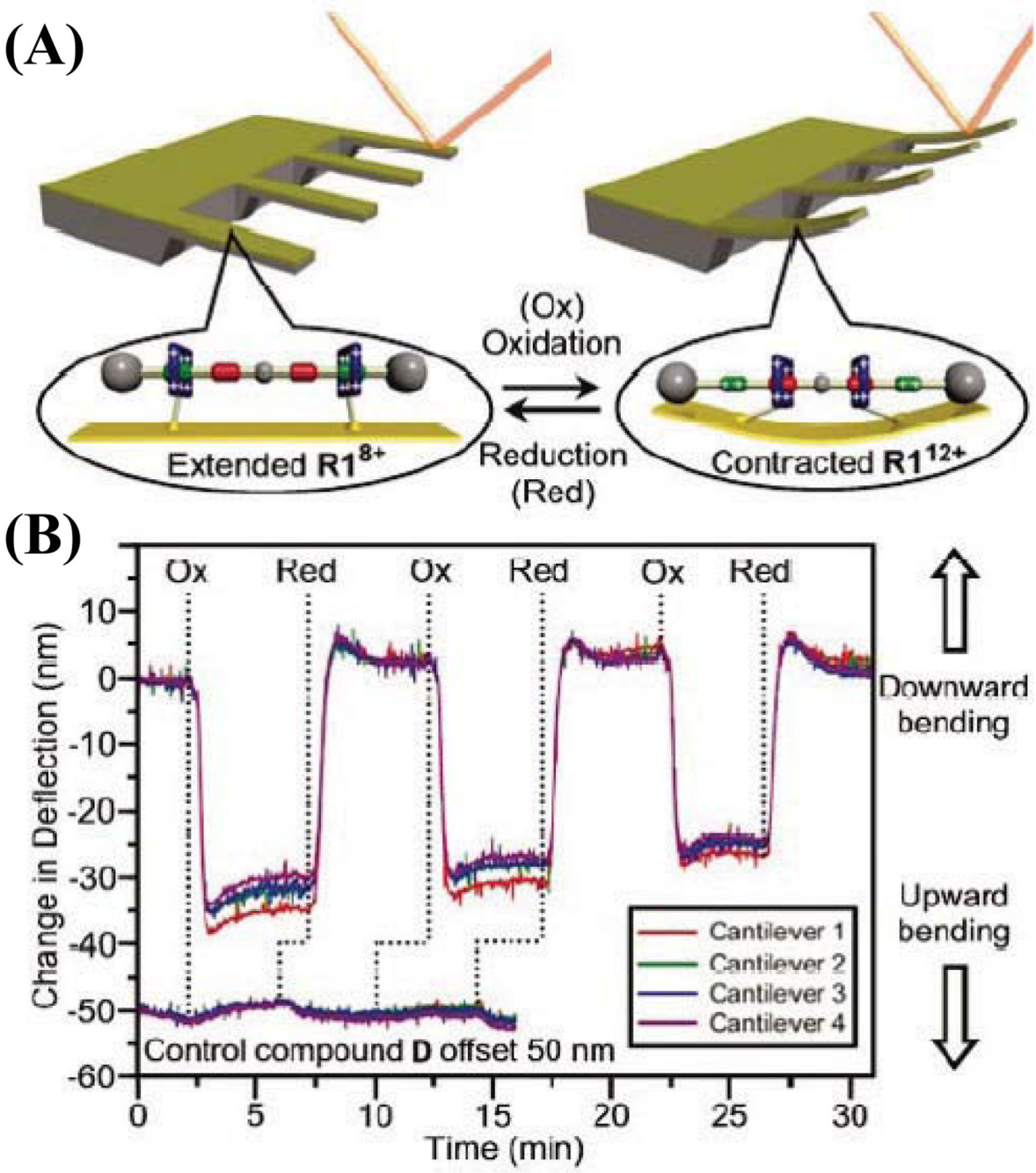

Figure 24.

Actuation of micro-cantilever beams by synthetic molecular linear motors. (A) Conceptual representation showing the actuation mechanism. (B) Reversible bending of four micro-cantilever beams actuated by synthetic molecular linear motors. (Reprinted with permission from Huang et al., Appl. Phy. Lett., 2004, 85:5391 – 5393, Copyright 2004, American Institute of Physics)

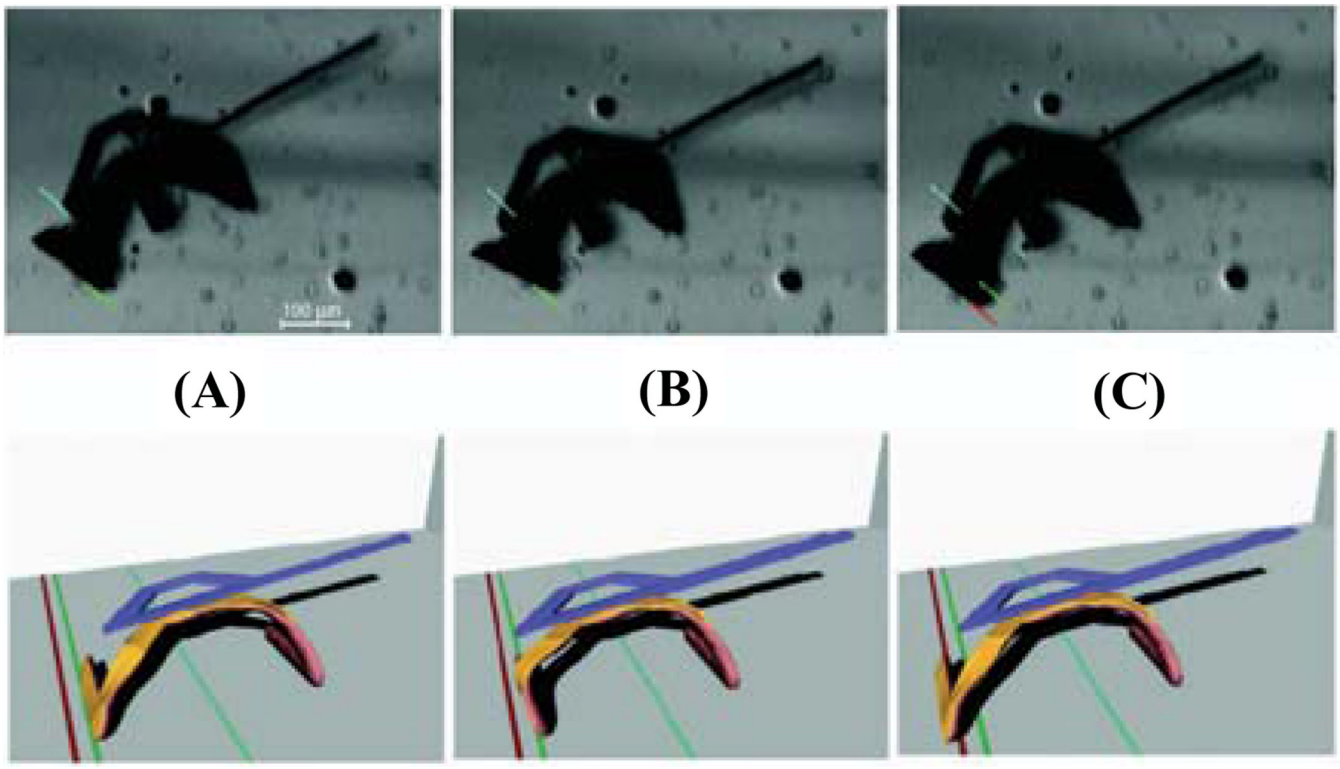

Figure 25.
MEMS actuator powered by self-assembled muscle. (A) Before muscle contraction. (B) During muscle contraction. (C) After relaxation of the muscle. Scale bar, 100μm (Reprinted by permission from Macmillian Publishers Ltd: J. Xi et al., Nat. Mater., 2005, 4:180–184, copyright 2005)

Table 1

Structural dimensions of selected molecular components

Molecular Component	Monomer Dimensions			Polymer Dimensions		Ref.
	L_1(nm)	L_2(nm)	L_3(nm)	D (nm)	P (nm)	
DNA *	-	-	-	2	3.4	(10)
Actin *a*	3.3	5.0	5.6	~ 7	~ 37	(93)
Tubulin *a***	4.6	6.5	8.0	~ 22	-	(129,130,132)
Fimbrin *a*	3.3	6.6	8.8	-	-	(114,115,351)
α-actinin *e*	-	~3–4	30–40	-	-	(116,117)
Filamin *e1*	-	-	~ 80	-	-	(119)
Spectrin *e1*	-	~ 10	150–200	-	-	(119)
Gelsolin *a*	3.6	5.5	8.5	-	-	(352,353)
Arps2/3 *a*	7–10	14.0	15.0	-	-	(122,354)

(Notations: L_1, L_2, L_3 (linear dimensions), D (diameter), P (periodicity);

a denotes the dimensions are obtained from atomic structural models;

e denotes the dimensions are estimated from electron micrograph with the sample prepared by negative staining;

e1 denotes the dimensions are estimated from electron micrographs, accounting for + 1nm due to sample preparation from Pt/Carbon Sputtering;

* denotes the B-form DNA;

** denotes 13-protofilament microtubule)

Table 2

Mechanical properties of biopolymers at the single molecule level

Biopolymer	Persistence Length (μm)	Torsional Rigidity (nN·nm^2)	Flexural Rigidity (nN·nm^2)	Ref.
F-actin	4–18 [a]	50–80	15–73	(100,109,110,112,355)
Microtubule	6300 [b]	-	2.6×10^4 [c]	(138)
dsDNA	0.04–0.05 [d]	0.46	0.16–0.21 [e]	(50,54,55)

[a] (denotes part of the persistence length is inferred from the flexural rigidity data by Equation (8) at 298K;

[b] denotes persistence length for very long microtubule (i.e. $\gg$ 21pm). On the other hand, for short microtubule, there is a length dependency of the persistence length, see text;

[c] denotes the flexural rigidity is inferred from persistence length by Equation (8);

[d] denotes the persistence length is dependent on the buffer conditions [54];

[e] denotes the flexural rigidity is deduced from persistence length from Equation (8))

Table 3

Mechanical performance for selected natural and synthetic linear motor molecules

Motor Molecules	Step Size (nm)[a]	Speed (nm/s)[b]	Force (pN)	Ref.
Kinesin	+8.3 [c]	~ 600[d]	6±1[e]	(167,177,178)
Myosin V	+37 [c]	~ 300[d]	~ 3[e]	(160,180)
Myosin VI	−27 +11	~ 300[d]	~ 3[e]	(170)
[2]rotaxanes [f]	±1.4	-	~ 145[g]	(341)

[a] (denotes step size towards a + end or – end;

[b] denotes *in vitro* absolute velocity measurements;

[c] denotes center-of-mass step;

[d] denotes velocity under zero load and at saturated ATP;

[e] denotes stall force at saturated ATP;

[f] denotes a synthetic artificial linear motor which can perform reversible work depending on the chemical environments (341);

[g] denotes that the force value depends on the loading rate, the average force evaluated from the interaction energy and the actuation distance is ~320pN (341)).